PhD degree in Molecular Medicine

(Curriculum in Molecular Oncology)

European School of Molecular Medicine (SEMM),

University of Milan and University of Naples "Federico II"

Settore disciplinare: Bio/11

Genetic dissection of the Myc-induced DNA Damage Response

Sara Rohban

Fondazione Istituto Italiano di Tecnologia (IIT), Milan

Matricola n. R09852

Supervisor: Dr. Stefano Campaner
IIT, Milan

Anno accademico 2014-2015

Table of contents

List of abbreviations

53BP1	p53 Binding Protein
ATM	Aaxia Telangiectasia Mutated
ATR	Ataxia-Telangiectasia and Rad3-related
ATRIP	ATR-Interacting Protein
bHLHZip	basic Helix-Loop-Helix Leucine Zipper
BrdU	Bromodeoxyuridine
CDK	Cyclin-Dependent Kinases
ChIP	Chromatin Immunoprecipitation
CPT	Camptothecin
CTCF	CCCTC-binding factor
CTD	C-Terminal Domain
DDR	DNA Damage Response
DNA-PKcs	DNA-dependent Protein Kinase catalytic subunit
DRIP	DNA-RNA Immunoprecipitation
DSB	Double-Strand Break
EdU	5-Ethynyl-2´-deoxyuridine
ER	Estrogen Receptor
FACS	Fluorescence-Activated Cell Sorting
HR	Homologous Recombination
HU	Hydroxyure
iPOND	isolation of Proteins On Nascent DNA
IR	Ionizing Radiation
MDC1	Mediator of DNA damage Checkpoint 1
MEF	Mouse Embryonic Fibroblast
NHEJ	Non-Homologous End-Joining
OHT	4-hydroxy-tamoxifen
PI	Propidium Iodide
PIKK	PI3K-like kinase family
POS	Reactive Oxygen Species
RS	Replication Stress
SC	Synaptonemal Complex
SL	Synthetic Lethal
SMC1	Structural Maintenance of Chromosomes
ssDNA	single-strand DNA
SV	Synthetic Viable
UV	Ultraviolet

Table of figures

Abstract

In pre-cancerous lesions the overexpression of oncogenes such as Myc not only drives aberrant cellular proliferation, but also triggers a strong DNA damage response (DDR) that is in part due to DNA damage accumulating at the level of stalled replication forks. This oncogene-induced DDR is an effective barrier to cancer development and represents a relevant tumor suppressive mechanism. Conversely, at later stages of malignancy DDR signaling may function in favor of cancer progression. Such tumor promoting role of DDR may be needed for cancer cells to avoid accumulation of cytotoxic DNA damage under high level of oncogene-induced replication stress. Recently it has been shown that targeting regulators of replication checkpoint such as ATR or Chk1 in Myc-overexpressing cells caused apoptosis and prevented tumor formation, suggesting a crucial role for this pathway in ensuring cancer cell viability and offering the chance of developing new targeted therapies against cancer cells.

In an effort to identify the modulators of Myc-induced replicative stress, we carried out a high-throughput RNAi screen based on immunofluorescence detection of ϒH2AX, a DNA damage marker. Quantification of the number of cells and the percentage of ϒH2AX-positive cells, identified hits that exhibited differential cell viability (synthetic lethal hits) and/or enhanced ϒH2AX signal (DDR-up hits) in Myc-overexpressing cells compared to normal cells. Validated hits encompass a variety of pathways and biological processes and have different molecular functions. As a proof of principal, we selected SRSF3 and Cdk12 and confirmed the synergistic effect of Myc overexpression and depletion of SRSF3 or Cdk12 on accumulation of cytotoxic DNA damage response as marked by H2AX phosphorylation.

For further mechanistic investigations, we selected Rad21, a component of the cohesin complex, which was also reported as a Myc-synthetic lethal candidate previously. Using

small inhibitory RNAs against Rad21, we confirmed that depletion of Rad21, increased ϒH2AX level and subsequently led to cell death, selectively in Myc-overexpressing cells. We provide evidence that while Rad21 is necessary for proper and efficient DNA synthesis, replication reinforcement imposed by Myc overexpression in Rad21-depleted cells results in replicative stress. In addition, we observed that Myc, as a transcription factor, could partially rescue transcriptional alterations due to Rad21 depletion. The conflicts between DNA replication and transcription in Rad21-depleted cells upon Myc activation may be the source of increased R-loops detected in these cells.

In summary, by means of a genetic loss of function screen we identified several candidates that may be involved in protecting Myc-overexpressing cells against ample replicative stress, thus revealing targets for potential therapeutic intervention in Myc-driven cancers.

1 Introduction

1.1 DNA Damage Response (DDR)

1.1.1 DDR signaling

1.1.1.1 The importance of DNA damage response

The genome in each cell is under constant attack by agents that can damage its DNA. These threats against DNA integrity can originate from exogenous sources such as ultraviolet (UV), ionizing radiation (IR) or DNA-damaging chemicals in contaminated foods. In addition, DNA damage may also arise endogenously, for example, as a result of defects in DNA replication or by chemical modifications due to reactive chemical intermediates like free oxygen radicals generated during oxidative respiration (Sancar et al., 2004). These lesions should be resolved before mitosis takes place in order to avoid that the damaged DNA is passed to daughter cells. To combat these assaults, cells have evolved a series of mechanisms termed DNA-damage response (DDR) to sense the DNA lesions, signal their presence and activate repair mechanisms and other effector pathways (Zhou and Elledge, 2000). As a consequence of the activation of the DDR signaling, cells can cope with DNA damage by transient or permanent arrest in cell cycle progression or by undergoing programmed cell death.

In the next part, the molecular mechanisms of the cellular response to DNA damage is briefly reviewed followed by discussions on its role in cancer.

1.1.1.2 How DDR is regulated

As mentioned above, DNA can be damaged in a variety of ways by either exogenous or endogenous agents. Reactive oxygen species (ROS) -generated as the by-products of oxidative respiration- and ionizing radiation can break the phosphodiester bonds in the backbone of the DNA helix. When the two single strand breaks in the opposite DNA strands are close together, this may result in a double-strand break (DSB),

a vicious form of DNA damage which poses a severe threat for the integrity of the genome (Kastan and Bartek, 2004). Alkylating/intercalating agents can cause intra-strand or inter-strand crosslinks that should be resolved before DNA replication begins. Inhibitors of DNA topoisomerases can lead to single or DSBs depending on the type of enzyme inhibited and the cell cycle phase (Froelich-Ammon and Osheroff, 1995). Inducing oncogenes, as will be discussed later, at least partly by boosting S-phase entry and DNA synthesis may cause replication stress (Macheret and Halazonetis, 2015). Under such conditions, if DNA polymerases stall, MCM replicative helicases continue unwinding DNA ahead of the replication fork, leading to the generation of single strand breaks. Then, if the replication process fails to restart, replisome components dissociate and the replication fork can collapse, leading to the formation of DSBs (Zeman and Cimprich, 2014). Therefore, despite the variety of potential DNA lesions, their processing often leads to the generation of single or double strand breaks that serve as the signals for initiating the DDR signaling pathway. Depending on the type of the DNA damage, the DDR pathway relies on the activation of different members of the PI3K-like kinases family (PIKKs): ATM (ataxia telangiectasia mutated), ATR (ataxia-telangiectasia and Rad3-related) and DNA-PKcs (DNA-dependent protein kinase catalytic subunit) (Harper and Elledge, 2007).

Although protein kinases ATM and ATR belong to a same PIKK family with a common target motif (Ser/Thr-Gln-Glu), gene disruption studies have shown little genetic redundancy of these proteins. For example, cells derived from ataxia-telangiectasia (A-T) patients (with heterozygous ATM mutation) as well as *atm*$^{-/-}$ mice display hypersensitivity to ionizing radiation and defects in DNA damage checkpoints. However, these cells are not sensitive to ultraviolet or replication inhibitors (Klose et al., 2006, McKinnon, 1987, Barlow et al., 1996, Canman et al., 1998, Painter and Young, 1980). On

the other side, ATR is an essential gene and hypomorphic mutant of ATR, unlike ATM-deficient cells, is sensitive to UV and inhibitors of DNA replication (Brown and Baltimore, 2000, Cliby et al., 1998, Wright et al., 1998, de Klein et al., 2000). For these reasons, it is commonly believed that ATM is mainly responsible for detecting and signaling the presence of DSBs, whereas ATR is engaged in the cellular processes that affect the progression of replication fork such as DNA damage generated by replication fork stalling and UV radiation. Single protein analyses as well as various screens for finding the ATM and ATR substrates identified over 700 proteins that become phosphorylated in response to IR or UV (Matsuoka et al., 2007, Stokes et al., 2007). One of the most enriched categories in these studies was the DNA replication module including MCMs, ORC (origin recognition complex) and DNA polymerases, arguing the impact of DDR on DNA replication and G1/S checkpoint. The other top enriched module was DNA repair. Several factors known to have a role in various DNA repair processes - such as excision repair, mismatch repair, crosslink repair, homologous recombination (HR) and transcription-coupled repair were classified in this group which could explain the cooperation between DDR pathway and repair mechanisms to maintain genome stability. Besides these two most enriched groups, there were a large number of modules whose connection to DDR have not yet been well elucidated. These include pathways like RNA splicing, nonsense mediated decay, the spindle checkpoints, chromatin remodeling and a number of transcription factors. Prospective studies can further clarify the link between DDR and these modules.

Although the downstream effectors of the other DDR-protein kinase, DNA-PK, are still largely unknown, it seems that this kinase is a DSB sensor required for non-homologous end-joining (NHEJ). Upon generation of a DSB, this protein is recruited to the site of the

damage via the Ku70-Ku80 heterodimer and by its catalytic subunit -that has DNA-end binding activity- promotes rejoining of the DSB (Durocher and Jackson, 2001).

1.1.1.3 DNA damage signal initiation

In response to DSBs, a complex called MRN, consisting of Mre11-Rad50-Nbs1, senses the damage and along with chromatin structural changes around DSBs, such as histone acetylations, favor the recruitment of ATM to the broken DNA (Price and D'Andrea, 2013, Uziel et al., 2003, Sulli et al., 2012). ATM exists as an inactive dimer but once recruited to a DSB, the dimer dissociates and this conformational change exposes certain residue (serine 1981) to ATM autophosphorylation that is crucial for maintaining ATM activation (Bakkenist and Kastan, 2003). Once activated, ATM orchestrates a signaling cascade based on its kinase activity. Among the ATM substrate there is also the MRN complex whose phosphorylation is important for recruiting other substrates like BRCA1 and SMC1 (structural maintenance of chromosomes 1) to ATM, thus the MRN complex serves also as an amplifier of the ATM-dependent DNA damage signaling. ATM can also phosphorylate other nucleoplasmic substrates such as p53 (Shiloh and Ziv, 2013).

Unlike ATM, whose activity is minimal in unstressed cells but is stimulated in the presence of damage, in vitro kinase assay indicated that ATR kinase activity remains constant after treatment with genotoxic agents, suggesting that ATR activity may be regulated by subcellular localization (Abraham, 2001). ATR exists in a complex with the ATR-interacting protein (ATRIP) and localizes with single-strand DNA (ssDNA) by means of ATRIP interaction to RPA, that is present on abnormal stretch of ssDNA. In this way, single strand DNA decorated by the RPA complex is the initial signal that plays two main roles: it recruits the ATR protein through its regulatory subunit ATRIP and it recruits RAD17 clamp loader. RAD17 clamp loader then becomes phosphorylated and activated by ATR to recruit PCNA-related 911 complex (RAD9-RAD1-HUS1) to

ssDNA. ATR can also phosphorylates TopBP1 which binds 9-1-1 complex and was shown to stimulate ATR kinase activity through interaction with ATRIP (Harper and Elledge, 2007, Zou and Elledge, 2003, Cortez et al., 2001).

1.1.1.4 DDR mediators

Mediators are the modulators of ATM and ATR that act as recruiters of additional substrates as well as scaffolds to assemble complexes. The ATM-mediated mediators include MDC1 (mediator of DNA damage checkpoint 1), 53BP1 (p53 binding protein 1) and BRCA1 (Harper and Elledge, 2007, Stewart et al., 2003). The accumulation of mediators into the DNA damage foci depends on ATM-dependent phosphorylation of histone H2AX on ser139 (termed ϒH2AX). In such a case the mediators serve as the bridges between ϒH2AX and the MRN complex to facilitate ATM signaling (Stucki and Jackson, 2006). Similarly, Claspin functions as a mediator in ATR signaling and is required for ATR-mediated phosphorylation of the downstream targets (Shechter et al., 2004).

1.1.1.5 Effector kinases Chk1 and Chk2

The most important ATM and ATR substrates are the checkpoint-transducer serine/threonine kinases Chk2 and Chk1. As mentioned earlier, regardless of the limited cross-talks between the two pathways, ATM preferentially phosphorylates Chk2 whereas ATR activates Chk1. In this fashion, the DNA damage signal sensed by ATM and ATR at the site of the damaged DNA is conveyed to mobile messenger kinases Chk1 and Chk2 to activate the subsequent responses in cells (Figure 1.1) (Reinhardt and Yaffe, 2009).

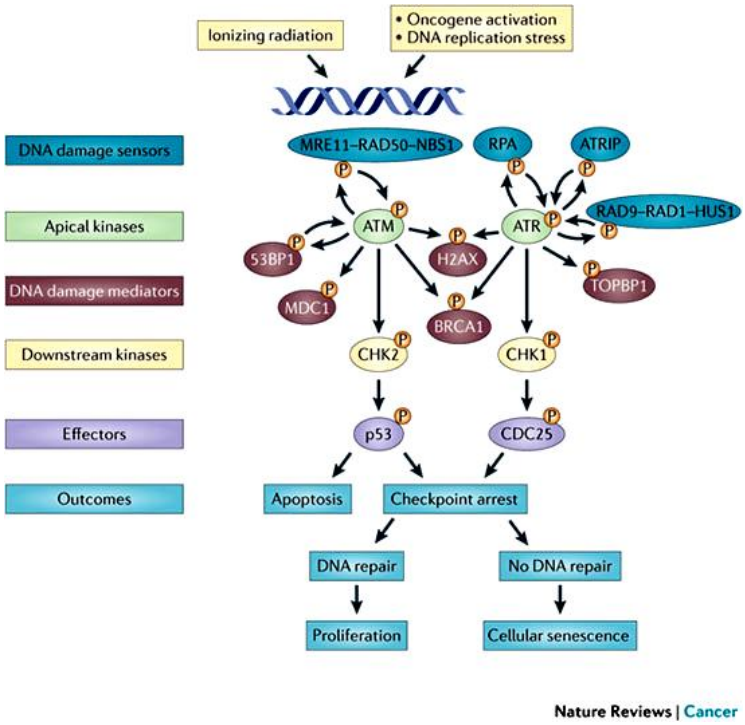

Figure 1.1. The DNA damage response signaling pathway
The DDR pathway is composed of two main DNA damage sensors the MRN complex and the RPA/RAD9-RAD1-HUS1 complexes that detect DSB and ssDNA respectively. These sensors then recruit PIKK kinases ATM and ATR to the site of DNA damage. Upon activation, ATM and ATR conduct a signaling pathway that relies mainly on the phosphorylation of the DNA damage mediators and subsequently the downstream kinases Chk2 and Chk1. The outcome of the DDR is determined by the activity of the DDR effectors that are activated by Chk2 and Chk1 kinases. Adapted from "Crosstalk between chromatin state and DNA damage response in cellular senescence and cancer" by G. Sulli, R. Di Micco R and F d'Adda di Fagagna, 2012, *Nature Reviews Cancer*, 12, p. 710.

1.1.2 The outcome of DDR signaling: checkpoint activation

A quick outcome of the DNA damage response induction is to halt cell cycle progression until the lesions are resolved. In eukaryotic cells control of cell growth and division involves molecular circuits known as "checkpoints" that ensure that the earlier process such as DNA replication or mitosis have been properly completed (Elledge, 1996). DNA damage response can lead to cell cycle blockage through activation of these checkpoints, a process called activation of the DNA damage checkpoint. These checkpoints act mainly on cell cycle regulators like cyclin-dependent kinases (CDKs) and CdK inhibitors in order

to delay cell cycle progression. Alongside the cell cycle arrest, the checkpoint kinases can also trigger cellular responses such as DNA repair, apoptosis and cellular senescence (d'Adda di Fagagna, 2008, Niida and Nakanishi, 2006, Sancar et al., 2004).

The G1 checkpoint response which results in G1 arrest in face of DNA damage, is mostly dependent on the p53-MDM2-p21 pathway stimulated by ATM/Chk2 or ATR/Chk1. ATM and ATR directly phosphorylate the p53 transcription factor particularly on serine 15 residue, located within the amino-terminal transactivation domain (Banin et al., 1998, Hirao et al., 2000, Shiloh, 2003, Tibbetts et al., 1999, Wahl and Carr, 2001). Also the ubiquitin ligase MDM2 that normally binds p53 and targets it to ubiquitin-mediated degradation is phosphorylated by ATM and ATR, leading to down-regulation of MDM2 function and p53 stabilization (Maya et al., 2001, Shinozaki et al., 2003). All these events contribute to the accumulation of p53 and the enhancement of its transcriptional activity. One of the important transcriptional targets of p53 is the inhibitor of cyclin-dependent kinase p21, which by inhibiting Cyclin E/Cdk2 blocks G1/S transition. As a result of inhibition of Cyclin E/Cdk2 kinase activity, E2F is preserved in the repressed transcriptional form bound to RB and thus is unable to activate the expression of the subset of genes required for S-phase entry and progression (Bartek et al., 1997, Bates and Vousden, 1996, Bartek and Lukas, 2001).

In the late G1 and early S-phase in response to DNA damage, Cdc25A -a phosphatase that removes inhibitory phosphate from Cyclin E/Cdk2 and Cyclin B/Cdk1 complex to promote progression into S-phase and mitosis respectively- becomes phosphorylated by Chk1. This phosphorylation creates a phosphodegron motif in the protein and subsequently leads to Cdc25A ubiquitination by the $SCF^{ß\text{-}TRCP}$ ubiquitin ligase and its rapid degradation. Following the decrease of Cdc25A, the Cyclin E (A)/Cdk2 complex is inhibited and the loading of Cdc45 -an essential replication factor- on replication origins

is prevented, causing a delay in S-phase progression (Bartek et al., 2004, Donzelli and Draetta, 2003). In addition, phosphorylation of Cdt1 -an important licensing factor for DNA replication- during S-phase induces the ubiquitin-mediated destruction of chromatin-loaded Cdt1 and leads to the disassembly of the pre-recombination complex and a blockage of origins firing and DNA replication (Kondo et al., 2004, Arias and Walter, 2007).

The G2 checkpoint (also known as the G2/M checkpoint) is activated in the case of persistent un-resolved DNA lesions occurred in the S-phase or when cells face DNA damage during G2, and has the function of preventing damaged cells from initiating mitosis (Nyberg et al., 2002, Xu et al., 2002). The key target of G2 checkpoint is the mitosis-promoting activity of the Cyclin B/Cdk1 kinase. Likewise G1/S checkpoint, down-regulation of Cdc25A in response to DNA damage signaling is an important event in the regulation of the G2 checkpoint response (Donzelli and Draetta, 2003, Mailand et al., 2002). Furthermore, Plk1 (which promotes ubiquitin-mediated proteolysis of Wee1 through creation a phosphodegron motif in the protein in normal G2/M transition) is inhibited in an ATM/ATR dependent manner and this leads to stabilization of Wee1 and inhibition of CDKs in the face of DNA damage (Harper and Elledge, 2007, Smits et al., 2000). Plk1 in normal cells phosphorylates and thus targets Claspin, an ATR coactivator, to $SCF^{ß\text{-}TRCP}$-mediated degradation, thus leading to reduced Chk1 signaling and preventing cell-cycle arrest (Gewurz and Harper, 2006). Noteworthy, the sustained G2 arrest may also partly rely on the transcriptional activity of p53, leading to the up-regulation of cell cycle inhibitors such as p21 and Gadd45a (growth arrest and DNA damage inducible 45 alpha) (Bunz et al., 1998, Taylor and Stark, 2001). DDR signaling cascade is schematically represented in figure 1.2.

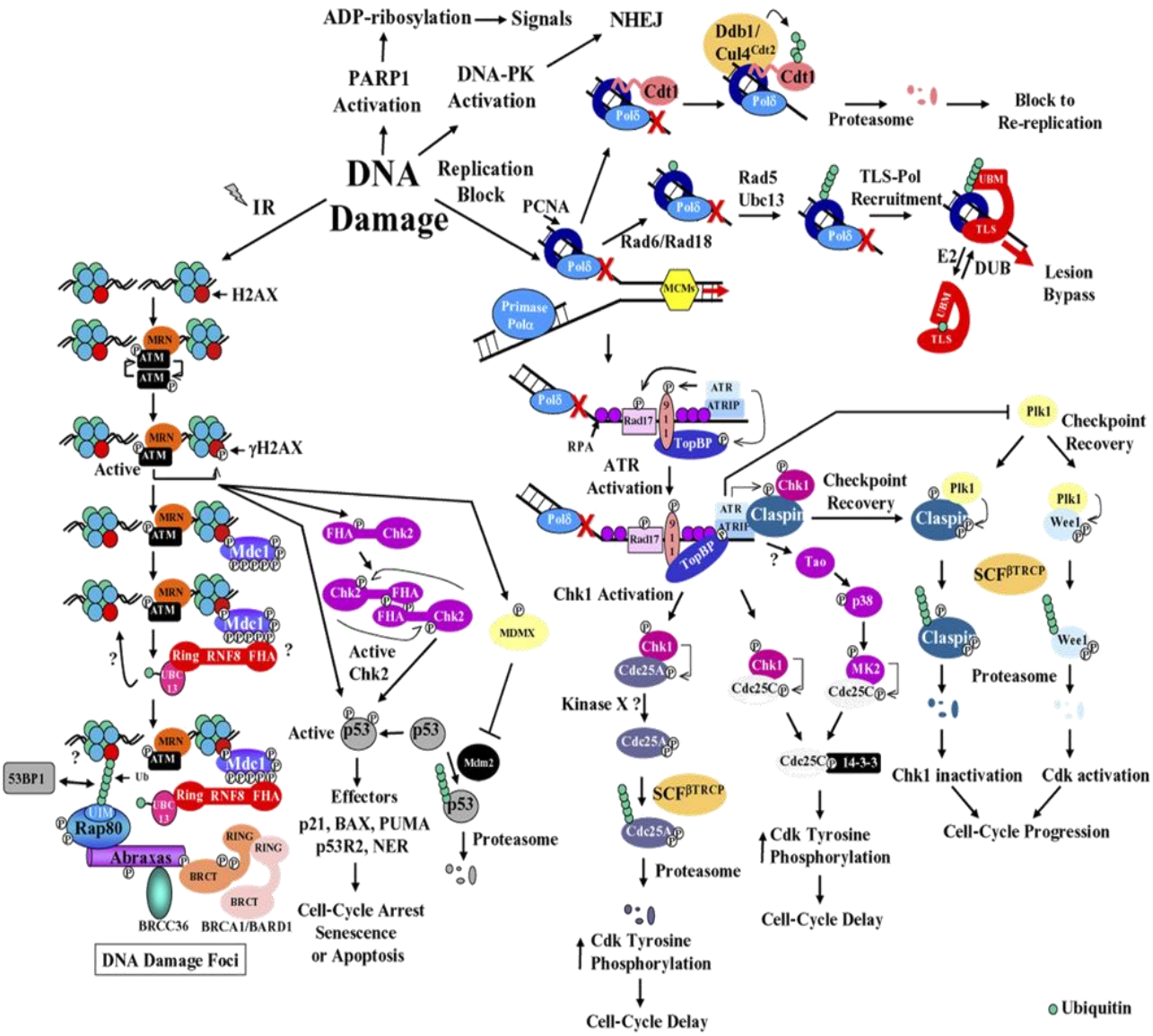

Figure 1.2. DNA damage response signaling cascade and its physiological consequences

A schematic representation of the various DDR pathways discussed in the text. Adapted from "The DNA Damage Response: Ten Years After" by J. W. Harper and S. J. Elledge, 2007, *Molecular Cell*, 28, p. 740.

1.1.3 The impact of DDR on cancer

Genome instability is a hallmark of almost all human cancers. Most carcinogens act by generating DNA damage. In addition, individuals with inherited DDR defects are commonly prone to develop tumors (Kastan and Bartek, 2004). Aberrant cellular proliferation -caused by activation of oncogenes- also has been shown to contribute to

genome instability by inducing DNA replication stress and ongoing DNA damage formation (Macheret and Halazonetis, 2015, Halazonetis et al., 2008). Therefore, the cellular responses to DNA damage in the frame of checkpoints activation and repair pathways play a crucial role in maintaining genome stability, while breach in these pathways increase the risk of cancer development. Indeed, not only mutations in DNA repair genes lead to cancer predisposition, but so do certain mutations in the components of DDR signaling pathway and DNA damage checkpoints. For example, loss of ATM or inactivating mutations in NBS1 or MRE11 predisposes individuals to lymphoma and leukemia development (Shiloh and Kastan, 2001, Stewart et al., 1999, Varon et al., 1998). In the case of ATR, hypomorphic mutant mice displayed enhanced tumorigenesis, presumably because of the defective DNA-mismatch repair (Fang et al., 2004). Also $H2AX^{\Delta/\Delta}p53^{-/-}$ mice (Bassing et al., 2003, Celeste et al., 2003) or mice lacking 53BP1 (Ward et al., 2003) showed checkpoint defects and cancer predisposition. The inherited mutations in one allele of Chk2 are also found in individuals with extremely cancer-prone Li-Fraumeni syndrome (Bell et al., 1999). The inheritance of a single mutated allele of either BRCA1 or BRCA2 also increases the incidence of breast and ovarian cancer, possibly by the loss of heterozygosity of the second allele (King et al., 2003).

1.1.3.1 Oncogene-induced DDR model

Overexpression of several oncogenes has been shown to associate with DDR activation and cancer development (Halazonetis et al., 2008). The first evidences from the analysis of precancerous lesions of various origins, demonstrated that the DNA double strand break checkpoint pathway is indeed frequently activated in pre-invasive tissues (Gorgoulis et al., 2005, Bartkova et al., 2005). For example, precancerous lesions of lung showed enhancement in several markers of DNA DSBs such as phosphorylated histone H2AX and 53BP1 foci, phospho-Chk2 and accumulated p53. In addition, these pre-

cancerous lesions showed sign of apoptosis. However, progression to carcinoma was associated with p53 or 53BP1 inactivation and decreased apoptosis (Gorgoulis et al., 2005). Further studies on different pre-invasive lesions (like hyperplastic lung tissues, dysplastic nevi, superficial bladder lesions and colorectal adenomas) demonstrated that the activation of DNA damage checkpoints occurs frequently at pre-cancerous stages and is associated with cell cycle arrest or apoptosis (Bartkova et al., 2005, Bartkova et al., 2006, Gorgoulis et al., 2005, Di Micco et al., 2006).

More investigations on the cause of DNA damage and the subsequent DDR response in pre-cancerous lesions, indicated that these lesions have high level of activated oncogenes rather than telomeres erosion or mutation in genes responsible for genomic instability (Halazonetis et al., 2008, Bartkova et al., 2005, Bartkova et al., 2006). In line with these observations, overexpression of oncogenes, such as Cyclin E, Cdc25a and E2F1, in cultured cell lines mimicked the characteristic of pre-cancerous lesions regarding the activated DNA damage response (Bartkova et al., 2005). Besides activation of ATM-Chk2 pathway, several targets of the ATR pathway, like Chk1 and Rad17, were also found to be phosphorylated in the cells overexpressing various oncogenes (Bartkova et al., 2005), linking the oncogene-induced DDR to replicative stress. As the overexpression of these oncogenes promotes S-phase entry, it was proposed that the DNA damage response might be a consequence of unscheduled DNA synthesis in oncogene-overexpressing cells. Supporting this idea, U2OS cells overexpressing Cyclin E displayed longer replication tracks in DNA combing and increased amounts of hyperphosphorylated form of single strand DNA binding replication protein A (RPA) (Bartkova et al., 2006). Based on these evidences, oncogene-induced DNA damage model was proposed for cancer development and progression. Based on this model, activation of an oncogene in precancerous tissues causes aberrant proliferation and may lead to replication stress (RS)

defined as inefficient DNA replication due to replication fork stalling and/or collapse (Gaillard et al., 2015, Halazonetis et al., 2008, Macheret and Halazonetis, 2015, Bartkova et al., 2005). The discovery that fragile sites (difficult-to-replicate genomic sites) showed higher likelihood of loss of heterozygosity than other sites of the genome in precancerous lesions (Gorgoulis et al., 2005, Tsantoulis et al., 2008) further supported the hypothesis that oncogene-induced RS may arise early during cancer development. Activation of the DNA damage response pathway in pre-cancerous lesions leads to the activation of a tumor suppressive barrier imposed by the DNA damage checkpoints controlled by the ATM/Chk2 pathway leading to a proliferative arrest and/or apoptosis, largely mediated by p53 activation. Additional mutations in genes involved in the DNA damage response (DDR) –such as ATM or p53 inactivation mutations- will breach this barrier thus favoring genomic instability and cancer progression (Halazonetis et al., 2008, Macheret and Halazonetis, 2015).

Noteworthy, although many of the DNA damage response factors act as tumor suppressor genes in early stage of cancer development, more recently it was proposed that in later stage of malignancy, DDR may function in favor of cancer progression (Bao et al., 2006, Santos et al., 2014). Such tumor promoting role of DDR may be needed for cancer cells to avoid accumulation of ample cytotoxic DNA damage under high level of oncogen-induced replication stress. The elevated resistance to DNA-damaging chemotherapies observed in highly malignant tumors could be at least in part related to this phenomenon (Bao et al., 2006). Therefore, it has been proposed that DDR inhibitors might increase the efficacy of radio- and chemo-therapy. Chk1 inhibitors were among the first DDR inhibitors examined by the pioneer studies on this topic. For example, it has been shown that Chk1 inhibition sensitizes p53-deficient tumor cells (but not normal cells) to different DNA-damaging agents (Chen et al., 2006, Vitale et al., 2007). These observations also

raised the concept of synthetic lethality to target cancer cells with the intrinsic property of having high levels of oncogene-induced replicative stress. In agreement with this notion, ATR and Chk1 inhibitors -by inducing massive S-phase DNA damage- are particularly toxic for cells overexpressing oncogenes such as Cyclin E, Ras and c-Myc (Gilad et al., 2010, Murga et al., 2011, Toledo et al., 2011).

1.2 Myc oncogene

1.2.1 An introduction on Myc protein

Myc is a master transcriptional regulator whose target genes are involved in cell cycle progression, cell growth, differentiation, metabolism and apoptosis (Meyer and Penn, 2008). Myc protein belongs to the basic Helix-Loop-Helix Leucine Zipper (bHLHZip) transcription factor family. The bHLHZip domain in C-terminal domain (CTD) of the Myc protein is responsible for site-specific DNA binding and its heterodimerization with its protein partner Max. Besides CTD, Myc family members also show high homology in regions at the N-terminal domain (NTD) called Myc Box regions (MB1 and MB2) that are uniquely present in Myc family members and are required for Myc transcriptional activity (Oster et al., 2002). The Myc-MAX complex can activate gene transcription by several mechanisms. Myc, through interaction with TRRAP, recruits histone acetyltransferase (HAT) complexes to the chromatin to activate transcription of different target genes (McMahon et al., 2000). Myc can also regulate gene transcription through interaction with IN1/hSNF5 (a component of the SWI/SNF chromatin remodeler complex) which modifies chromatin in an ATP-dependent manner (Cheng et al., 1999). Accumulating evidence showed that Myc is also involved in RNA polymerase II elongation through interaction with components of the RNA polymerasee II CTD kinase P-TEFb like Cdk9 and Cyclin T1 (Eberhardy and Farnham, 2002).

Myc can also function as a transcriptional repressor of many genes, the best characterized are genes involved in cell cycle arrest and adhesion (Kleine-Kohlbrecher et al., 2006), however the mechanism of gene repression by Myc is less understood than the mechanism of transcription activation. The presence of Myc-MAX complex at the promoter of repressed target genes suggests that Myc acts directly in the down-regulation of these genes (Kretzner et al., 1992). Indeed it has been shown that Myc interacts with transcriptional activators bound to initiator elements (Ir) or transcriptional enhancers such as YY1, Miz-1 and NF-Y, thus by tethering and inhibiting the activity of these transcription factors represses the transcription of the target genes (Kleine-Kohlbrecher et al., 2006). Myc was also shown to contribute to transcriptional repression by promoting chromatin modifications (such as histone deacetylation) through recruiting DNA methyltransferase Dnmt3a and histone deacetyltransferase to Miz1-bound sites (Brenner et al., 2005, Kurland and Tansey, 2008). Noteworthy, by regulating the expression of microRNAs, Myc is also able to indirectly repress the expression of the target genes (Chang et al., 2008).

Given the significant role of Myc in gene regulation, it is estimated that this protein is bound to ~25,000 sites in human genome including RNA pol III- and pol I-dependent genes as well as non coding RNAs (Adhikary and Eilers, 2005). This global transcriptional regulatory role of Myc reveals its pleiotropic role in virtually every aspect of cell behavior (Figure 1.3).

1.2.2 The role of Myc in cellular processes

1.2.2.1 Cellular growth

Myc directly binds virtually all genes involved in glycolysis and glutaminolysis including glucose and glutamine transporters as well as glutaminase, and thus potentiates cell

metabolism and protein synthesis (Dang, 2013, Wise et al., 2008). Imported glucose can participate in glycolysis pathway to produce pyruvate. Pyruvate can be further oxidized in the mitochondrion to be converted to acetyl-CoA, which can then participates in the elongation of the growing fatty acid chain. Moreover, the glycolytic intermediate 3-phosphoglycerate is a substrate for lipid biosynthesis as well as precursor for serine and glycine. Glucose can also enter into pentose phosphate pathway for the production of NADPH and ribose. Glutamine can be transported into the mitochondrion where it is converted to glutamate by glutaminase. Both pyruvate and glutamate can then enter tricarboxylic acid (TCA) cycle to generate ATP or provide the carbon skeleton for the *de novo* synthesis of pyrimidines and purines (Dang, 2013, Wise et al., 2008). In addition, Myc stimulates lipid biosynthesis through regulation of many enzymes in this pathway such as acetyl-CoA carboxylase, fatty acid synthetase and stearoyl-CoA desaturase (Zeller et al., 2003).

Considering the importance of mitochondria in biosynthetic pathways as well as ATP production, it is conceivable that Myc could be involved in mitochondrial biogenesis. The observation that Myc induction led to increase in mitochondrial mass and biogenesis, possibly through the activation of several genes such as PGC-1ß and p32, supports this notion (Kim et al., 2008, Li et al., 2005, Zhang et al., 2007). PGC-1ß and p32 are the potent inducers of mitochondrial biogenesis and respiration whose knock-down was shown to diminish mitochondrial function and respiration (Fogal et al., 2010, Zhang et al., 2007).

Myc also contributes to ribosome biosynthesis through its ability to activate gene transcription mediated by all three RNA polymerases I, II and III (Gomez-Roman et al., 2003, Grandori et al., 2005). Taken together, it is proposed that Myc by stimulation of cell metabolism coordinates cellular growth and proliferation with cell mass.

1.2.2.2 S-phase entry

Myc is an immediate early growth response gene whose induction following exposure to mitogens such as platelet-derived growth factor (PDGF) leads cells to enter S-phase (Dang, 2013). In the absence of mitogen, Myc overexpression is also able to drive quiescence cells to S-phase (Shichiri et al., 1993). Indeed, Myc promotes cell cycle progression by activation of a large number of genes such as Cyclin D1, Cyclin D2, Cyclin E1, Cyclin A2, Cdk4, Cdc25A, E2F1 and E2F2 (Bouchard et al., 1999, Hermeking et al., 2000, Zeller et al., 2003). Myc also suppresses the transcription of the cell cycle checkpoint genes (like Gadd45 and Gadd153) and Cdk inhibitors (like $p15^{INK4b}$, $p21^{Cip1}$ and $p27^{Kip1}$) (Gartel and Shchors, 2003, Gartel et al., 2001).

The ability of Myc to promotes G1/S transition and DNA synthesis not only stems from its transcriptional role, but it was also shown that c-Myc co-localizes with the sites of DNA replication and physically interacts with components of pre-replication complex (Dominguez-Sola et al., 2007). Depletion of c-Myc indeed led to inhibition of DNA replication and reduced number of active replicons. Using transcriptional-silent Xenopus cell free extract, Dominguez-Sola et al. showed that addition of recombinant c-Myc protein to the Myc-depleted DNA was able to fully rescue DNA replication defect (Dominguez-Sola et al., 2007). Therefore, it seems that the combination of transcriptional and non-transcriptional activity of Myc is needed for Myc-induced S-phase entry and DNA replication.

1.2.2.3 Differentiation

Down-regulation of c-Myc is a characteristic of cells committed to undergo differentiation and ectopic Myc expression blocks differentiation in a number of cultured cells (Meyer and Penn, 2008, Oster et al., 2002). Moreover, it was shown that during differentiation, MAX is down-regulated (Delgado et al., 1995), suggesting that not only

Myc expression is reduced but also its activity is turning down by the absence of its partner. As terminal differentiation is usually coupled with permanent cell cycle exit, the differentiation impairment in Myc-induced cells has been related to the ability of Myc to provoke cellular proliferation. However, it was also reported that Myc, without rescuing the cell growth arrest and possibly by repressing the expression of master regulators of a differentiation state, inhibits differentiation in a number of cellular models. For example, it was shown that Myc inhibits the p27-mediated differentiation of human myeloid leukemia K562 cell line by repressing the transcription of genes involved in erythroid lineage differentiation rather than bypassing the G1 arrest (Leon et al., 2014).

The importance of Myc on inhibition of differentiation was revealed particularly after the discovery of the role of Myc in inducing the pluripotency and maintaining the stemness property of "induced pluripotent stem cells" (Takahashi and Yamanaka, 2006). In addition, the anti-differentiation role of Myc seems to be a critical mechanism in Myc-driven tumorigenesis, as Myc inactivation in transgenic mice led to tumor regression and re-differentiation of tumor cells (Arvanitis and Felsher, 2005).

1.2.2.4 Apoptosis

Myc also has been shown to participate in the apoptotic response under diverse cellular challenge, most probably to limit uncontrolled cellular growth under these conditions (Hoffman and Liebermann, 2008). Ectopic expression of Myc was shown to induce apoptosis while Myc-null cells appeared to be resistant to diverse apoptotic stimuli (Evan et al., 1992, Shi et al., 1992, de Alborán et al., 2004). There are several mechanisms found by which Myc potentiates apoptosis in the cells, the well known characterized one is through the activation of p53. The level of p53 protein is kept in a low level by the activity of the p53 negative regulator MDM2 in unperturbed cells. Myc activation leads to increased ARF expression which counteracts MDM2 function, resulting in increased p53

protein. In addition, Myc overexpression has been linked to ATM activation, a kinase that is critical for p53 phosphorylation and activation (Oster et al., 2002).

It is noteworthy that p53 can cause either growth arrest or apoptosis, however deregulated expression of Myc was shown to abrogate p53-mediated growth arrest without affecting p53-mediated apoptosis. For example, Myc overexpression down-regulates several growth arrest genes like p21, gadd45a and gas1 that are transcriptionally activated by p53, favoring the p53-mediated apoptosis (Hoffman and Liebermann, 2008).

Myc-mediated apoptotic response can also occur independently of p53. For example, studies in p53 wild type and p53 null mouse embryonic fibroblast (MEF) cells were shown that in response to Myc the pro-apoptotic BH3-only protein Bim is induced independently of p53 status (Hemann et al., 2005). Taken together, it seems that the mechanism of Myc-induced apoptosis is dependent on the cell type and the apoptotic stimuli.

Myc can also disrupt the balance of pro- and anti- apoptotic factors and in this way sensitizes cells to undergo apoptosis. In precancerous B cells derived from EuMyc mice, it was shown that Myc suppresses the anti-apoptotic proteins such as BCL2 and BCL-X_L and activates the pro-apoptotic molecules like BIM and BAX (Meyer and Penn, 2008). In addition Myc has been shown to have an important impact on apoptotic signaling pathways through the release of mitochondrial cytochrome c to the cytoplasm, triggering caspase activation and eventually apoptosis (Oster et al., 2002).

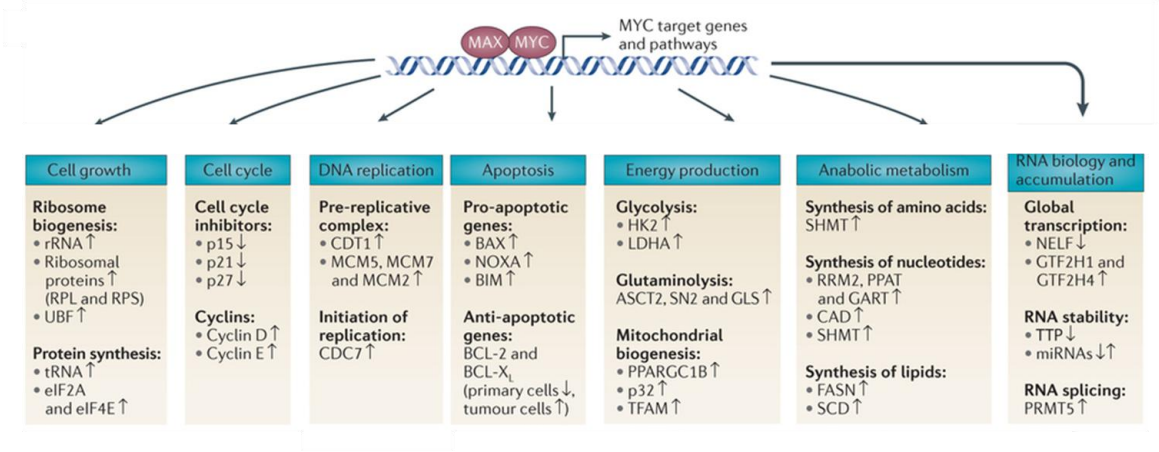

Figure 1.3. The main cellular processes regulated by Myc with some examples of Myc-target genes (up- or downregulated, as indicated by arrows)
Adapted from "MYC: connecting selective transcriptional control to global RNA production" by T. R. Kress, A. Sabo and B. Amati, 2015, *Nature Reviews Cancer*, 15, p. 594.

1.2.2.5 Cellular transformation

Being a product of an immediate early response gene, Myc expression is rapidly elevated following mitogenic stimulation in quiescent cells while in dividing cells its expression is maintained at a constant intermediate level throughout the cell cycle. Myc mRNA and protein have a very short half-lives, suggesting that Myc expression is tightly regulated in non-transformed cells in order to respond quickly to proliferative status of the cells (Meyer and Penn, 2008). The physiological control that regulates Myc expression and activity are disrupted in many human cancers. Besides, Myc deregulation also occurs as a consequence of gross genetic abnormalities that affect the *Myc* locus (such as viral-mediated insertional mutagenesis, chromosomal translocation and gene amplification) or other mechanisms that lead to aberrant Myc overexpression (transcriptional activation) of Myc gene (Meyer and Penn, 2008, Vita and Henriksson, 2006). However, the deregulated expression of Myc alone cannot transform normal cells, implying that additional mutations are required for Myc-induced transformation and tumor formation. For

example, Myc cooperates with Ras to promote cellular transformation and tumorigenesis. Indeed, Ras stabilizes Myc protein by phosphorylating the serine 62 residue through MAPK/ERK kinases and by inhibiting glycogen synthase kinase-3 (GSK3) through phosphatidylinisitol 3-kinase (PI3K) signaling. GSK3 can phosphorylate Myc at threonine 58 and thus provoke ubiquitin-mediated Myc degradation. Ras can also indirectly assists Myc-induced transformation. For example, several Myc target genes -that are involved in cellular proliferation- are bound and repressed by FOXO family of transcription factors. Activation of Ras-downstream kinase AKT leads to FOXO phosphorylation and its nuclear export, thus activation of the transcription of the Myc target genes (Adhikary and Eilers, 2005). Besides cellular proliferation, one of the predominant Myc-induced pathways that has a critical role in preventing unrestricted cell proliferation, is Myc-induced apoptosis. Supporting this notion, many oncogenes that collaborate with Myc to induce tumorigenesis including Bcl-2, Ras, Raf, and v-abl have an anti-apoptotic functions (Oster et al., 2002). A key arm of Myc-induced apoptosis relies on the activation of p53 through induction of $p19^{ARF}$ (an inhibitor of the MDM2 E3 ligase). Spontaneous inactivation of the $p19^{ARF}$-p53 pathway is also a frequent event in tumors arising in Eμ-c-myc transgenic mice (Henriksson et al., 2001). Interestingly enough, negative regulators of the $p19^{ARF}$ pathway such as Bmi-1, TBX2 and TWIST were shown to cooperate with Myc in driving tumor formation by inhibiting the p53-mediated apoptosis (Meyer and Penn, 2008, van Lohuizen et al., 1991).

1.2.3 Myc-induced DDR

Myc overexpression is associated with the activation of a DNA damage response in a number of cellular systems. For example, transient Myc overexpression in U2OS cells caused an increase in ϒH2AX and activation of ATM/ATR-dependent checkpoints. Moreover, splenic B cells derived from a transgenic mouse carrying a deregulated Myc allele (lambda-Myc) exhibited enhanced ϒH2AX foci particularly in geminin positive cells (S/G2 cells) (Dominguez-Sola et al., 2007).

Given the pleiotropic role of Myc in biological processes, it is likely that Myc induces DNA damage and affects genome stability in different ways. For example, Myc activation in normal human fibroblast cells increases ROS levels and induces DSBs and p53 activation as well as reduces clonogenicity. Moreover, treating the cells with an antioxidant led to a remarkable decrease in the DNA damage and improved cell survival after Myc activation (Vafa et al., 2002). As Myc has a prominent role in regulating numerous genes involved in intermediary metabolism and particularly in mitochondrial oxidative metabolism, ROS may accumulate as a by-product of such unscheduled metabolism (Dang, 2013).

There are also a number of studies linking the Myc-induced DNA damage response to S-phase, highlighting the impact of Myc on origin firing and DNA replication. The induced DDR in Myc-overexpressing cells, at least partly, could be due to the transcriptional role of Myc in promoting S-phase entry and progression (Meyer and Penn, 2008). In addition, Gautier and colleagues, by uncoupling the transcriptional role of Myc from its non-transcriptional function, showed that addition of recombinant Myc protein to the transcriptionally-compromised replicating Xenopus extracts led to replication perturbation and DNA damage (Dominguez-Sola et al., 2007). Further investigations by DNA combing experiments revealed that Myc-overexpressing cells possessed higher

percentage of asymmetric and unidirectional replication forks indicating that the DDR seen upon Myc overexpression may be a result of replication fork stalling and collapse. More studies revealed that Myc by acting upstream of Cdc45 -which facilitates DNA unwinding and the loading of DNA polymerase during DNA replication- causes an unscheduled origin firing and eventually leads to replicative stress (Dominguez-Sola et al., 2007, Srinivasan et al., 2013).

How does unscheduled origin firing lead to DNA damage? It is proposed that higher levels of origin firing -for example upon Myc activation- may exhaust the dormant origins that serve as the backups in case of replication fork stalling or precocious replication termination (Rohban and Campaner, 2015). Moreover, under replication stress conditions, replication elongation factors such as deoxyribonucleotides (dNTPs) and the enzymes needed for proper fork progression like DNA topoisomerases and DNA helicases may become limiting, leading to inefficient DNA replication, fork stalling and collapse (Bester et al., 2011). Considering the fact that Myc overexpression leads to its pervasive binding to accessible region of the genome, it is also possible that the increase in DNA replication as well as transcription in Myc-overexpressing cells may lead to genomic instability caused by the interference between the two processes and the formation of structure called R-loop (Zeman and Cimprich, 2014, Gaillard et al., 2015). R-loop is a structure in which a nascent RNA transcript is hybridized with the template DNA strand, leaving the other strand unpaired and vulnerable to nuclease attack (Aguilera and García-Muse, 2012). This DNA-RNA hybrid may form under different physiological and pathological conditions. For example, R-loop forms naturally in highly repetitive and GC-rich immunoglobulin genes contributing to class switch recombination. It could also happen that R-loops arise under unusual conditions, for instance at the sites of paused RNA polymerase or in the case of transcription-replication collision (Santos-

Pereira and Aguilera, 2015). Supporting this notion, it has been shown that early replicating fragile sites are indeed enriched in regions with high transcriptional activity (Barlow et al., 2013). Furthermore, the replication stress induced by Cyclin E, an oncogene that like Myc increases origin firing and alters replication dynamics, not only can be reversed by inhibiting replication initiation, but also blocking transcription rescues replicative stress effects and mitigates the DNA damage response. More direct evidence emphasizing the role of R-loop formation on Cyclin E-induced replicative stress came from an experiment in which overexpression of RNase H1, an enzyme required for resolving RNA-DNA hybrids, decreased the impaired replication fork progression in Cyclin E-overexpressing cells (Jones et al., 2013). Further studies have to be designed to confirm whether R-loop formation contributes to oncogene-induced DNA damage.

Despite the effect of Myc overexpression on replicative stress and DNA damage response, Myc induction confers long-term growth advantage, suggesting that Myc-induced replicative stress is somehow restrained or resolved in favor of an efficient cellular proliferation. Several studies have been conducted to find the critical molecules moderating Myc-induced replicative stress. One known example of such factors is WRN, a DNA helicase responsible for resolving DNA structures that form during S-phase, like those generated at stalled replication forks. WRN has been shown to co-localize with RPA and ATR at replication fork stalling sites and cells lacking functional WRN exhibit genomic instability and hypersensitivity to specific DNA damaging agents (Pichierri et al., 2011). In the context of Myc overexpression, WRN knock-down exacerbates Myc-induced DNA damage response *in vitro* and impaired Myc-driven tumorigenesis and tumor growth *in vivo* (Moser et al., 2012, Robinson et al., 2009). As WRN is a Myc target genes, it seems that Myc, through regulation of the expression of WRN and by relieving

topological stress generated from replication stress, safeguards the cells and ensures proficient cellular proliferation.

Another mechanism by which Myc copes with replication stress is to increase the rate of nucleotide biosynthesis. Genome-wide transcription analysis in human B cell line overexpressing Myc revealed a significant up-regulation of genes related to pyrimidine and purine metabolism besides genes involved in DNA replication and cell cycle (Liu et al., 2008, Zeller et al., 2003). Furthermore, Myc overexpression in cells undergoing replication stress induced by E6/E7 viral oncogenes or Cyclin E could rescue the perturbed replication -slow replication rate and enhanced ϒH2AX foci formation- mimicking the rescue achieved by supplementing the cells with exogenous nucleoside (Bester et al., 2011).

The other well-studied example of such Myc-induced failsafe pathway is the ATR-Chk1 signaling that was shown to alleviate Myc-induced replicative stress *in vitro* and promote malignant transformation *in vivo* (Murga et al., 2011). Chk1 expression is under the control of Myc and increased Chk1 levels have been reported in lymphomas. Inhibiting ATR or Chk1 in mice bearing Eu-myc lymphomas in short term triggered a strong increase of ϒH2AX signal and apoptosis and eventually led to tumor regression, suggesting that accentuating the Myc-induced RS by suppressing ATR/Chk1 limits transformation (Höglund et al., 2011, Murga et al., 2011, Ferrao et al., 2012).

1.3 Cohesin complex

1.3.1 An introduction on the cohesin complex

The cohesin complex was originally discovered as a major constituent of mitotic chromosomes required for holding post-replicative sister chromatid together. In recent years it was shown that, apart from its role in sister chromatid cohesion, cohesins participate in other processes such as DNA double strand break repair, recombination and gene transcription (Losada, 2014). A core of the cohesin complex consists of two members of the structural maintenance of chromosomes (SMC) family: SMC1 and SMC3. In addition, two non-SMC proteins RAD21 (Scc1 in yeast) and stromal antigen (SA, Scc3 in yeast) are associated with SMC1-SMC3 heterodimer to form the complex. It is believed that the cohesion complex embraces chromosomal DNA within a large tripartite ring, formed by its core subunits (Figure 1.4). Each SMC subunit is composed by two globular domains located at N- and C-terminal part of the protein which are separated by an antiparallel coiled coil domain and a flexible hinge domain in the middle portion of the protein. The hinge domain contains highly conserved glycine residues that facilitate the folding of the coiled coil region back onto itself and is also necessary for the formation of V-shaped SMC1/SMC3 heterodimer. The non-SMC protein RAD21, by bridging the two head domains of SMC1 and SMC3, acts as a ring closer, whereas SA does not seem to bind directly to SMC1-SMC3 heterodimer but rather associates with the complex through binding with RAD21 (Jessberger, 2002, Nasmyth and Haering, 2009, Horsfield et al., 2012). This ring shape structure of the cohesin complex is a requisite to almost all the functions ascribed to cohesin (**Error! Reference source not found.**).

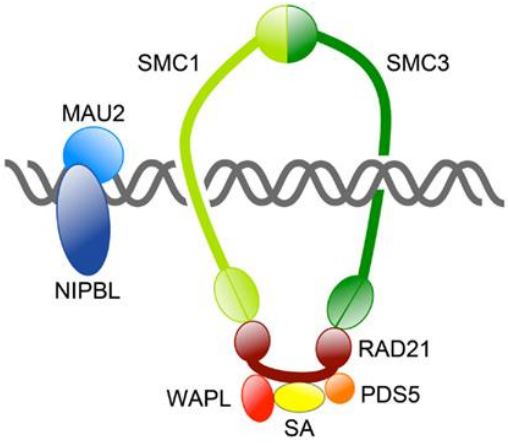

Figure 1.4. Architecture of the cohesin complex
The cohesin complex consists of SMC1, SMC3, RAD21 and SA subunits that bind together to form a tripartite ring with a diameter of about 40 nm. Cohesin's binding to DNA is assisted by the cohesin loader NIPBL, whereas WAPL (wings apart-like protein homologue) and PDS5 promote cohesin unloading. Adapted from "Diverse developmental disorders from the one ring: distinct molecular pathways underlie the cohesinopathies" by J. A. Horsfield, C. G. Print and M. Monnich, 2012, *Frontiers in Genetics*, *3*, p. 3.

1.3.2 The role of the cohesin complex

1.3.2.1 Cohesion and chromosome segregation

As mentioned above, the cohesin complex is essential for sister-chromatid cohesion and subsequently chromosomal segregation during mitosis. Cohesin was shown to load on chromatin in G1/S phase by the aid of the cohesin loader NIPBL, allowing the establishment of sister-chromatid cohesion in S-phase and maintenance of chromatid cohesion during the G2 phase of the cell cycle (Losada, 2014).

Cohesin functions are also regulated by a number of cohesin-binding proteins such as Wapl, Pds5 and sororin as well as modifications such as phosphorylation, acetylation and proteolysis. The ESCO1 and ESCO2 acetyl transferases have been shown to be needed for SMC3 acetylation in mammalian cells. ESCO1/2 were suggested to be recruited to the fork by interaction with PCNA and the replication factor C (RFC)-CTF18 clamp loader (RFC^{CTF18}). In vertebrates, SMC3 acetylation enables the binding of sororin to Pds5,

which counteracts Wapl's ability to remove cohesin from chromatin (Losada, 2014). In this way, SMC3 acetylation was suggested to convert cohesin ring that may obstruct the replication fork to an open ring, thus permitting fork advancement (Terret et al., 2009). In addition, several models have been proposed related to the interplay between replication and cohesin during S phase. One model proposes the involvement of specific replication factors such as translesion DNA polymerase that may facilitate DNA synthesis through sites of cohesin binding. Another model simply relies on the structural property of the cohesin ring whose large diameter (40 nm) may allow the replication machinery to pass through (Jessberger, 2003, Nasmyth and Haering, 2009).

In vertebrate cells, during prophase, the vast majority of the cohesin complex is dissociated from chromosomes by Wapl. This process is mediated by Plk1-dependent phosphorylation of SA2. The residual cohesins remain mainly associated with the centromeric regions which is protected from Wapl and Plk1 by shugoshin-protein phosphatase 2A complex. During the metaphase-anaphase transition, cysteine protease Separase is activated and by cleaving RAD21 leads to dissolution of the remainder cohesin complex allowing chromosome separation (Jessberger, 2002, Losada, 2014).

1.3.2.2 DNA damage response, repair and recombination

As cohesins act through a ring-shaped structure, it is conceivable to assume that they may also have a role in DNA recombination and repair, possibly by aligning and juxtaposing the two anti-parallel DNA strands. Indeed, SMC1 and SMC3 -the core components of the cohesin complex- were identified as two previously unknown subunits of the recombination protein complex RC-1. This complex by possessing subunits such as DNA polymerase epsilon, DNA ligase III and an endonuclease was shown to catalyze cell-free DNA strand transfer and DNA gap repair (Jessberger et al., 1993, Jessberger et al., 1996).

Cohesin appeared to also have a role in recombination during meiosis. In S. cerevisiae SMC3 and the meiotic homologue of RAD21, REC8, were shown to be closely associated with the synaptonemal complex (SC) until late prophase when REC8 dissociates from the chromosomal arms (Klein et al., 1999). The same observation was also made in mammalian cell, where SMC1 and SMC3 exhibited to co-localized with SC proteins SCP2 and SCP3 (Eijpe et al., 2000, Eijpe et al., 2003). In C. elegans, Rec8 depletion resulted in deficient chromosome synapsis in pachytene and pre-mature chromosome segregation in diakinesis suggesting that Rec8 has a role in meiotic homologous recombination (Pasierbek et al., 2001).

The cohesin subunits have also been shown to be involved in DNA damage response (Wu and Yu, 2012). Rad21 was originally identified in *S. pombe* as one of the Rad genes whose mutation in yeast led to cell sensitivity to DSBs (Birkenbihl and Subramani, 1992). The recruitment of the cohesin subunits to DSBs in human cells was shown by immunofluorescence, where SMC1 was shown to localize to laserbeam-induced DNA damage sites in a Mre11/Rad50-dependent manner (but not ATM or Nbs1) (Kim et al., 2002a). This was further supported by immunoprecipitation studies, demonstrating the cohesin enrichment around the DSBs generated by I-SceI cleavage (Potts et al., 2006, Ünal et al., 2004).

Moreover, in 2002 Kim et al. identified two serine residues in SMC1 (Ser 957 and Ser 966) that become phosphorylated by ATM upon ionizing radiation. Exposure of cells to ultraviolet radiation or the DNA replication inhibitor hydroxyurea (HU) also yielded SMC1 phosphorylation even in ATM deficient cells, probably through ATR kinase activity (Kim et al., 2002b). In another study, Kitagawa et al. observed that the level of the SMC1 phosphorylation, likewise NBS1 and H2AX phosphorylation, increased in an IR dose-dependent manner (Kitagawa et al., 2004). This data together with the detection

of phospho-SMC1 at the DNA damage foci by immunofluorescence, indicate that most likely SMC1 is phosphorylated and acts at the site of DNA damage.

SMC1 mutants in the phosphorylation sites (Ser 957 and Ser 966) exhibited impaired S-phase arrest after IR, though cells were arrested in G2 phase, suggesting that the lack of IR-induced S-phase checkpoint results in accumulation of cells in G2 over time (Kim et al., 2002b). Furthermore, by using cells lacking functional Nbs1 (NBS1-LB1 cell) or BRCA1 (HCC1937 cell) Kim and others showed that optimal phosphorylation of SMC1 is dependent on the presence of Nbs1 and BRCA1 at the site of DNA damage (Kim et al., 2002b). Although there are some discrepancies between different studies, these may be due to different DDR pathways activated by DNA damage stimuli and the crosstalks between ATM and ATR. Altogether, these results proposed a new function for SMC1 and showed that it can play a role in DNA damage-induced S phase checkpoint and modulation of radiosensitivity.

While it is not clear whether IR-induced phosphorylated SMC1 functions through canonical cohesin complex or as a single protein, overexpression of dominant-negative mutants for SMC1 phosphorylation did not raise significant increase in chromosomal breaks after IR, separating radiosensitivity phenotype from chromosomal breakage phenotype in these cells (Strom et al., 2004). There are also studies emphasizing on the role of other non-SMC subunits in DNA damage, reinforcing the role of cohesion on DNA damage response. For example, phosphorylation of RAD21 by Chk1 was shown to be critical for RAD21 acetylation and cohesion establishment in DNA damage sites (Heidinger-Pauli et al., 2008, Heidinger-Pauli et al., 2009). In addition cohesion-establishment factor, sororin, was shown to be required for efficient DNA damage repair during G2 in HeLa cells (Schmitz et al., 2007). Despite all these studies shedding light into the role of cohesin in DDR, a lot of unresolved questions left behind. For example,

what are the exact functions of the SMC proteins in DNA damage response and DNA repair? Do they simply provide a structural support to promote DNA repair, or do they preferentially bind to and thus mark the sites of DNA damage to recruit other DDR-proteins? As SMC proteins are the prominent protein whose function was evaluated in these studies, it is still not clear whether the role of SMC in DNA damage can be attributed to other subunits of the cohesin complex, whether these functions are carried out by SMC proteins alone or whether they act in a different unknown protein complex should be further studied.

1.3.2.3 Regulation of gene transcription

The cohesin complex has also a role in transcriptional regulation, in part due to its interaction with CCCTC-binding factor (CTCF). CTCF is the main insulator protein in vertebrates and is capable of activating or repressing gene expression by facilitating interactions between transcription regulatory sequences (Ong and Corces, 2014). Although not always bound to CTCF on chromatin, cohesins have been shown to stabilize CTCF-mediated chromosomal interactions and thus facilitating CTCF function. Down-regulation of cohesins resulted in the disruption of CTCF-mediated intrachromosomal interactions and affected gene expression. For example, in mouse embryonic stem (ES) cells the TATA-binding protein-associated factor 3 (TAF3), a component of the promoter recognition complex TFIID, not only is bound to promoters but also is found at CTCF- and cohesin-bound distal sites. By promoting the formation of a loop between two sequences, it is proposed that CTCF and cohesin tether distal regulatory elements, such as endodermal enhancers in this case, to their target promoters (Ong and Corces, 2014, Wendt et al., 2008).

Cohesins and the cohesin loader NIPBL were also found in association with mediator complex and RNA polymerase II (but not CTCF) at the enhancers and the core promoter

sites of actively transcribed genes in ES cells. Using 3C technology Kagey et al., observed an increased interaction frequency between core promoter and the enhancer of the pluripotency genes in ES cells compared to MEFs where these genes are silent and are not occupied by mediator and cohesin. Therefore, it is suggested that cohesins through their role in DNA loop formation may favor physical association of distal regulatory elements to the core promoter thus contributing to gene regulation (Kagey et al., 2010).

1.3.2.4 DNA replication

The cohesin complex was found to interact with components of the pre-replication complex, such as MCM proteins (Guillou et al., 2010). Furthermore, cohesins down regulation slowed down S-phase progression and this was shown to be independent of sister chromatid cohesion, regulation of gene transcription and checkpoint activation. Monitoring DNA replication by DNA combing showed a reduced fork density (number of forks divided by the total length of DNA fibers normalized by the percentage of cells in S-phase) in Rad21-depleted cells compared to control cells whereas the fork velocity was similar, indicating that the S-phase delay is most likely due to a reduced frequency of origin firing. Moreover, Genome-wide enrichment of cohesins, exhibited a significant enrichment of the cohesin complex at the genomic intervals located at origins rather than regions not harboring replication origins (Guillou et al., 2010, MacAlpine et al., 2010). Considering the architectural role of the cohesin complex, it is proposed that potential replication origins within a DNA region are grouped in a rosette-like structures where the replication factories tethered and make a favorable environment for DNA replication. Disrupting the cohesin-mediated structures caused formation of larger chromosomal loops, shown by increased halo radius signal, and reduced frequency of origin firing (Guillou et al., 2010, Losada, 2014).

Cohesin was shown to have a role in replication of telomeric regions. MEFs lacking cohesin subunit SA1 (which is responsible for telomeric cohesion) showed reduction in the fraction of replicating telomeres and defects in chromosome segregation (Remeseiro et al., 2012).

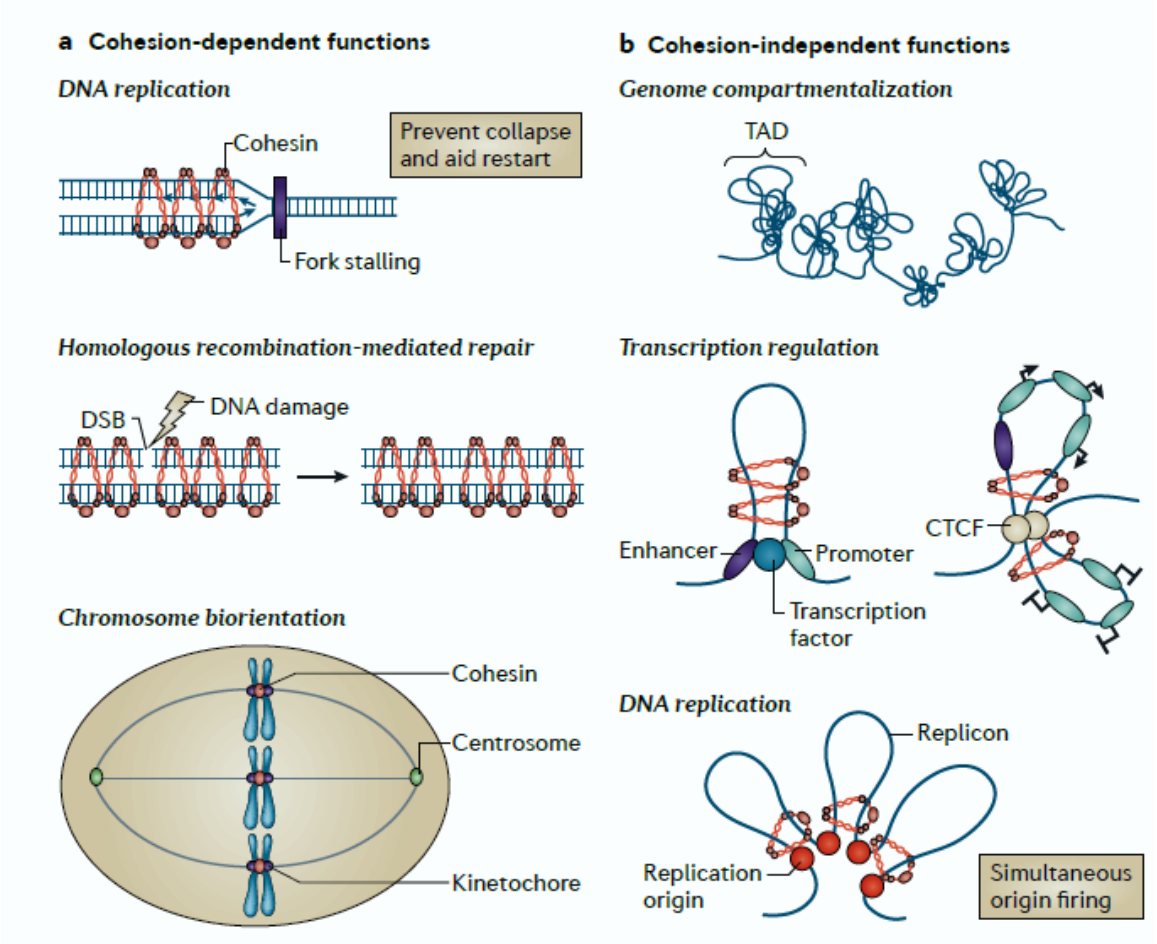

Figure 1.5. Cohesin functions

(A) Cohesion-dependent functions. The cohesin complex by embracing the double strand DNA in the replication sites is important to stabilize the stalled replication forks and to facilitate replication fork restart. In the case of double strand break, the cohesin complex can also hold two sister chromatid together and promotes homologous recombination-mediated repair. In mitosis, cohesin-mediated cohesion ensures faithful chromosome segregation. (B) Cohesion-independent function. The cohesin complex by establishing and maintaining the large chromosomal interaction is important for genome organization as well as promoting transcription and replication. Adapted from "Cohesin in cancer: chromosome segregation and beyond" by A. Losada, 2014, *Nature Reviews Cancer, 14*, p. 392.

1.3.3 Cohesins in human diseases

Human diseases caused by mutations in genes associated with the cohesin complex are termed cohesinopathies. One of such diseases is the Roberts/SC phocomelia syndrome that is caused by mutations in the acetyltransferase ESCO2 that is needed for cohesion establishment. Heterozygous mutations in SMC1, SMC3 or NIPBL are the cause of another cohesinopathy called Cornelia de Lange syndrome (CdLS). Cohesionopathies are characterized by a variety of developmental abnormalities such as growth failure, mental retardation, limb defects and craniofacial anomalies. In addition, cells derived from patients with cohesinopathies are hypersensitive to variety of DNA-damaging agents like mitomycin C and camptothecin, presumably related to the role of cohesin in homologous recombination repair. However, these cells do not exhibit massive defect in sister chromatid segregation, instead the developmental defects in the patients suggest that cohesin is crucial for developmental gene expression programs during embryogenesis (Bose and Gerton, 2010). Indeed gene expression profiling in several mutant cell lines derived from CdLS patients identified around 400 deregulated genes involved in embryonic and tissue development, hematological and immune system development. Furthermore, not only cohesins have been shown to preferentially bind to promoter regions of active genes, but also there was a correlation with reduced cohesin binding in the vicinity of misregulated genes in mutant cells, suggesting that cohesin may play a role as a transcription factor (Liu et al., 2009). The findings of transcription factor dense cluster forming almost invariably around cohesins also provided evidence for the role of cohesin in mediating gene expression presumably by formation of loops between enhancers and promoters or stabilization of transcription factor binding.

Cohesins mutations are also found in a variety of human cancer samples. For example, mutations in STAG2 were found in urothelial bladder cancer, glioblastoma, Ewing's

sarcoma and melanoma. Also mutations in genes encoding the cohesin subunits and NIPBL were identified in colorectal cancer, AML and other myeloid neoplasms. Overall, mutations in STAG2 are often truncating and usually affect one allele. Considering that STAG2 gene in located on the X chromosome, the high rate of mutation in this gene may not have a huge impact on chromosome segregation, as SA1 can partially compensate this loss. In contrast to STAG2, mutations in other cohesin genes including SMC1 and NIPBL are mostly missense. The consequence of these missense mutations in protein function still is not clear (Losada, 2014).

It is mainly believed that cohesins dysfunction may accelerate tumorigenesis by increasing genome instability. Although chromosome missegregation and the subsequent aneuploidy could be deleterious for cell survival, it may also be beneficial for tumor development. However, a study in yeast revealed that sister-chromatid cohesion and chromosome segregation are not affected even when cohesin levels are reduced to 13% of wild-type levels. Studies on cells derived from heterozygous NIPBL mice, which recapitulates several phenotypes of CdLS, also showed normal mitosis, instead transcription was disrupted at several loci (Heidinger-Pauli et al., 2010). These results suggest that transcriptional regulation could be more sensitive to the reduction in the levels of functional cohesin present in the cell, proposing that mutations in cohesin may promote tumorigenesis mainly by affecting the transcription of oncogenes and tumor suppressor genes.

Aim of the study

In the context of Myc-induced DNA damage response, we propose that Myc, when overexpressed, may co-opt several intracellular pathways that may function to protect cells from excessive replicative stress and DNA damage, thus allowing efficient cellular proliferation. The identification of such pathways will not only improve our mechanistic understanding of Myc-induced cellular transformation, but may also have relevant clinical implications to selectively target Myc-overexpressing cancer cells.

The aim of the current study was to identify the modulators of Myc-induced DDR by means of RNAi screen followed by further characterization of the mechanism of action of some hits.

2 Materials and methods

2.1 siRNA screen

2.1.1 MEF immortalization

R26-MycER primary mouse embryonic fibroblast (MEF) cells were spontaneously immortalized using 3T3 protocol. Briefly primary MEF cells growing in a 10-cm dish were washed with PBS (Lonza®) and trypsinized with 1 ml of 0.05% trypsin-EDTA (Lonza®). After cell detachment, trypsin was diluted into 5 ml of growth media and the cells were counted by Neubauer chamber. 3×10^5 cells were seeded in a 6-cm dish (Nunc™) and were grown in normal oxygen (20% O_2) incubator. Subsequent passages were done every 3 days in a manner described above. Growth curve was determined from cell count at each passage. The immortalized cells were further subcloned by limiting dilution following colony picking and expansion.

2.1.2 Optimization of siRNA reverse transfection conditions

The efficiency of siRNA delivery into Bz1 R26-MycER MEF cell line was tested by comparing the performance of Lipofectamine RNAiMAX (Lifetech) and DharmaFECT1 (Dharmacon, Thermo Fisher Scientific) transfection reagents in 96-well plate format. In brief, three different concentration of the transfection reagents (0.1, 0.2 and 0.3 µl per well) were used to reverse transfect three different cell densities (2000, 3000 and 5000 cells per well). A toxic siRNA (siTOX, Dharmacon, Thermo Fisher Scientific) was used to assess the transfection efficiency based on cell death induction. For reverse transfection, the transfection reagent was diluted in an appropriate volume of Opti-MEM (Gibco, 20 µl per well) and then transferred to the wells of a 96-well plate. After 5 minutes incubation time, 30 µl of diluted siRNA in Opti-MEM was added to the transfection reagent in the wells and mixed. The lipid-siRNA complex was allowed to form during 20 minutes incubation at room temperature. Afterwards, 50 µl of cell

suspension (in 2X medium) was added to the complex to reach the final volume of 100 µl. All the siRNAs were used at 25 nM final concentration during transfection. Forty-eight hours post transfection, cell viability was measured by MTT (3-[4, 5-dimethylthiazol-2-yl]-2, 5 diphenyl tetrazolium bromide) assay (Sigma).

Once the best performing transfection reagent defined, the assay was scaled down into 384-well plate format. To this purpose, first the optimal cell density in 384-well format was determined by seeding different cell numbers (400, 625, 800, 1250, 1600 and 2500 cells/well) in a 384-well plate and measuring the cell growth at different time points using the CellTiter-Glo assay (Promega). The selected cell density was then used for testing different volumes of DharmaFECT1 reagent per 384-well (0.2, 0.15, 0.12 and 0.1 µl). The toxic siRNA (siTOX) and a pool of non-targeting siRNAs (siGENOME Non-Targeting siRNA Pool #2, Dharmacon, Thermo Fisher Scientific) were used as the positive and negative controls respectively.

2.1.3 Automated high-throughput siRNA transfection

The mouse siGenome SMARTpool library was obtained from Dharmacon (Thermo Fisher Scientific) in 384-well format. Each well in the library contains a pool of four distinct siRNA oligos targeting different sequences of the target transcript. Five library plates were analyzed targeting a total of 1400 druggable genes plus positive controls for monitoring transfection efficiency (SMARTpool siGENOME Plk1 siRNA), assay specific positive control (SMARTpool siGENOME Rad21 siRNA) and a siRNA targeting the Renilla Luciferase gene (siGENOME Rluc siRNA) as negative control for data normalization.

The esiRNA custom libraries were purchased from Sigma (MISSION® esiRNA, Sigma) in 384-well format. esiRNAs are endoribonuclease-prepared siRNA pools comprised of a

mixture of siRNAs that all target a same gene. Control esiRNAs targeting mouse Plk1, Kif11, Rad21 and Rluc were purchased in individual tubes and included in the final 384-well plates.

Silencer pre-designed siRNA library was obtained from Ambion (Silencer®, Ambion) in 384-well plate. Three different individual silencer siRNAs were chosen for each gene. Silencer siRNAs against mouse Kif11, Rad21 (#150458) and negative control #2 were also used as controls.

For screening, 800 Bz1 R26-MycER immortalized MEF cells/well were reverse-transfected in 384-well black, gelatin-coated optical plates (Corning) using the Freedom EVO automated liquid handler system (Tecan) with 0.13 µL/well of DharmaFECT1 transfection reagent (Dharmacon, Thermo Fisher Scientific) and 25 nM Dharmacon SMARTpool or Ambion silencer siRNA or 50 nM of Sigma esiRNA. After transfection, cells were cultured for 48 hours under standard conditions (37°C in humidified atmosphere, with 5% CO2), in the SteriStore automated incubator (HighRes Biosolutions). A total of 6 replicates plates (3 ethanol- and 3 OHT-treated) were transfected for each of the library plates.

2.1.4 Fixing and immunofluorescence staining

Forty-eight hours post siRNA transfection, cells were fixed by adding 40 µl of 4% Paraformaldehyde (PFA) directly to the medium to reach a final concentration of 2%. The plates were then incubated at room temperature for 15 minutes. After that, the medium was aspirated and the plates were washed twice with PBS. Then cells were permeabilized by adding 20 µl of 0.1% Triton X-100 (in PBS) to each well. After 10 minutes, cells were washed with PBS and blocked with 20 µl of blocking buffer (PBS + 2% BSA + 10% goat serum) for 30 minutes. Cells were then rinsed twice with PBS and incubated with 25 µl of

anti-phospho-Histone H2AX (Ser139) antibody (Merck Millipore, Cat#05-636) dilution (1:1500 in 2% BSA) for 1 hour at room temperature. Afterwards, cells were washed two times with PBS and then incubated with 25 µl of secondary antibody dilution (1:400 Alexa Fluor® 488 goat anti-mouse antibody in 2% BSA, Invitrogen Cat#A11001). and DAPI (1:4500 in PBS) for 1 hour. Following 3 washes with PBS, 70 µl of PBS was left in the plates and the plates were sealed and stored at 4°C until imaged.

2.1.5 Image acquisition and processing

Cells were imaged on the Olympus ScanR wide-field microscope which allows fully automated image acquisition. ϒH2AX-Alexa 488 fluorescence was acquired using BP470-495 excitation filter and BP510-550 emission filter (U-MNIBA3; Olympus) meanwhile DAPI was acquired by BP360-370 excitation filter and BP420-460 emission filter (U-MNIBA3; Olympus). Image acquisition was done with 10X objective, and six different fields of view were recorded for each well, thus covering most of the entire area of a 384-well format.

The acquired images were analyzed using a custom image analysis algorithm (by Dr. Adrian Andronache in IIT Screening unit, available upon request), developed and executed in the Acapella software development/run-time environment (Perkin Elmer). The algorithm used some Perkin Elmer proprietary procedures, such as the nuclei detection on the DAPI channel. The image analysis procedure was run on every single field of view acquired on two channels, and eventually merged the results for each individual well by summing or averaging single parameters, according to their definition (see the following paragraphs, provided by Dr. Adrian Andronache).

Step 1: Background removal and uneven illumination correction

The image analysis algorithm starts with the background removal and uneven illumination correction for all the images on both input channels. This step is performed using a sliding parabola transform which divides the input image into two parts: background and foreground (signal). The curvature of the parabola was set up to 1/500 pixels, so that it does not affect the real signal from the images.

Step 2: Nuclei segmentation and local background definition

First, using Perkin Elmer (PE) proprietary algorithms, we identified all the individual nuclei from the DAPI channel. Then we defined the local background of every nucleus using the Voronoi tessellation. Voronoi tessellation divides the image space by defining region boundaries equally distanced from the neighboring given centers (i.e. nuclei). In order to not extend too much from the nuclei, a maximum border distance of 50 pixels away from the nuclei was imposed. Once the nuclei were segmented and their Voronoi regions were estimated, we defined individual foreground and background masks for every nucleus, these masks were further used to extract phenotype descriptors for every cell.

Step 3: Preliminary features extraction

For all the detected objects (nuclei having both a foreground and an associated local background), a series of basic parameters were directly extracted or derived from the different images to describe the morphology and phenotype of individual cells. First, from the nuclei segmentation we estimated the radius, the area, and the shape of every single nucleus. Second, the nuclear DAPI intensity was defined as the difference between the average intensities of each individual foreground and background nuclei. The DNA content was defined as the product of the DAPI intensity and the nuclear area. Third, from the Alexa 488 channel we estimated all the ϒH2AX related features as described in the following paragraph.

Step 4: ϒH2AX foci and pan-nuclei definition

The ϒH2AX foci were defined using a local adaptive thresholding approach. Using the previously defined nuclear masks, we calculated the average Alexa 488 intensities of every nucleus in the population of negative controls (siRluc). This resulted in the threshold that differentiates background from ϒH2AX signal. Further on, this threshold was used to segment the ϒH2AX foci from the Alexa 488 channel on every single nucleus (within the foreground masks) on all the screened wells. A local adaptation of the threshold was performed for every single nucleus, by correcting for the Alexa 488 background level extracted from the individual local background mask. All nuclei with ϒH2AX foci covering more than 70% of their surface were declared (labeled) as "pan-nuclear ϒH2AX".

Step 6: Phenotype descriptive parameters

For every single well, the information extracted from all the 6 field of view was finally integrated and the following main phenotype description parameters reported:

N°_Of_Nuclei: the total number of nuclei from all the 6 fields of view, remained after the different filtering described previously;

N°_Of_PanPosNuclei: the total number of pan-nuclear ϒH2AX nuclei from all 6 fields of view;

Percent_Of_PanPos: the percent of pan-nuclear ϒH2AX nuclei with respect to the total number of nuclei from all 6 fields of view;

Dapi_Intensity: the average DAPI intensity of all detected nuclei;

DNAContent: the average DNA content of all detected nuclei;

NuclearArea: the average nuclear area of all detected nuclei;

ϒH2AX_Intensity: the average Alexa488 intensity of all detected nuclei;

ϒH2AX_AreaCoverage: the average ϒH2AX foci area coverage of all detected nuclei.

Each well of an assay plate was associated a phenotype descriptive vector (an array of the 8 previously main parameters) and eventually tabulated and associated the biological and technical annotation according to the plate-layout design and siRNA-database definition.

2.1.6 Statistical data processing and analysis

The statistical data processing and analysis was performed independently on two of the main phenotype descriptor parameters extracted by the image analysis: the viability (i.e. the N°_Of_Nuclei) and the DNA damage response (DDR) (the percentage of pan-nuclear ϒH2AX nuclei: Percent_Of_PanPos). The data of each screened siRNA was available in triplicates sample values for each of the two chemical treatments ethanol (EtOH) and OHT. Each assay plate had a series of control wells (with negative and positive controls for transfection and assay-specific positive control) and multiple experimental samples. From here on, the data of a single well will denote the specific parameter value of any well, independent from nature of the transfection reagent class (negative or positive controls or experimental samples).

The statistical data processing and analysis is organized in the following 5 main steps:

intra plate normalization of raw data (on each individual assay plate);

intra-treatment data dimensionality reduction;

inter-treatment data dimensionality reduction;

hit metric estimation;

hit calling.

The intra-plate normalization of raw data ensures the removal of inter-plate variability. This operation is done on every assay plate with respect to the median data of all the

negative controls present on the analyzed plate (siRluc). The normalization procedure was performed only on the viability parameter, as the percent of pan-nuclear ϒH2AX nuclei is internally normalized to the number of nuclei of a given well. All the samples presenting a very low viability (i.e. less than 100 nuclei within a well) were discarded from following statistical data processing and analysis of both viability and percent of pan-nuclear ϒH2AX parameters.

The intra-treatment data dimensionality reduction merges the replicates (triplicates) values of the wells on the assay plates. This operation estimates the median of the transfection samples replicates in order to assign one single data value for each well (siRNA) within each experimental condition (EtOH and OHT treatments).

The inter-treatment data dimensionality reduction is the operation of combining and confronting the parameter values of single wells in between the different experimental conditions. As such, the viability-ratio was estimated for all the wells by dividing normalized viability in OHT-treated to EtOH-treated samples. At the same time, the DDR-gain was estimated as the difference between the percent of pan-nuclear ϒH2AX nuclei in OHT-treated and the EtOH-treated samples.

Both viability-ratio and DDR-gain previously estimated underwent the classical Z-score hit metric estimation. Using a plate-wise approach, the primary screen data was using as reference the entire population of experimental samples, using the assumption that most of the siRNAs have a null effect. Similarly, using the plate-wise approach, the hit metrics applied on the data of the deconvolution/validation screens used as reference the population of negative samples present on the analyzed plate.

The final step of the statistical data processing and analysis is the hit calling. The Z-score $\leq$ -2 and Z-score $\geq$ 1.25 was set to identify the set of genes whose knockdown decreased the viability ratio of OHT versus EtOH-treated cells (called synthetic lethality hits) and

the set of genes whose knockdown increased the viability ratio of Myc-activated cells compare to non Myc-activated control cells (called synthetic viability hits) respectively. For DNA damage response (DDR) hit identification, four different methods, all established from median absolute deviation (MAD)-based Z-score, were evaluated in a pilot test composing 280 genes. The evaluated methods were: (1) difference in ϒH2AX enhancement in OHT samples compared to EtOH-treated samples, (2) robust regression, (3) ratio of ϒH2AX in EtOH versus OHT-treated samples and (4) principal component analysis (PCA). Eventually we chose "difference in the percentage of ϒH2AX enhancement" as a standard method for the analysis of all libraries. Hits were called DDR-up if the Z-score of DDR-gain (OHT-EtOH) in triplicates, was ≥ 2.

2.1.7 Enrichment analysis

Functional classification was performed using PANTHER (http://pantherdb.org), DAVID (https://david.ncifcrf.gov) and Ingenuity Pathway Analysis (IPA, http://www.ingenuity.com) tools.

2.2 Cell culture

2.2.1 Cell infection

10 µg of the retroviral plasmids together with packaging plasmids were used to transfect Phoenix Ecotropic or Amphotropic packaging cells (10-cm dish) using Calcium Phosphate. 24 hours post transfection the medium was replaced with new medium. The virus supernatant was collected 48 and 72 hours post transfection and filtered through a 0.45 µm filter. Next, the medium of the target cell was replaced with the virus supernatant, polybrene was immediately added to the medium (8 µg/ml) and the cells were put in the 37°C incubator for at least 3 hours. Afterwards the medium was replaced

by fresh medium. Depending on the cell density and growth, 24-48 hours after incubation, cells were trypsinized and split into antibiotic-containing medium.

2.2.2 Cell lines and culture conditions

Immortalized R26-MycER MEF cell lines (Bz1 and Bz5), U2OS and U2OS-MycER cells were cultured in DMEM (Lonza®) containing 10% FBS supplemented with 1% penicillin, 1% streptomycin and 2 mM Glutamine in 5% CO_2 incubator. Primary MEFs were cultured in DMEM containing 10% FBS supplemented with 1% penicillin, 1% streptomycin, 2 mM Glutamine, 1% non essential amino acids and 25 µM ß-mercaptoethanol under hypoxia condition (3% O_2).

2.2.3 siRNA transfection

For transfection, cells were grown in media without antibiotics. Bz1 R26-MycER MEF cell line and U2OS cells were reverse-transfected with DharmaFECT1 (Dharmacon, Thermo Fisher Scientific) and Lipofectamine RNAiMAX (Lifetech) transfection reagent respectively, according to the manufacture's instruction. All siRNAs were used at 25 nM final concentration during transfection. OHT was added in the time of transfection at 400 nM final concentration.

2.3 Cell survival assay

MTT assay was done by adding 20 µl of sterile MTT solution (5 mg/ml MTT, Sigma, in PBS) to 100 µl of medium in each well of 96-well plate. The plate was incubated for 4 hours at 37°C cell culture incubator. After this time the medium was removed and 150 µl of DMSO was added to each well. The plate was then agitated on an orbital shaker for 15 minutes and then was diluted (if necessary) and read at 590 nm with luminometer. An extra well containing no cells with medium was used as a blank for normalization.

CellTiter-Glo® (Promega) assay was performed according to the manufacturer's protocol. Briefly a vial of CellTiter-Glo® buffer was thawed and was equilibrated to room temperature. Then the appropriate volume (10 ml) of the buffer was transferred to the bottle containing CellTiter-Glo® substrate. After mixing, an appropriate volume of the CellTiter-Glo® reagent (the volume equal to the volume of the medium) was added directly to the room temperature equilibrated opaque-walled white plate (Costar®) and the contents were mixed for 20 minutes on an orbital shaker. The luminescence was then read by the CellTiter-Glo protocol in Promega GloMax® reader.

2.4 Flow cytometry and cell cycle analysis

Asynchronous growing cells were pulsed labeled with bromodeoxyuridine (brdU) for 30 minutes prior to harvesting. As a negative control, no BrdU control was included. Cells were trypsinized, fixed with ice-cold 70% ethanol and stored at 4°C until further analysis. Cells were then washed in PBS + 2% BSA and treated with 1 ml of 2N HCl for 20 minutes to expose labeled DNA. HCl was then neutralized with addition of 3 ml of sodium borate (0.1 M, pH 8.5) for 2 minutes. After spinning down the cells were washed twice with PBS and the pellet was resuspended in anti-BrdU antibody (1:5, BD Biosciences) and incubated for 1 hour at room temperature. Cells were then quickly washed and incubated for 30 minutes with secondary fluorescence labeled antibody. After washing, cells were resuspended in propidium iodide (2.5 µg/ml) + RNase A (250 µg/ml) and kept at 4°C overnight.

For ϒH2AX/DNA synthesis staining, cells were pulsed with EdU (5-ethynyl-2´-deoxyuridine, 10 nM) for an appropriate time and then were trypsinized and fixed with ice-cold 70% ethanol. Fixed cells were then washed with PBS containing 1% BSA. Then cells were permeabilized with 100 µl of 0.25% Triton-X 100 in PBS for 10 minutes at room temperature. After a washing step with PBS, the cell pellet was resuspended in 500

µl of PBS + 10% Goat serum. Following 30 minutes incubation, the cells were stained with mouse anti phospho-H2AX (1:200 in PBS + 1% BSA) for 2 hours. Then cells were washed once with PBS + 1% BSA and spun down. The cell pellet was resuspended in secondary goat anti-mouse FITC antibody (1:50 in PBS + 1% BSA) and incubated for 1 hour at room temperature. After a washing step, cell pellet was resuspended in 200 µl of Click-iT® (Life technologies) reaction solution (175 µl PBS + 4 µl $CuSO_4$ + 1 µl Alexa 647 azide + 20 µl 1X Click-iT EdU buffer additive). After 30 minutes incubation at room temperature, cells were washed with PBS + 1% BSA and the pellet was resuspended in 500 µl of propidium iodide (2.5 µg/ml) + RNase A (250 µg/ml) and stored at 4°C until FACS analysis. Cell cycle analysis performed on FACSCalibur flow cytometer using Cell Quest Pro software. Flow cytometry data analysis was performed using FlowJo software (vX.0.7).

2.5 Immunostaining and Immunoblotting

For immunostaining, growing cells on coverslips were first washed twice with PBS and then fixed with paraformaldehyde (4%) for 10 minutes at room temperature. For RPA staining pre-extraction was carried out before fixation, by treating the cells first with ice-cold cytoskeleton buffer (10 mM Pipes pH 6.8, 100 mM NaCl, 300 mM sucrose, 3 mM $MgCl_2$, 1 mM EGTA and 0.5% Triton-X 100) for 5 minutes on ice and then with ice-cold cytoskeleton stripping buffer (10 mM Tris-HCl pH 7.4, 10 mM NaCl, 3 mM $MgCl_2$, 1% Tween 40 (v/v) and 0.5% v/v sodium deoxycholate). After 5 minutes incubation on ice, cells were rinsed three times with ice-cold PBS and then fixed with 4% paraformaldehyde for 10 minutes at room temperature.

Fixed cells were then permeabilized with 0.2% Triton-X 100 in PBS for 10 minutes at room temperature. After a brief wash with PBS, the cells were incubated with blocking solution (2% BSA in PBS) for 30 minutes. Primary antibodies were diluted in PBS

containing 1% BSA. Incubations with the primary antibodies were performed at room temperature for 1 hour. Cells were then washed and incubated with secondary fluorescently labeled antibodies for 45 minutes. DAPI staining (1:5000) was applied for 5 minutes at room temperature to stain DNA. After a washing step with PBS, coverslips were dried and mounted on Mowiol-based mounting media.

For BrdU immunofluorescence, after permeabilization, cells were first treated with DNaseI (Neb) at 37°C for 30 minutes and then were incubated with anti-BrdU antibody.

For western blotting, cells were washed twice with ice-cold PBS and then lysed in an appropriate volume of lysis buffer containing 20 mM Hepes pH 7.5, 0.5 M NaCl, 5 mM EDTA, 10 % Glycerol and 1% Triton-X 100, supplemented with protease and phosphatase inhibitors. After sonication, lysates were centrifuged and the supernatant was recovered. The protein concentration was determined according to Bradford (Bio-Rad Laboratories). Cell extract was separated on 4-15% gradient precast TGX^{TM} polyacrylamide gel (Bio-Rad Laboratories) and was blotted onto nitrocellulose membrane using Trans-Blot® Turbo^{TM} transfer system (25 V, 1 A, 30 minutes). Following 1 hour blocking in TBST containing 5% BSA, blot was incubated with primary antibody for overnight at 4°C. Secondary peroxidase-coupled antibodies were incubated with the blot at room temperature for 1 hour. ECL-based chemiluminescence (Bio-Rad Laboratories) was detected on BioRad ChemiDoc system and the image was processed using Image Lab 4.0 (Bio-Rad Laboratories). The used antibodies were: H2AX-pS139 (Biolegend, #613402), Rad21 (Santa Cruz, sc-54325), RPA32 (Merk Millipore, NA19L), Chk1 (Santa Cruz, sc-8408), Chk1-pS345 (Cell Signaling, #2348), p53-pS15 (Cell Signaling, #9286), Vinculin (Sigma, V9131), H3 (Abcam, Ab1791).

2.6 DNA combing

Asynchronously growing cells were sequentially labeled with 25 µM IdU for 30 min followed by a brief wash with PBS and then 30 min incubation with 200 µM CldU in the cell culture medium. After labeling, cells were trypsinized, harvested and then embedded in agarose plugs until further analysis. The plugs were treated with proteinase K, then DNA was extracted and combed on silanized coverslips. DNA fibers were incubated first with a mouse anti-ssDNA antibody (Chemicon) followed by Alexa 546 coupled-secondary antibody (Molecular Probes) staining. Incorporation of halogenated nucleotides was detected with specific antibodies (IdU: mouse anti-IdU/BrdU, Becton Dickinson; CldU: rat anti-CldU/BrdU, Abcam) and visualized with appropriate secondary antibodies. Images were acquired automatically with a spinning disk confocal microscope, and the individually labeled DNA molecules were manually measured with ImageJ.

2.7 RNA extraction and analysis

RNA was extracted using RNeasy total RNA extraction kit (Qiagen). Briefly cells were lysed by adding RLT buffer and the lysate was passed through a 20 gauge needle for several times. Then one volume of 70% ethanol was added to the collected lysate in a 1.5 ml microtube and mixed well. The mixture was then transferred to an RNeasy spin column and centrifuged at ≥ 8000 xg for 15 minutes. The flow through was discarded and the column was washed with 350 µl of RW1 buffer. After a centrifuge step and discarding the flow through, DNase treatment was performed by adding 80 µl of DNaseI solution (10 µl of DNaseI stock + 70 µl of RDD buffer) to the column. After 15 minutes incubation, the column was washed first with 350 µl of RW1 buffer and then twice with 500 µl of RPE buffer. Finally the flow through was discarded and the empty column was

centrifuged at full speed for 1 minute. RNA was eluted by adding 30-50 µl of RNase-free water into the column and centrifuge for 1 minute at 8000 xg. The extracted RNA was quantified using Nanodrop (ThermoFisher).

Extracted and purified RNA was then used for cDNA synthesis with Superscript reverse transcriptase synthesis kit (invitrogen). 1 µg of RNA was combined with 1 µl of OligodT and 0.1 µl of Random primers, the final volume was reached to 30.5 µl by RNase-free water and then incubated at 70°C for 5 minutes. The samples were then quickly chilled at 4°C for 5 minutes. Then, 19.5 µl of RT reaction (5 µl 25mM $MgCl_2$ + 10 µl 5X reaction buffer + 2.5 µl 10 mM dNTP mix + 1 µl RNase inhibitor + 1 µl Reverse Transcriptase) was added to each sample. The reverse transcription protocol was then started by 5 minutes incubation at 25°C and was followed by 60 minutes at 42°C. At the last step, RT enzyme was heat-inactivated by 15 minutes incubation at 70°C.

Synthesized cDNA was used for subsequent Real-time RT-PCR. Quantitative RT-PCR reaction was performed using SYBR PCR master mix (Applied Biosytems, 10 µl SYBR master mix, 4 µl of 4 µM primer mix, 6 µl cDNA) in a BioRad CFX96 system. The data was analyzed using the $2^{-\Delta\Delta Ct}$ method. The primers used in real-time PCR are listed in table 1.

For RNA-seq, total RNA was purified using QIAzol reagent (QIAGEN). DNase treatment was then performed with RNase-free DNase (QIAGEN). 5 ug of purified RNA was first treated with Ribozero rRNA removal kit (Illumine) and then precipitated with ethanol. RNA quality and removal of rRNA were checked with the Agilent 2100 Bioanalyser (Agilent Technologies). Libraries for RNA-seq were then prepared with the TruSeq RNA Sample Prep Kit v2 (Illumine) following the manufacturer instruction.

Table 2.1 List of primers and the sequences used in this study

PRIMER NAME	SEQUENCE (5'→ 3')
Rplpo-F	TTCATTGTGGGAGCAGAC
Rplpo-R	CAGCAGTTTCTCCAGAGC
Rad21-F	ATTGACCCAGAGCCTGTGAT
Rad21-R	GGGGAAGCTCTACAGGTGGT
Nipbl-F	AAAGGGAGCGCTTCTCAAA
Nipbl-R	CAGCCTCCTGTGGGTAAGAA
Smc3-F	CCGTGCTTTCACTATGGACTG
Smc3-R	CAAGTCGAGACTTCCTTGTGTC
SRSF3-F	GCAGTCCGAGAGCTAGATGG
SRSF3-R	TTCACCATTCGACAGTTCCA
Ccd12-F	AGAAGGAACCTATGGCCAAGTA
Cdk12-R	TCTCACCTTCTTCAGAGCCACT
Cyclin K-F	CACCCTCACAACTTGAAGGAC
Cyclin K-R	CCAGTTGCCAGGGTATCATAG
Cdk13-F	CCATGAAACCAAAGAAGCAA
Cdk13-R	ACTAGGATCCAAGGCAAGCA
Fancd2-F	AACTTGGAGGAGATTGATGGTC
Fancd2-R	CGCTCTTTAGCAGACATGGA
ATR exon9/10-F	CTGCAGAGCTCCCATGAAG
ATR exon9/10-R	GACAATGTCAGAATCATCTTTGACT
ATR exon10-F	CTCTTCACGGCATGTTTTATTCTG
ATR exon10-R	TGGCTTTCAAGTTCCTACAGAAG

2.8 Native isolation of proteins on nascent DNA (iPOND)

Native iPOND was performed according to the protocol published by Leung et al. (Leung et al., 2013). Exponentially growing cells (50×10^6 cells) were labeled with EdU (final concentration 10 uM) for 10 minutes. For thymidine chase, the EdU-containing medium was discarded, cells were rinsed with 37°C and CO_2 equilibrated medium to remove residual EdU and then the medium containing 10 uM thymidine was added to the cells. Cells were then incubated at 37°C in the incubator for 1 hour. EdU pulse or thymidine chase was stopped by discarding EdU/thymidine containing media and ice-cold nuclei extraction buffer (20 mM Hepes pH 7.2, 50 mM NaCl, 3 mM $MgCl_2$, 300 mM sucrose and 0.5% NP40) was immediately added to the monolayer cells in the dish. After 15

minutes incubation, cells were collected using cell scraper and then spun down for 10 minutes at 2500 ×g. After two washes with ice-cold PBS, the cell pellet was resuspended in 5 ml of Click reaction mix (25 uM biotin-azide, 10 mM (+)-sodium L-ascorbate, 2 mM$CuSO_4$ in PBS, the negative control had DMSO instead of biotin-azide) and the samples were rotated at 4°C for 1 hour. The cells were then spun down for 10 minutes at 2500 ×g at 4°C. The click reaction mix was discarded and after a washing step with PBS, the cell pellet was resuspended in 500 ul of lysis buffer B1 (25 mM NaCl, 2 mM EDTA, 50 mM Tris-HCl pH 8.0, 1% NP40 plus protease and phosphatase inhibitors). After 15 minutes incubation on ice, the lysate was sonicated for 10 seconds on ice. The samples were then centrifuged at max speed for 10 minutes at 4°C and the supernatants were discarded. The steps of lysis, sonication and centrifuge were repeated twice to remove soluble proteins and other non-chromatin proteins. After the second Centrifugation, the cell pellet was resuspended in 500 µl of lysis buffer and the samples were sonicated 10 times each step 10 seconds with 10 seconds interval on ice. After centrifugation at max speed, the supernatant was transferred to a new eppendorf tube and an equal volume (500 µl) of lysis buffer B2 (150 mM NaCl, 2 mM EDTA, 50 mM Tris-HCl pH 8.0, 0.5% NP40 plus protease and phosphatase inhibitors) was added to the samples. At this step, an appropriate aliquot of cell lysate was preserved as an input. The samples were then incubated overnight with streptavidin-coated dynabeads (invitrogen) on a rotating wheel, at 4°C. The following day, the dynabeads were collected using magnetic stand and the beads were washed four times with B2 buffer. Finally after a quick centrifuge (960 ×g, 3 minutes) the residual B2 buffer was discarded and the beads were resuspended in 20 ul of 5× Laemmli buffer. The iPOND together with input samples were boiled at 95°C for 15 minutes and then run into the gel.

2.9 Chromatin Immunoprecipitation (ChIP) and DNA-RNA Immunoprecipitation (DRIP)

First cells were fixed by adding 37% formaldehyde to the medium of tissue culture plate to a final concentration of 1% for 10 minutes. Next the cross linking was quenched by adding 2.5 M Glycine diluted to a final concentration of 125 mM while the plates were slowly shaking. After 5 minutes, the cells were rinsed three times with PBS and then scraped off the plates and spun down in a falcon tube. The pellet of ~ 10^8 cells was then resuspended in 5 ml of cell membrane lysis buffer 1 (50 mM Hepes-KOH pH 7.5, 140 mM NaCl, 1 mM EDTA, 10% glycerol, 0.5% NP-40 and 0.25% Triton X-100) containing protease and phosphatase inhibitors. After 10 minutes of incubation on ice, the lysate was centrifuged and the pellet was resuspended in 5 ml of lysis buffer 2 (10 mM Tris-HCl pH 8.0, 200 mM NaCl, 1 mM EDTA, 0.5 mM EGTA) supplemented with protease and phosphatase inhibitor while gently rocking for 10 minutes at room temperature. Nuclei were collected by centrifugation and the nuclear pellet was resuspended in 3 ml of nuclei lysis buffer 3 (10 mM Tris-HCl, 100 mM NaCl, 1 mM EDTA, 0.5 mM EGTA, 1% Na-Deoxycholate, 2.5% N-lauroylsarcosine and protease and phosphatase inhibitor mixture). The suspension was then sonicated 7 cycles (30-seconds pulses followed by 30-seconds rest periods) using a Branson 450 CE sonicator (20% sonication amplitude, 6.4 mm probe diameter) on ice to shear chromatin to an average length of about 300-1000 bp. After that, 300 µl of 10% Trition-X 100 was added to the sonicated lysate and chromatin was split to two 1.5-ml microcentrifuge tubes and was spun down at maximum speed to pellet the debris. The supernatant was aliquoted to the new microcentrifuge tubes. Dynabeads protein G (100 µl, invitrogen) that were washed and pre-blocked with PBS + 0.5% BSA, were incubated with 10 µg of the antibody, overnight at 4°C on a rotating wheel. Next day the beads were washed three times with 1 ml of blocking solution and then 100 µl of

resuspended beads in blocking solution was added to the cell lysates and rotated in a rotating wheel, overnight at 4°C. The day after, the beads were collected using a magnet and washed six times with pre-chilled wash buffer (50 mM Hepes-KOH pH 7.6, 500 mM LiCl, 1 mM EDTA, 10% NP-40 and 7% Na-Deoxycholate) and once with 1 ml of TE containing 50 mM NaCl. The residual buffer was removed by spinning down the beads at 960 xg for 3 minutes and the beads were resuspended in 150 µl of elution buffer (TE + 2% SDS) and incubated at 65°C for overnight. As the input, 1% of sheared chromatin was eluted in a same manner. Next day, the beads were spun down at maximum speed for 1 minute and the supernatant was transferred to a new tube. The DNA was purified using Qiaquick kit (Qiagen) according to the instructions, quantified using Qubit® dsDNA HS assay kit and further analyzed by real-time PCR. 2-10 ng of ChIP DNA was prepared for Illumina Genome Analyzer sequencing with TruSeq ChIP Sample Prep Kit (Illumina).

3 Results

3.1 Setting the siRNA screen

3.1.1 Choosing an appropriate Myc-overexpressing cellular model

To identify regulators of the Myc-induced DNA damage response (DDR) we performed a high-throughput automated siRNA screen based on the quantitative detection of DDR at single cell level.

To set up the screen, we took advantage of a conditional Myc-overexpressing cellular system in which Myc is fused to the Estrogen Receptor (ER). This system has the advantage to allow a quick transcriptional-independent activation of Myc upon 4-hydroxy-tamoxifen (OHT) treatment. In order to find a proper cellular model where Myc induced-DDR is robust enough to be detected by the immunostaining assay, we tested human osteosarcoma U2OS cell line and 3T9 immortal mouse embryonic fibroblast (MEF) cell infected with MycER construct. We also examined the primary embryonic fibroblast MycER-overexpressing cells that were derived from a knock-in mouse (homo- and heterozygous) where the MycER cDNA was inserted in the ROSA26 locus, under the control of R26 promoter (termed R26-MycER MEF). These cells were treated with OHT for 48 hours and Myc-induced DDR was measured by western blot analysis of ϒH2AX, a DNA damage marker (Figure 3.1).

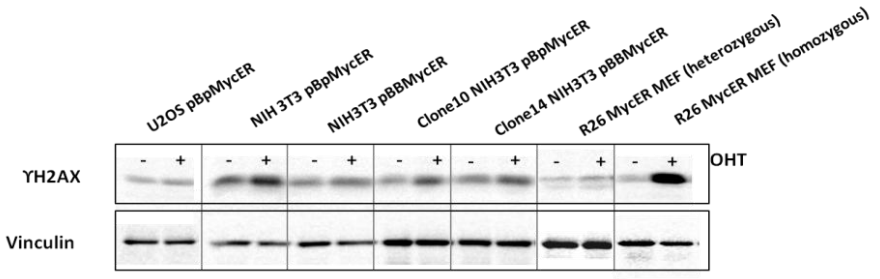

Figure 3.1. Western blot analysis of ϒH2AX in stably MycER-overexpressing cells

U2OS-MycER, NIH/3T3-MycER immortalized MEF cells and clones (#10, #14) and R26-MycER primary MEF cells (hetero- and homozygous) were cultured. Myc overexpression was induced by adding OHT (400nM) to the culture medium. Ethanol was used as solvent control. After 48 hours, OHT-treated and ethanol-treated cells were harvested and subjected to ϒH2AX western blotting. Vinculin was used as a loading control (pbpMycER: pbabe-puroMycER, pBBMycER:pbabe-bleoMycER).

Based on the robustness of the ϒH2AX signal, homozygous R26-MycER MEF cells were chosen for the screen. To ensure the consistency of the cells during the entire screening process, two immortalized clones were generated from two independent preparations of primary MEF cells (named Bz1 and Bz5) by using the 3T3 protocol (Figure 3.2A). Because Myc-induced DDR is known to engage the p53 pathway (Eischen et al., 1999, Zindy et al., 1998) we checked p53 status of the immortalized lines by Sanger sequencing. Sequencing of the p53 gene revealed a homozygous point mutation (K129T) in Bz5 line, while the p53 gene was wild-type in Bz1 cell line. Consistent with the sequencing result, western blot analysis in Bz1 line showed that p53 protein is stabilized as a result of Myc activation compared to negligible level of the protein in control cells. In contrast, Bz5 line appeared to have a robust accumulation of the p53 protein independently of Myc activation, implying that p53 -most likely due to the loss of function nature of the mutation- is stabilized (Figure 3.2B). In addition, the p53-mutated cell line (Bz5) unlike the p53-WT line that was diploid, showed a polyploid FACS profile characterized by 4n and 8n peaks (Figure 3.2C). As p53 mutation and polyploidy may

affect and bias the result of our screen, we decided to carry out the RNAi screen with the Bz1 R26-MycER MEF line which is p53-WT and diploid.

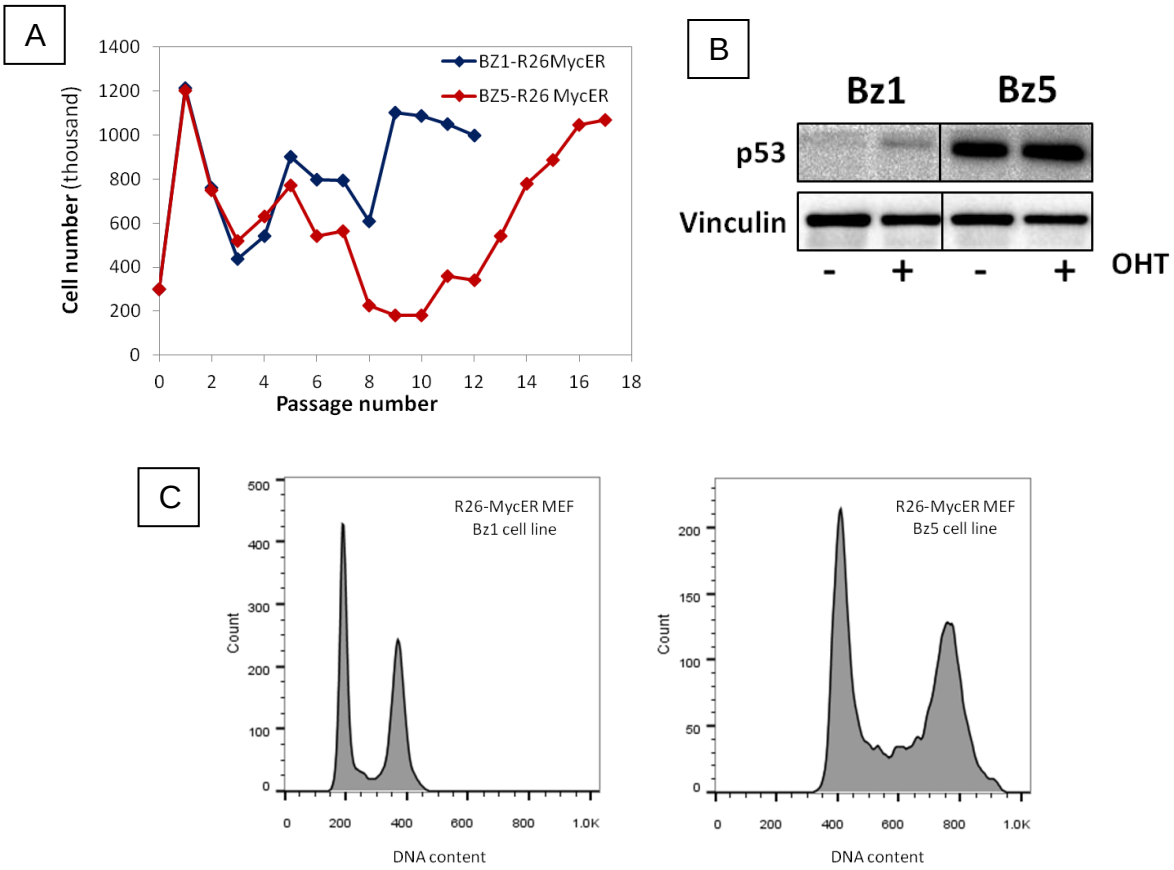

Figure 3.2. Generating and characterization of immortalized cells from R26-MycER primary MEFs

Two independent preparations of primary MEF cells (Bz1 and Bz5) were passaged on a 3T3 protocol until the immortalized cells were established. (A) Growth curve of Bz1 and Bz5 MEF cells during continuous passages in culture in normal oxygen condition (20%). Under this condition many of primary MEFs undergo senescence, however some may acquire mutations and become immortal. Blue and red curves show the growth of Bz1 and Bz5 R26-MycER MEF cells respectively. (B) Western blot analysis of p53 (top panel) and vinculin (bottom panel) in Bz1 and Bz5 immortal MEF clones. (C) FACS profile of propidium-iodide-stained cells. Immortalized Bz1 line showed diploid DNA content profile whereas Bz5 clone displayed discrete 4n and 8n peaks (freshly isolated cells from mouse thymus were used as a control of diploid cells).

3.1.2 Establishing ϒH2AX immunofluorescence assay for quantitative detection of the Myc-induced DNA damage response

The readout of the RNAi screen was based on immunofluorescence detection of ϒH2AX. For this reason, first the DNA damage induced by Myc in Bz1 R26-MycER MEF cell line was evaluated by ϒH2AX immunostaining. Western blot analysis of Myc-activated cells showed a progressive enhancement in H2AX phosphorylation up to 48 hours of Myc activation (Figure 3.3). Consistent with ϒH2AX western blot analysis, Myc overexpression caused a marked increase in the number of nuclear ϒH2AX foci (speckles) detected by immunofluorescence (Figure 3.4A). Based on the robustness of the Myc-induced DDR at 48 hours post OHT treatment, this time was chosen as the endpoint of the screen.

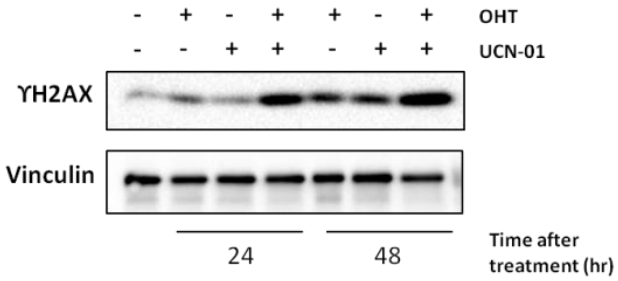

Figure 3.3. Western blot analysis for detection of DDR activation in R26-MycER MEF cell line upon Myc activation and Chk1 inhibition
Bz1 R26-MycER cells were treated with OHT or ethanol and with UCN-01 or DMSO and then were harvested 24 and 48 hours post treatment for measuring H2AX phosphorylation by western blotting. Vinculin was used as a loading control. The final concentration of OHT and UCN-01 was 400 nM and 10 μM respectively.

To evaluate the dynamic range (signal to background ratio) of the immunofluorescence assay, a massive Myc-induced replicative stress was triggered in Bz1 R26-MycER MEF cell line by coupling Myc activation with UCN-01 treatment, a Chk1 inhibitor previously shown to provoke cytotoxic DDR in Myc-overexpressing cells. This treatment mimics the situation of targeting a tumor maintenance gene (such as Chk1) in cells with high levels

of Myc (Murga et al., 2011), thus causing a robust DNA damage. Indeed treating Myc-overexpressing Bz1 MEF line with Chk1 inhibitor (UCN-01) led to a strong enhancement of ϒH2AX signal, as detected by western blotting (Figure 3.3). Immunostaining of the cells for ϒH2AX, displayed mostly a uniform staining in the nuclei (referred to pan-nuclear signal, Figure 3.4B). Given the broader dynamic range of pan-nuclear signal compared to the ϒH2AX foci, we used pan-nuclear signal as a quantitative assessment of DDR in our screen.

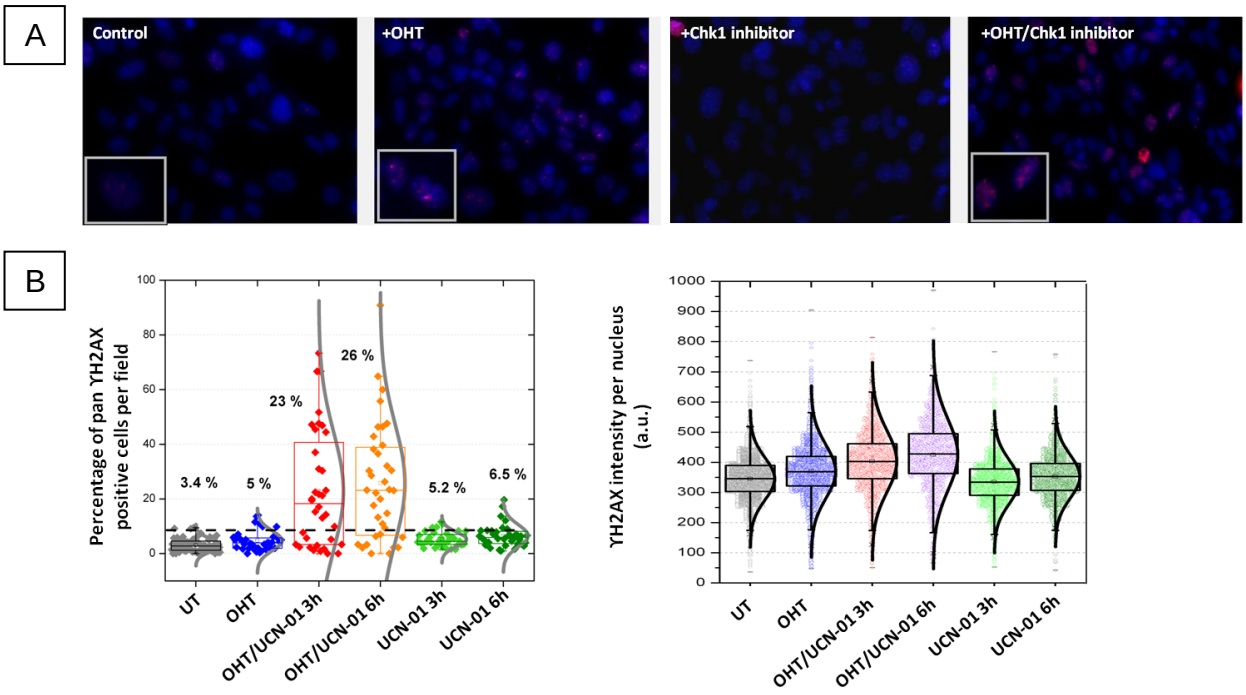

Figure 3.4. Immunofluorescence detection of ϒH2AX foci and pan-nuclear signal in Bz1 R26-MycER MEF cell line

Cells were treated with OHT or ethanol for 48 hours. UCN-01 or DMSO was added the last 3 or 6 hours of treatment. After fixation, the cells were stained with ϒH2AX (red) and counterstained with DAPI (blue). (A) Representations of immunofluorescence staining for ϒH2AX in untreated cells (control), OHT, UCN-01 and double treated cells. (B) Quantification of ϒH2AX signal. Left plot shows the percentage of the pan-nuclear stained cells. Median values are depicted for each treatment. Right plot shows the total intensity of the ϒH2AX signal (speckles and pan-nuclear staining) per nucleus. a.u. arbitrary units. Final concentration for OHT was 400 nM and for UCN-01 was 10 μM. (The analysis was done by Dr. Fernanda Ricci in IIT screening unit).

3.1.3 Optimization of siRNA transfection

To set the siRNA transfection conditions in Bz1 R26-MycER MEF cell line, we tested different cell transfection reagents and different cell densities to find the optimal transfection condition with the highest transfection efficiency and the lowest cell toxicity. To this intent, different concentration of two widely used siRNA transfection reagents (Lipofectamine RNAiMAX and DharmaFECT1) were used to reverse transfect Bz1 R26-MycER MEF cell line at three different cell densities in a 96-well plate. The transfection efficiency was assessed by measuring cell viability upon delivery of a toxic siRNA (siTOX) into the cells. Measured cell viability with MTT and CellTiter-Glo assays after 48 hours of siRNA transfection showed a good performance of DharmaFECT1 transfection reagent compared to Lipofectamine RNAiMAX (Figure 3.5). Among the tested conditions, 2000 cells with 0.2 µl of DharmaFECT1 yielded higher siRNA transfection efficiency (higher toxicity by siTOX) and low toxicity with no siRNA.

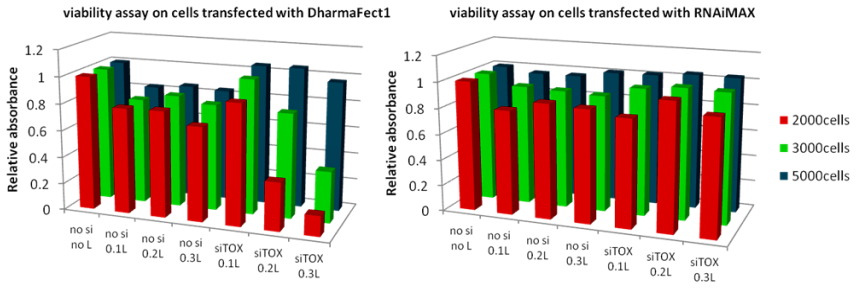

Figure 3.5. Optimization of siRNA transfection in Bz1 R26-MycER MEF in 96-well plate format

Cells (at different densities: 2000, 3000 and 5000 per well) were reversed transfected with 2.5 pmol of a toxic siRNA (siTOX) or no siRNA using different amounts of the transfection reagents Lipofectamine RNAiMAX and DharmaFECT1. Cell viability was measured 48 hours post transfection by the colorimetric MTT assay. Relative absorbance normalized to the mean absorbance of untransfected cells (no siRNA, no lipid) is presented. The experiment was repeated another time with comparable results. Assays were performed in triplicates. No si: no siRNA, L: lipid.

The transfection conditions set in 96-well format, were further scaled down and re-tested in a 384-well plate. To do this, first the optimal cell density in 384-well format was determined by seeding different cell numbers and monitoring the cell growth over time (Figure 3.6A). We chose to seed 800 cells per well of 384-well plate since at this cell density cells were growing exponentially till 48 hours, which was the endpoint of the siRNA screen. The selected cell density was then used for testing different volumes of DharmaFECT1 reagent per well. Similarly to the set up experiment done in 96-well plate, we used siTOX for monitoring cell viability and assessing the transfection efficiency. Comparing the results, we chose the volume of transfection reagent (0.15 µl per well) that resulted in higher toxicity by siTOX and low toxicity by a pool of non-targeting siRNAs (Figure 3.6).

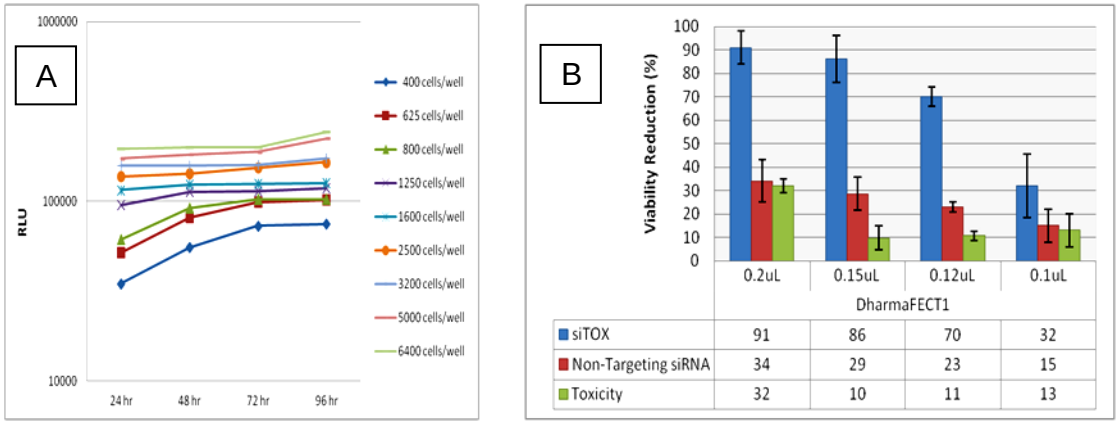

Figure 3.6. Assessing the optimal siRNA transfection condition in 384-well plate format

First, the optimal initial cell density was determined by seeding Bz1 R26-MycER MEF cell line at different cell densities in a 384-well plate and monitoring the cell growth over time. Once identified, the optimal cell density was used to set up the volume of the DharmaFECT1 transfection reagent. (A) Growth rate of Bz1 R26-MycER MEF line measured by CellTiter-Glo viability assay. (B) Viability reduction of siRNA-transfected cells after 48 hours measured by CellTiter-Glo. siTOX (blue bars) was used to assess the transfection efficiency while non-targeting siRNA pool (red bars) and lipid only (green bars) were used as the negative controls. The initial cell density was 800 cells per well. The experiment was repeated another time with a comparable results. (The data was generated by Dr. Michela Mattioli in IIT screening unit).

3.1.4 Selection of appropriate controls for the siRNA screen

Like all the assays, for RNAi screen several negative and positive controls were needed. For the negative control, we tested a number of neutral siRNAs that do not target any transcript in murine cells (siRNAs against GFP, Renilla luciferase and non-targeting siRNA pool #2, Dharmacon, Thermo Scientific). Among those, the siRNA against Renilla luciferase (siRluc) served as the best negative control in terms of low toxicity and low impact on the basal ϒH2AX in the cells, giving results that were comparable with untransfected cells (data not shown). To ascertain the siRNA transfection efficiency in our screen, we took advantage of the siRNAs targeting essential genes like Plk1 and Kif11 that upon delivery, due to prolonged mitotic arrest, cause cell death in transfected cells.

In addition to these transfection controls, we also needed a number of positive controls for Myc-induced DDR and for synthetic lethality. Despite the fact that UCN-01 treatment synergized with Myc in inducing DNA damage and eventually led to cell death, we observed that siRNA against Chk1 was not potent in inducing synthetic lethality and in increasing H2AX phosphorylation. As Chk1 is also a Myc target gene, we observed an up-regulation of Chk1 mRNA level in siChk1-transfected cells upon Myc activation compared to Chk1-depleted cells with endogenous level of Myc (Figure 3.7A). In line with the RT-qPCR results, the ϒH2AX western blot analysis in Bz1 R26-MycER MEF line showed no synergy between Myc overexpression and Chk1 depletion (Figure 3.7B).

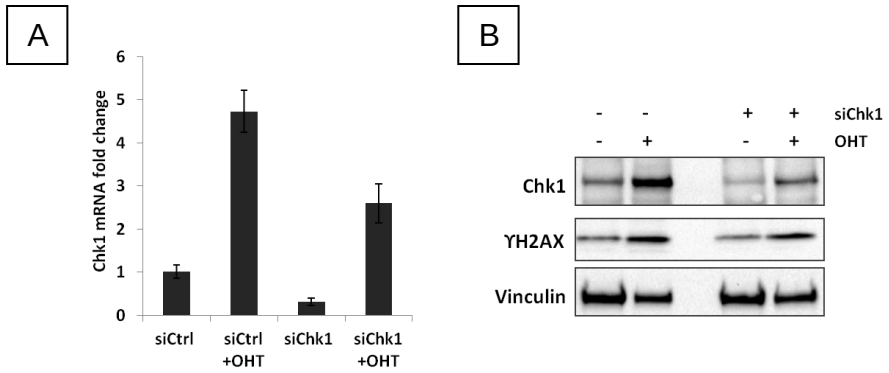

Figure 3.7. Chk1 depletion in Bz1 R26-MycER MEF line by means of siRNA

Bz1 R26-MycER line was transfected with siChk1 or a non-targeting siRNA (siCtrl) and was treated with OHT or ethanol at the same time. After 48 hours, cells were harvested for RT-qPCR and western blot analyses. (A) RT-qPCR analysis of Chk1 mRNA expression level upon Myc activation in siChk1-transfected cells compared to control cells. mRNA expression level was normalized with a housekeeper gene (RPLPO) and is plotted relative to the siCtrl-transfected cells. Error bars show the standard deviation. (B) Western blot analysis of Chk1 and ϒH2AX in cells. Vinculin was used as a loading control. The experiment was done once. siCtrl: control siRNA, siChk1: siRNA against Chk1.

The fact that Chk1 depletion by siRNA was not effective in inducing Myc-induced DDR, because of the positive regulation of Myc on the Chk1 gene, led us to examine a number of other genes whose knock-down previously shown to induced DDR and cell death selectively in Myc-overexpressing cells (Toyoshima et al., 2012). Among the tested genes, we noticed that Rad21 silencing led to a marked increase in phosphorylation of H2AX upon Myc activation (Figure 3.8A). Furthermore, Rad21 knock-down caused a significant reduction in the number of Myc-overexpressing cells compared to control cells with endogenous level of Myc (Figure 3.8B). Therefore Rad21 was selected as a positive control for either Myc-induced DDR and for synthetic lethality.

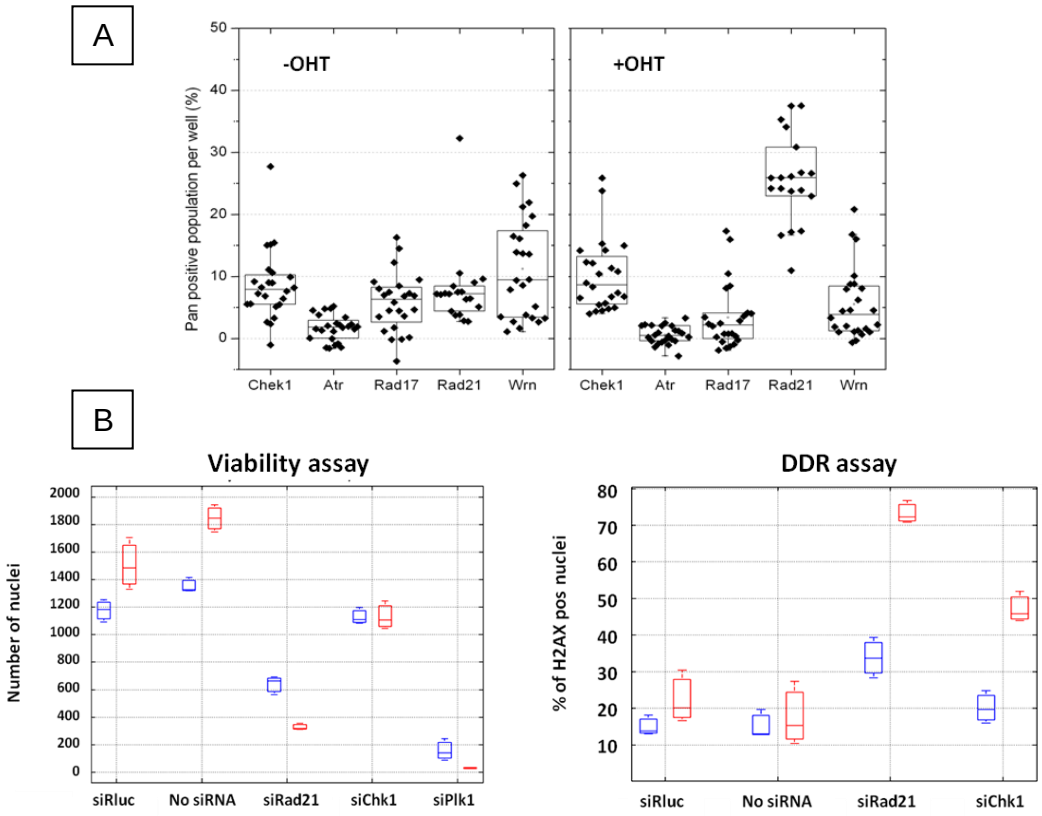

Figure 3.8. Immunofluorescence analysis of Myc-induced DDR in Bz1 R26-MycER MEF line transfected with a number of previously-published Myc-synthetic lethal candidates

Cells were transfected individually with siRNAs targeting Chk1, ATR, Rad17, Rad21, Wrn and Rluc and simultaneously were treated with OHT or ethanol. After 48 hours, cells were fixed and stained for ϒH2AX and DAPI. (A) Quantification of the percentage of ϒH2AX pan-stained nuclei in the transfected cells. The experiment was done manually in a 96-well plate. (B) Quantification of the number of nuclei and the percentage of ϒH2AX pan-positive nuclei in siRad21-transfected cells in comparison with the control cells in the presence or absence of OHT. siRNA transfection was performed automated in a 384-well plate. The assays were performed in triplicates. (Data was produced by IIT screening unit).

3.2 A high-throughput siRNA screen for identification of modulators of Myc-induced DDR

The RNAi screen was carried out in Bz1 R26-MycER MEF line in two conditions: (i) OHT- and (ii) ethanol-treated (high and normal Myc level respectively). We used a library that targeted around 1400 druggable genes from Dharmacon, arrayed in five 384-

well format plates, each well containing a pool of four individual siRNAs targeting a same gene. Forty-eight hours post siRNA transfection and OHT/ethanol treatment, cells were fixed and then stained with ϒH2AX antibody to measure the DNA damage response, and counterstained with DAPI to estimate the cell viability. Images were acquired using Olympus ScanR microscope for further analysis. Having three technical replicates for each condition (normal Myc and high Myc level) enabled us to perform statistical testing of the obtained results. As mentioned before, besides having negative control, siRNA against Renilla luciferase (siRluc), we chose siRad21 that was shown to increase DNA damage and lead to synthetic lethality in Myc-overexpressing cells, as a positive control for the assay.

We assessed cell viability based on the number of DAPI-stained nuclei to identify genes whose depletion caused differential viability in Myc-overexpressing cells (Myc-OE) compared with the control cells (Myc-N). To do so, first the viability data of each well in a given plate was normalized to the median of the viability in siRluc-transfected cells (negative control) of that plate in order to correct inter-plate and inter-day variability. Taken the normalized viability, we then calculated the viability ratio of Myc-OE cells over Myc-N cells. Applying a stringent threshold of Z score of $\leq$ -2 on viability ratio of Myc-OE over Myc-N cells enabled us to identify the potential Myc synthetic lethal (Myc-SL) hits. This analysis revealed 51 high confidence hits. We also defined a class of low confidence hits (45 hits) by using a less stringent Z score $\leq$ -1.5 and the viability ratio < 0.7 (Figure 3.9A).

To identify negative regulators of Myc-induced DDR (DDR-up hits), the enhancement in the background-corrected intensity of ϒH2AX in Myc-OE cells compared to control cells, was analyzed with four different methods, all based on MAD Z score in a pilot experiment (with approximately 280 genes). Evaluating these methods, we obtained a

good overlap between the hits coming from different methods. We then chose “difference in the percentage of ϒH2AX pan-positive nuclei” as a standard method for analyzing the entire screen. Applying this method we found 58 candidates whose knock-down significantly increased ϒH2AX signal in Myc-OE cells (Figure 3.9B). Furthermore, using a ϒH2AX-intensity threshold according to the negative (siRluc) and positive (siRad21) replicates in a given plate, we identified additional 59 candidates in this group that caused elevated ϒH2AX (Figure 3.9D). Quantification of ϒH2AX intensity in Myc-SL hits also showed a higher signal in a number of the cases (Figure 3.9C), whether this is the cause or the consequence of the synthetic lethality is an interesting issue to be addressed.

Although the screen was aimed mainly on identification of negative regulators of Myc-induced DDR, we were also able to identify two other groups of hits: (i) a group of 25 hits (termed synthetic viable hits) which showed increased viability compared to negative control (siRluc) in Myc-overexpressing cells (normalized viability ratio of Myc-OE/Myc-N $\geq$ 1.25,Figure 3.9E) and (ii) a group composed of 37 candidates that showed reduced ϒH2AX in OHT-treated cells compared to control cells (Percentage ϒH2AX pan-positive nuclei (OHT - EtOH) <0, referred to DDR-down hits, Figure 3.9D). Interestingly ATM was among the synthetic viable (SV) hits whose depletion increased the number of Myc-overexpressing cells. This observation was in consistent with the tumor suppressive role of ATM in Myc-driven tumors, most likely by regulating p53-mediated Myc-induced apoptosis (Pusapati et al., 2006). Moreover, we also found some shared hits between two SV and DDR-down groups (Figure 3.9E). One possible explanation could be that those hits which reduced DNA damage may exert their function by blocking Myc-induced apoptosis thus increasing cell viability. Also, the synthetic viability could be simply a consequence of reduced DDR in these cells.

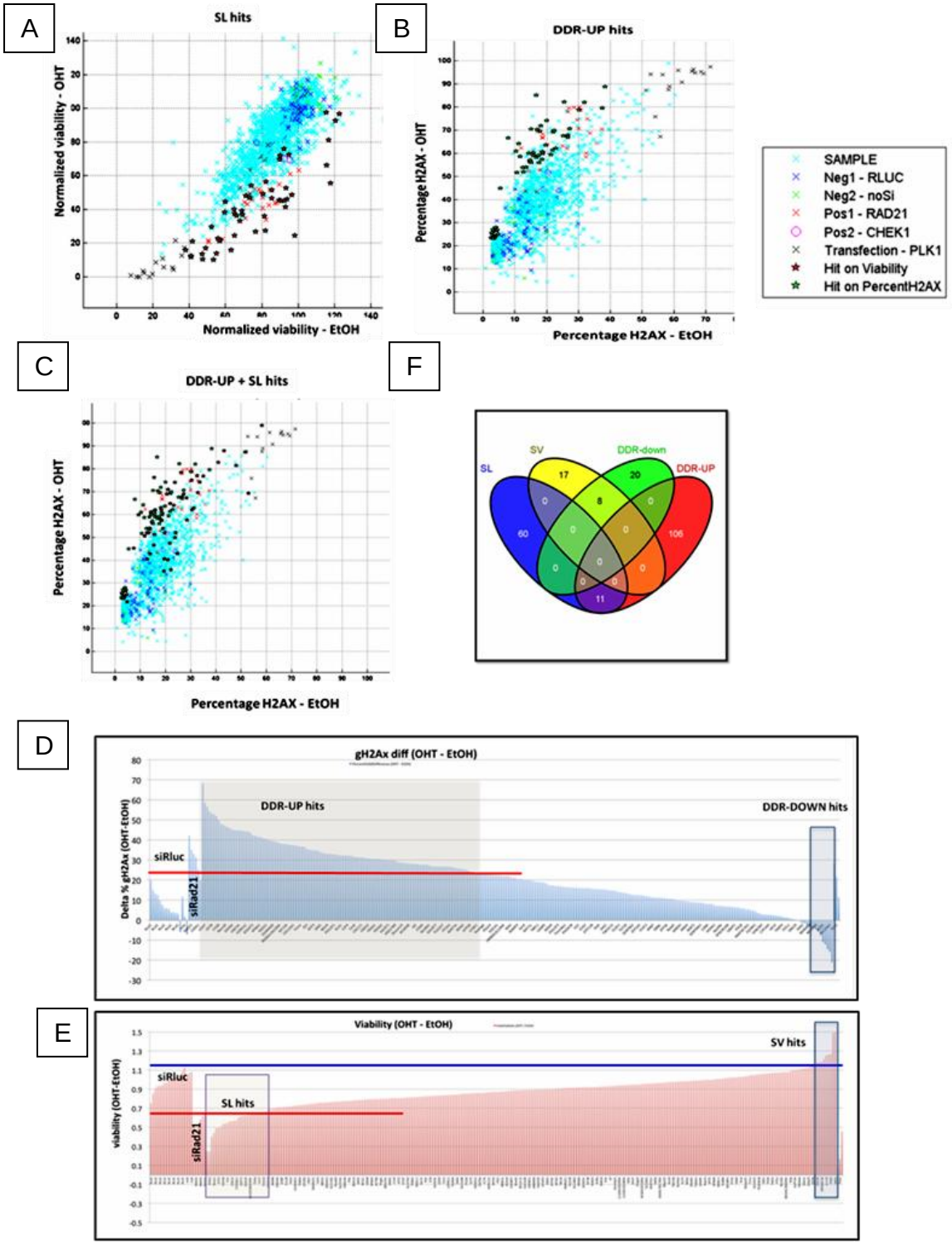

Figure 3.9. Summary of siRNA screen and the identified groups of hits (see figure legend next page)

(A, B, C) Scatter plots of the R26-MycER cell line (OHT/EtOH-treated) transfected with single siRNAs depicted as blue cross. (A) The normalized viability in OHT-teated (Y-axis) and ethanol-treated (X-axis) cells. Potential synthetic lethality hits are shown with red stars. (B) Percentage of ϒH2AX pan-positive cells in OHT-treated cells compared to ethanol-treated cells. Potential DDR-up hits are shown as green stars. (C) DDR-up and SL hit distribution as a function of the percentage of ϒH2AX pan-positive nuclei is delineated. (D, E) Representation of DDR (up panel) and viability (low panel) hits in a given library: (D) difference in the percentage of ϒH2AX positive cells between OHT- and ethanol-treated cells was shown for each single siRNA. A ϒH2AX-based threshold (blue line) was set to identify DDR-up hits. Blue square shows DDR-down hits; (E) viability ratio (OHT/EtOH) of the same plate. Red and blue lines were set to discriminate synthetic lethal (SL) and synthetic viable (SV) hits respectively. (F) Venn diagram showing the overlap between hits. SL: synthetic lethality, SV: synthetic viability, EtOH: ethanol.

3.3 Secondary screen for verification of the initial hits

False positivity may happen in every RNAi screen due to the off-target effect of siRNAs, for this reason we further validated our primary hits with a secondary screen using different siRNAs. The majority of primary hits were screened by Mission esiRNAs (Sigma). Each esiRNA is a pool of siRNAs resulting from endoribonuclease cleavage of long double strand RNA. As the starting material in esiRNA preparation is cDNA, these silencers are guaranteed to effectively target a specific real gene with lower off-target effect than single or pooled siRNAs. For the minority of the primary hits for which a targeting esiRNA was not available, three different individual silencer siRNAs (Ambion) were used in the secondary screen. Since for some hits, in the primary screen, the synthetic lethality was accompanied with ϒH2AX enhancement, it was not possible to discriminate if the synthetic lethality is the cause or the consequence of the increased ϒH2AX. Because of this reason, the synthetic lethal and DDR-up hits from the secondary screen were all classified as “positive hits” regardless whether they were called as synthetic lethal or DDR-up previously in the primary screen. With this criterion, overall 43 out of 201 tested genes from esiRNA custom library were called as positive hits in

both primary and secondary screens. Among Ambion siRNA custom library, 7 out of 74 genes (with at least two out of three single siRNA called as positive) were detected to cause synthetic lethality and/or to increase ϒH2AX in both screens. In addition, among the initial identified SV and DDR-down hits we verified 3 hits by the secondary screen. One possible reason for the low rate of hit validation in the SV/DDR-down class could be the lower dynamic range of the signal in this group, which reduced our confidence in calling the SV and DDR-down hits. The summary of the number of tested genes, initial positive hits and the validated hits is shown in table 3.1.

Table 3.1. Summary of number of tested genes and number of positive hits in the primary and secondary siRNA screen

Screen		Tested genes		Hits		
Druggable	Primary screen	1400		205 (14%) (non-redundant)	DDR-up	117
					SL	102
	Verification screen	esiRNA	147	50/147 (34%)	DDR-up/SL	50
		Ambion	58	11/58 (19%)	DDR-up/SL	11

3.4 Bioinformatics and network analysis

To biologically and functionally annotate the verified hits, we used PANTHER and David functional classification tools. PANTHER showed the distribution of the hits in a variety of biological pathways including metabolism, cell cycle and cellular proliferation (Figure 3.10). However, considering the distribution of all the tested genes (as background), the verified hits were not enriched in any particular process. DAVID functional analysis on hits also showed different clusters related to a variety of processes such as translation and protein synthesis, nuclear envelope and pore complex, intracellular transport, transcriptional regulation, mitochondrion and apoptosis.

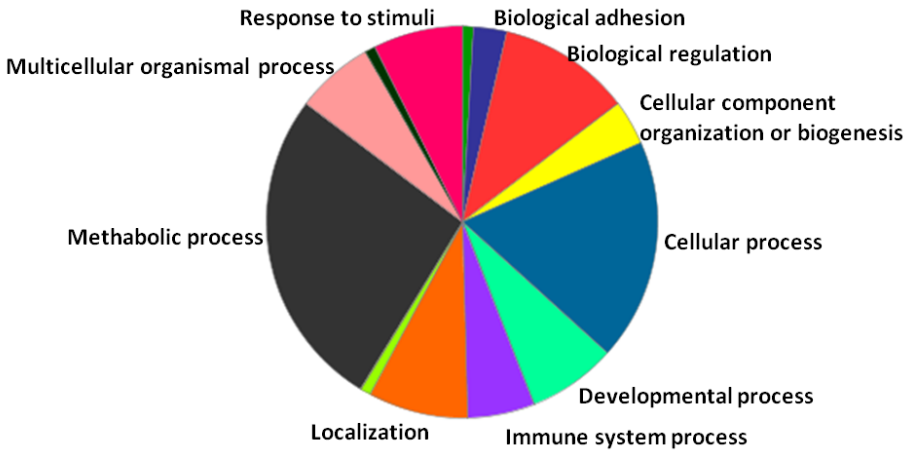

Figure 3.10. Functional classification of the verified hits
PANTHER representation of the biological process of all verified "positive hits" from screening.

3.5 A biased primary screen against DDR genes

In a complementary approach to the unbiased screen described above, we also chose a subset of genes that were linked to the maintenance of genome stability by previous study (Paulsen et al., 2009). With this aim, we selected around 1200 genes based on a previous genome-wide siRNA screen done in Cimprich lab (Paulsen et al., 2009). Whereas the aim of the RNAi screen by Paulsen and colleagues was to find the genes that affect genome stability in unperturbed cells (measured by ϒH2AX immunofluorescence), we were looking for genes whose knock-down would not largely affect the population but synergize with Myc-induced DDR to enhance ϒH2AX and/or to induce cell death. Therefore we chose mostly the genes from the Paulsen et al. hit list that moderately increased ϒH2AX without having a severe impact on the viability of the cells. Screening this collection of genes revealed 66 synthetic lethal hits and 39 DDR-up hits, among them 23 were called in both groups. Interestingly, the SL and DDR-up hits showed a strong enrichment in the "nucleic acid binding" class and in particular the "RNA binding protein" class of proteins (Figure 3.11). By gene ontology analysis, these hits revealed to

have a role in mRNA processing and splicing. RNA post-transcriptional modification and splicing was also one of the enriched categories in Paulsen et al. study. The role of RNA processing machinery in preserving genome integrity is not very well known and has become the subject of some recent studies. Besides the RNA processing machinery, we also found eight hits as coding genes regulating protein degradation. Further validation is required to understand the role of these genes in Myc-overexpressing cells.

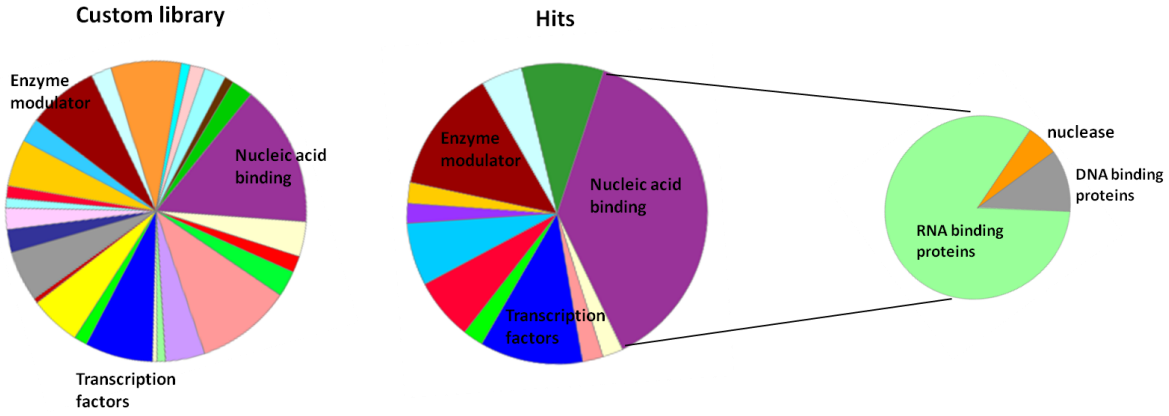

Figure 3.11. Classification of the custom screen genes based on the encoded protein

Classification of the total tested genes in custom library (A) and the positive (SL and DDR-up) hits (B) are shown. The subsets of the "nucleic acid binding" class in the hit category is further expanded in the pie chart.

3.6 Validating the synthetic lethal interaction between Myc and SRSF3

As mentioned above, the mRNA processing and splicing cluster was one of the most enriched group of positive hits arose from the custom siRNA screen. Therefore we decided to further validate one hit (SRSF3) from this group that was also among the positive hits of primary and secondary validation screens.

We rationalized that if there is a dependency of Myc-overexpressing cells on the splicing factor SRSF3, we may obtain the same phenotype in other cell types as well. With this notion, we intended to validate the synthetic lethality between Myc overexpression and

SRSF3 depletion in U2OS cells overexpressing the conditional MycER fusion protein (hereafter termed U2OS-MycER). U2OS-MycER cells were reverse transfected with three different siRNAs against SRSF3 and a non-targeting siRNA (siControl) and, simultaneously, cells were treated with OHT (to activate Myc) or ethanol (as control). Cell viability assay at 48 hours post transfection/treatment showed a reduction in viability of the SRSF3-depleted cells overexpressing Myc compared to control cells or SRSF3-silenced cells with normal Myc level (Figure 3.12).

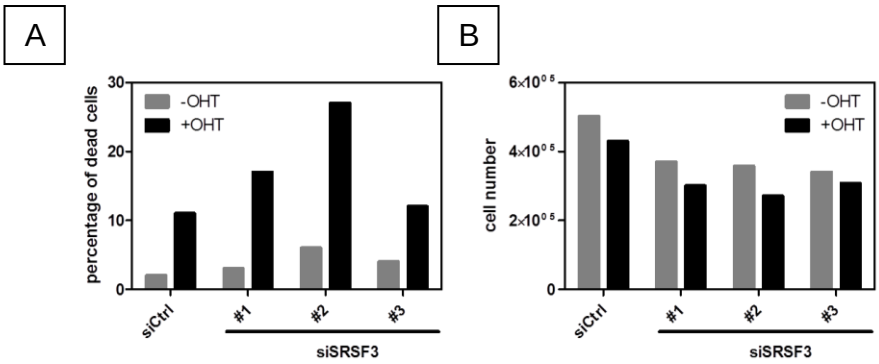

Figure 3.12. The effect of SRSF3 depletion on cell viability and cell proliferation of U2OS-MycER cells

1.5×10^5 cells were reverse transfected independently with three different siRNAs against SRSF3 and a non-targeting siRNA (siCtrl) and were simultaneously treated with OHT or ethanol. At 48 hours post transfection cells were collected and counted by trypan blue. (A) percentage of dead cells and (B) total number of live cells are plotted. The experiment was performed once.

Consistent with the screen data, western blot analysis of H2AX phosphorylation displayed a significant enhancement of ϒH2AX in Myc-overexpressing cells depleted of SRSF3 (Figure 3.13B). It should be noted that although high knock-down level of SRSF3 (as achieved by siSRSF3 #2, Figure 3.13) had cytotoxic effect on cells and led to increased ϒH2AX even in the absence of Myc overexpression, the intermediate knock-down level of SRSF3, at least up to 48 hours, did not affect largely the cell viability and the basal level of ϒH2AX in cells.

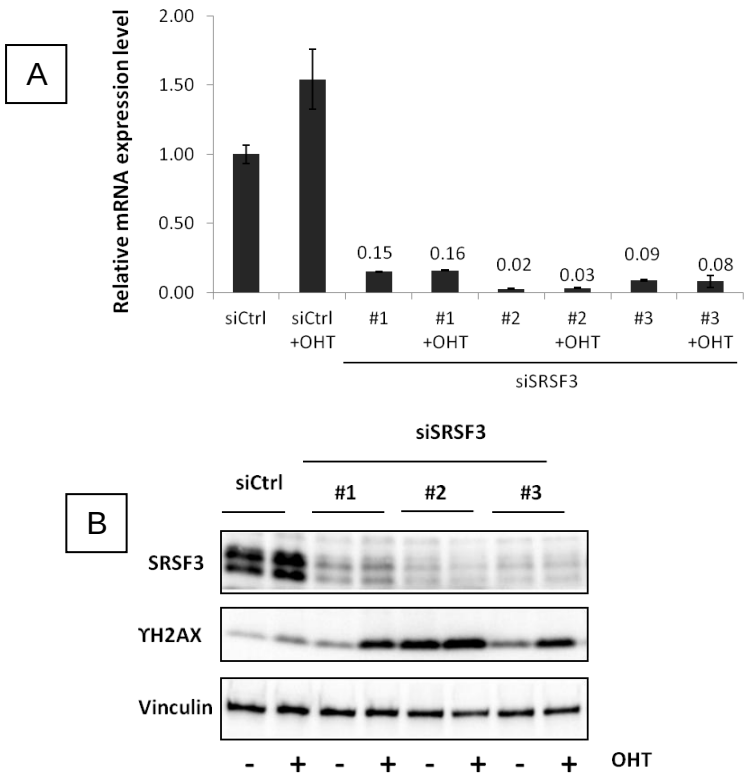

Figure 3.13. The effect of SRSF3 knock-down in U2OS-MycER cells
Cells were transfected with three different siRNAs against SRSF3 and a control siRNA (siCtrl) and treated with OHT or ethanol at the same time. At 48 hours post transfection/treated cells were harvested for RT-qPCR and western blot analyses. (A) RT-qPCR analysis of SRSF3 expression level in transfected cells. Relative mRNA expression was measured using ΔCt method, normalized with a housekeeper gene (RPLPO) and is plotted relative to the control (siCtrl) cells. Values are the mean ± sd. (B) Western blot analysis for SRSF3 (upper panel), H2AX phosphorylation (middle panel) and vinculin (bottom panel) in transfected cells.

We also analyzed the cell cycle profile of SRSF3-depleted cells by EdU incorporation. FACS analysis revealed a significant decline in EdU positive population in cells transfected with two different siRNA against SRSF3 (Figure 3.14). Myc overexpression in these cells caused a reduction in the percentage of G1 and an increase in the percentage of G2/M population.

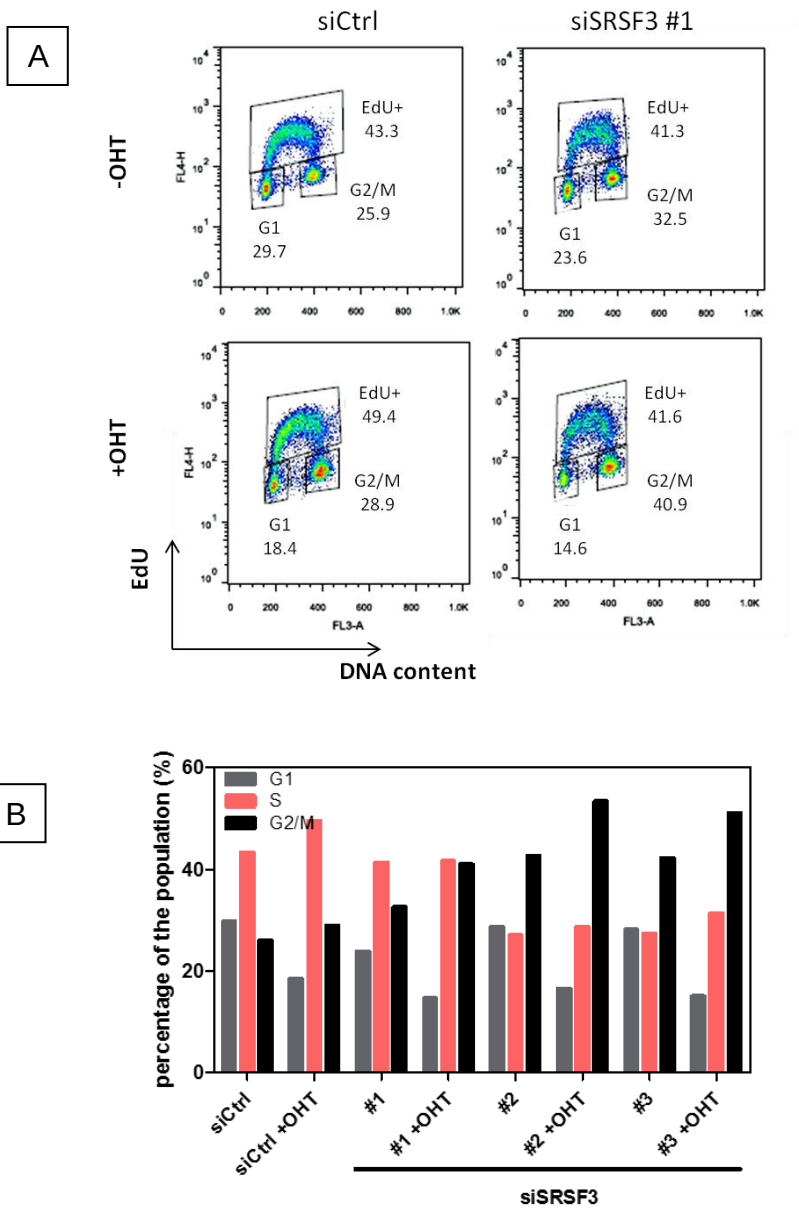

Figure 3.14. FACS analysis of EdU incorporation in U2OS-MycER cells transfected with three different siRNAs against SRSF3
(See figure legend next page)

At 48 hours post transfection and Myc activation, cells were pulsed with EdU for 90 minutes, then harvested and subjected to EdU staining followed by propidium iodide staining. (A) Representative FACS profiles of cells transfected with siCtrl and a siRNA against SRSF3 (siSRSF3 #1) showing the EdU positive cells and the population of cells in G1 and G2/M phase of the cell cycle. (B) The percentage of cells in each phase of the cell cycle, as determined by EdU staining, is plotted. FACS analysis was performed once.

Moreover, FACS analysis on Myc-overexpressing siSRSF3-transfected cells stained with ϒH2AX and propidium iodide, displayed that ϒH2AX-positive cells were distributed in all cell cycle phases (Figure 3.15), suggesting that the accumulation of DNA damage in these cells may be the cause of synthetic lethality.

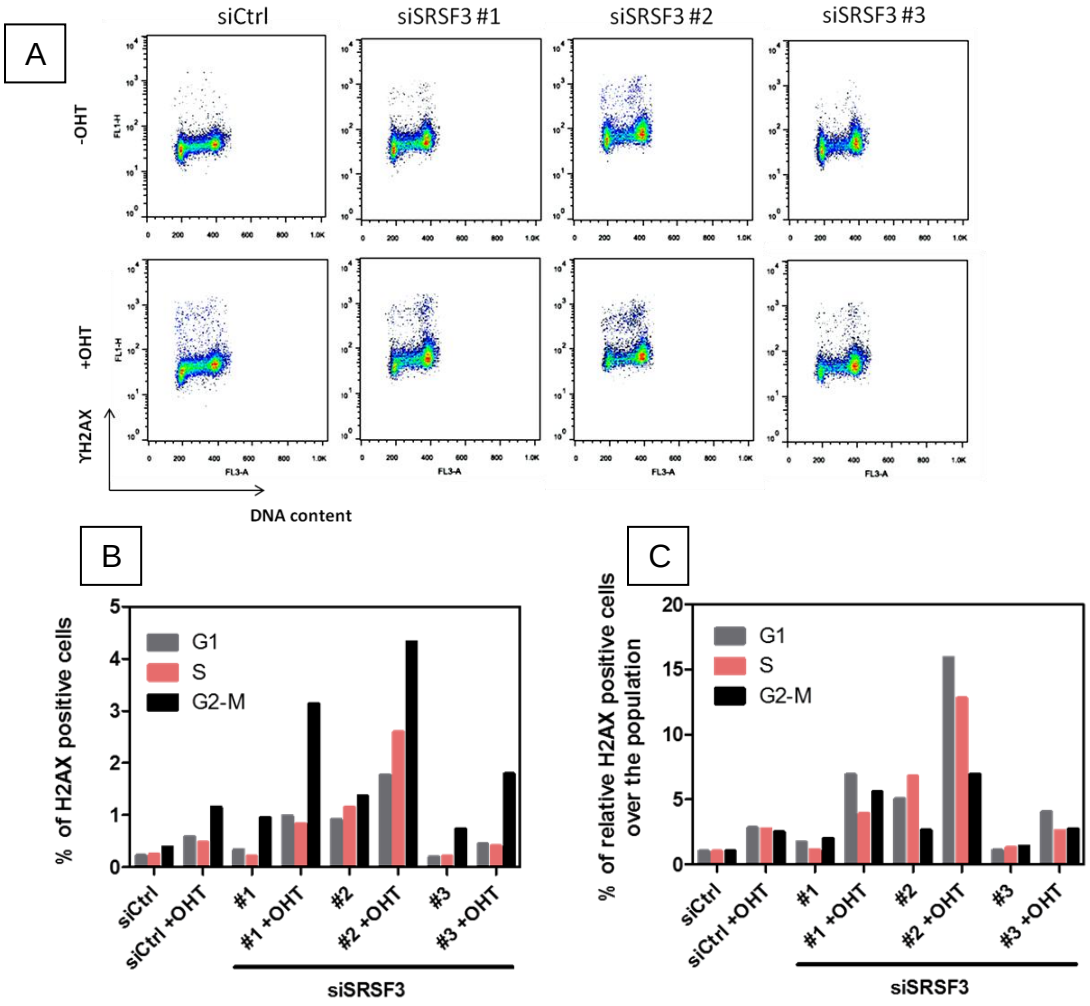

Figure 3.15. Cell cycle distribution of ϒH2AX-positive cells upon SRSF3 depletion and Myc activation (See figure legend next page)

After 48 hours from transfection, cells were pulsed with EdU for 90 minutes, then collected, stained for EdU, ϒH2AX and propidium iodide and followed by FACS analysis. (A) FACS profiles of the transfected showing ϒH2AX-positive cells as a function of DNA content (B) Percentage of ϒH2AX-positive cells in each phase of the cell cycle is plotted. (C) Percentage of ϒH2AX-positive cells in different phase of the cell cycle normalized to the parental population is plotted. FACS analysis was performed once.

3.7 Validating the Myc-Cdk12 synergy in enhancing DDR

We also selected Cdk12, a DDR-up hit, for further validation in U2OS-MycER cells. Of note, Cdk12 depletion was also found in Toyoshima et al. study (Toyoshima et al., 2012) as a Myc synthetic lethal hit. Recently it has been shown that Cdk12 together with its cyclin partner, Cyclin K (CCNK), has a critical role in maintaining genomic stability, presumably via regulation of expression of DDR genes. Cdk12 or Cyclin K depletion was shown to sensitize cells to a variety of DNA damaging agents (Blazek et al., 2011, Liang et al., 2015). Therefore we decided to examine the effect of Cdk12, Cdk13 (the paralog of Cdk12) and Cyclin K depletion under Myc-induced replicative stress condition. Gene knock-down was achieved by transfecting U2OS-MycER cells with two individual siRNAs targeting Cdk12, Cdk13 and Cyclin K. Real-time RT-PCR analysis after 48 hours from transfection validated the knock-down of the corresponding genes (Figure 3.16).

.

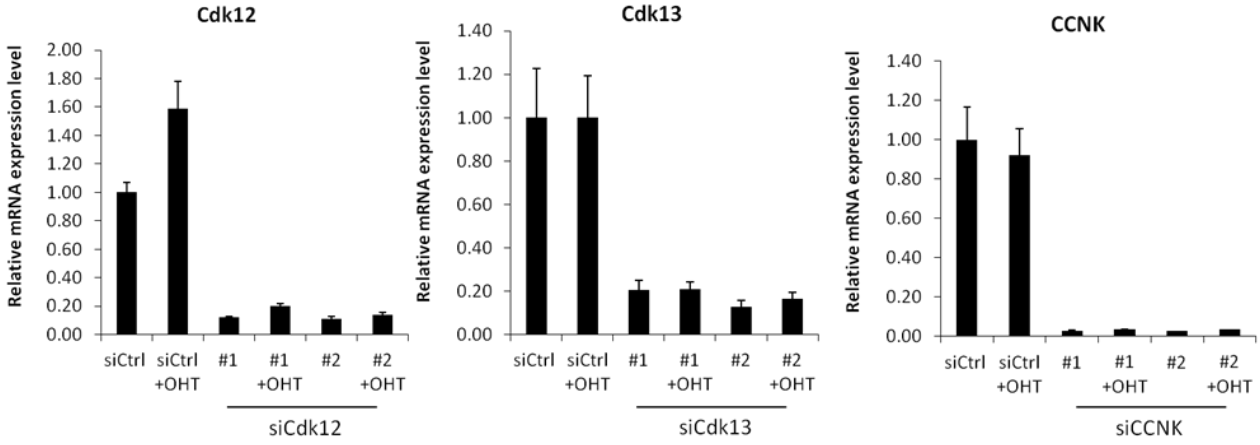

Figure 3.16. Quantitative RT-PCR analysis of Cdk12, Cdk13 and CCNK expression level in siRNA-transfected cells

Two different siRNAs were used for each gene silencing. Relative mRNA expression was measured using ΔCt method, normalized with a housekeeper gene (RPLPO) and is plotted relative to the control (siCtrl) cells. Values are the mean ± sd.

We then examined the cell viability and cell growth of Myc-activated or non-activated cells depleted of Cdk12, Cdk13 and Cyclin K. Indeed, cell viability was not largely affected in siCdk12-transfected cells (with endogenous or high level of Myc). In contrast, Myc-overexpressing cells depleted of Cdk13 and Cyclin K exhibited a significant higher level of dead cells and the cell proliferation was reduced in these cells, while siCdk13- or siCCNK-transfected cells with endogenous level of Myc just showed a slight increase in cell death (Figure 3.17).

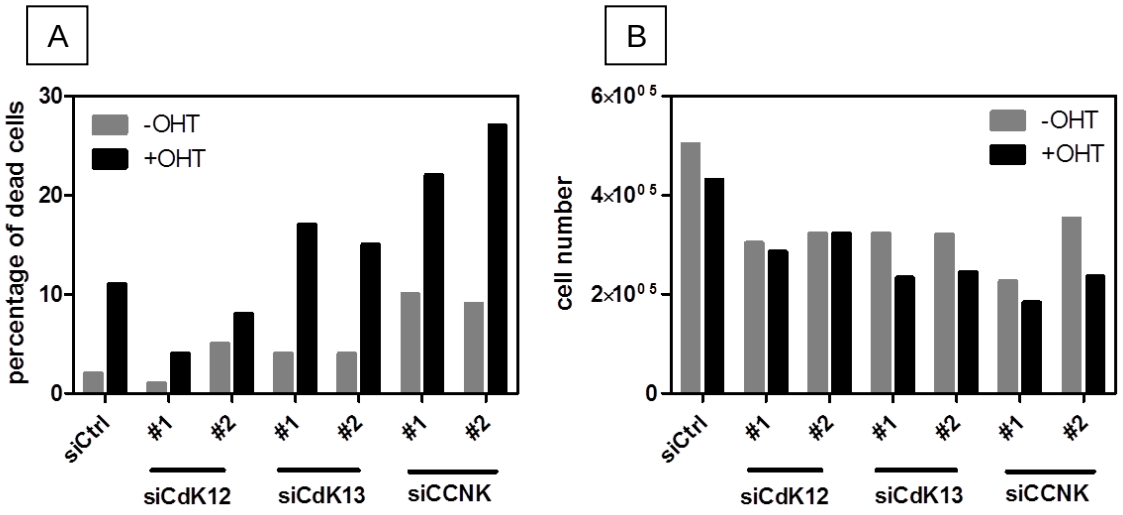

Figure 3.17. The effect of Cdk12, Cdk13 and Cyclin K depletion on cell viability and cell proliferation of U2OS-MycER cells
1.5×10^5 cells were reverse transfected with two individual siRNAs (#1 and #2) against each gene. At 48 hours post transfection, cells were collected and counted by trypan blue. (A) Percentage of dead cells and (B) total number of live cells are plotted. The experiment was performed once.

Since in our siRNA screen the depletion of Cdk12 in Myc-activated cells yielded a higher percentage of ϒH2AX-positive cells, we examined the level of H2AX phosphorylation in the transfected cells by western blot analysis. Cdk12 depletion by both siRNAs significantly increased ϒH2AX levels in Myc-overexpressing cells but not in cells possessing normal Myc level. Similarly, Cdk13 and Cyclin K depletion (dependent on the

siRNA) also synergized with Myc-activation to enhance H2AX phosphorylation (Figure 3.18).

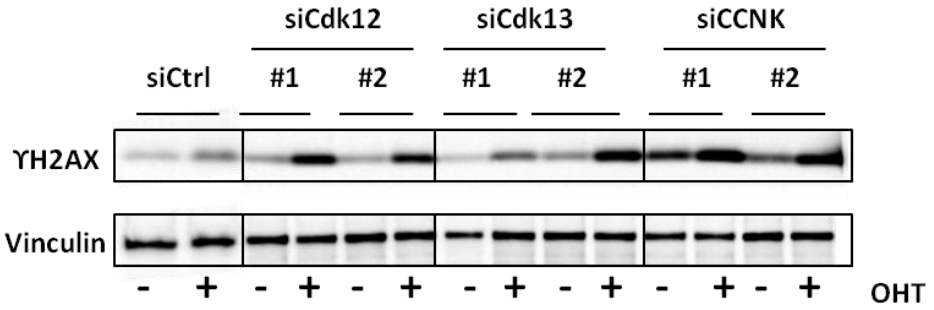

Figure 3.18. Western blot analysis for H2AX phosphorylation in U2OS-MycER cells transfected with siRNAs against Cdk12, Cdk13 and Cyclin K
Two different individual siRNAs (#1 and #2) were used for gene knock-down. A non-targeting siRNA (siCtrl) was used as a control. Cells were treated with OHT or with ethanol at the same time of transfection, and harvested 48 hours post treatment. Vinculin was used as a loading control. Western blot analysis was performed twice with consistent results.

The Cdk12/Cyclin K complex has been shown to regulate the expression of long and complex genes (such as DNA damage response genes) through phosphorylation of C-terminal domain of RNA polymerase II (Blazek et al., 2011, Liang et al., 2015). Therefore, we sought to investigate the expression of some DDR genes that was shown to be deregulated upon CdK12/Cyclin K depletion in previous studies (Blazek et al., 2011, Liang et al., 2015). Myc-activated and non-activated cells depleted of Cdk12, Cdk13 and Cyclin K as well as siCtrl-transfected cells, were harvested at 48 hours post transfection and analyzed for expression of ATM, FANCD2 and ATR genes. To our surprise, quantitative RT-PCR of the tested DDR genes did not show any significant reduction in the mRNA level (Figure 3.19). Therefore, more thorough analysis is needed to investigate the possible role of Cdk12/Cyclin K in regulating DDR genes.

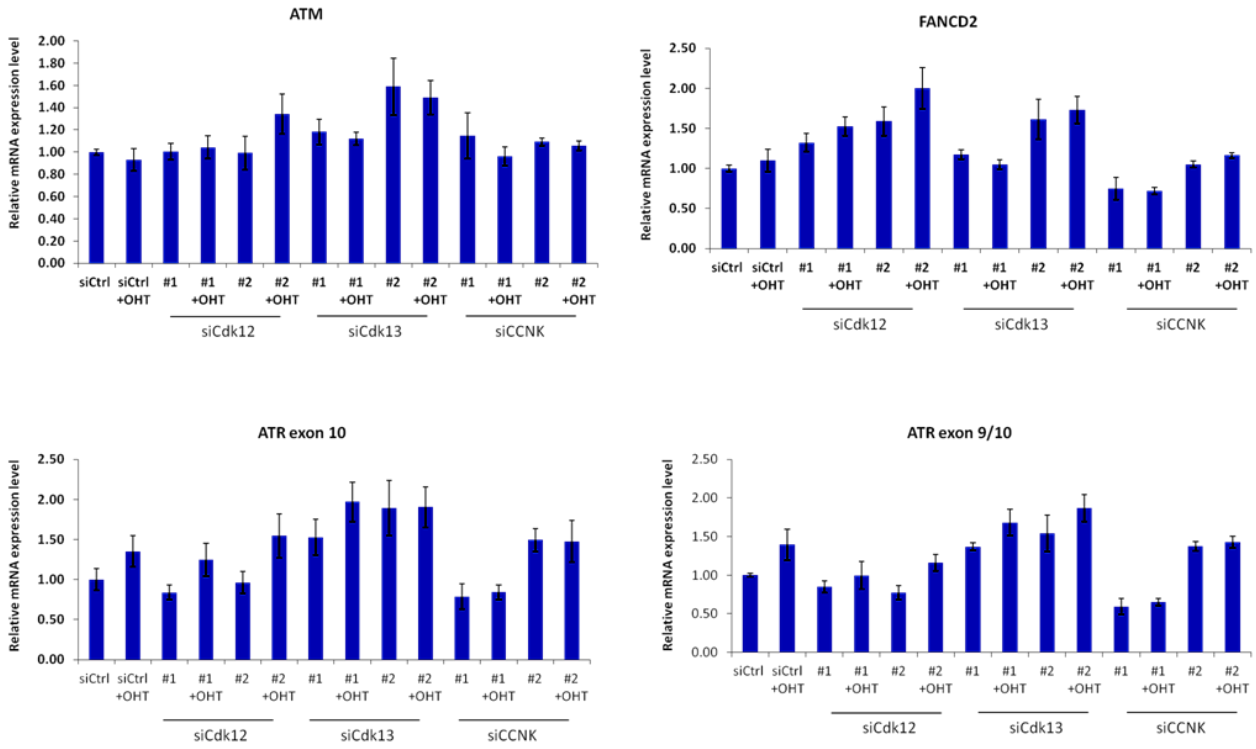

Figure 3.19. Quantitative RT-PCR analysis of ATM, FANCD2 and ATR expression level in Cdk12, Cdk13 and Cyclin K-silenced cells

Two different siRNAs (#1 and #2) were used for each gene silencing. Primers for amplifying ATM and FANCD2 are either exon-exon spanning or intron-flanking. For ATR amplification, one intron-flanking primer pair (ATR exon9/10) and one intron-spanning primer pair (ATR exon10) were used. Relative mRNA expression was measured using ΔCt method, normalized with a housekeeper gene (RPLPO) and is plotted relative to the control (siCtrl) cells. Values are the mean ± sd.

In summary, we validated synergistic effect of Myc-induced DDR with depletion of two hits from siRNA screen (Cdk12 and SRSF3) in U2OS-MycER cells. Further studies are needed for unraveling the mechanism behind these effects.

3.8 Validation of the synthetic lethal interaction linking the Myc oncogene to Rad21 depletion

During the set-up of the RNAi screen, by comparing the identified hits with the positive control (siRad21) we saw very robust synthetic lethality and a remarkable enhancement of ϒH2AX in Rad21-depleted cells upon Myc activation. In addition, the fact that this synthetic lethality is observed in different cellular models (R26-MycER MEF, shown in figure 3.8, and NMuMG-MycER cells, data not shown) proposed a strong interaction between Myc and Rad21. As the mechanism of this synthetic lethal interaction has not been investigated, we sought to explore some underlying mechanisms that might account for this effect.

3.8.1 Rad21-Myc synthetic lethality is subsequent to the accumulation of cytotoxic DNA damage

To validate Myc-SL with Rad21 depletion we selected the human osteosarcoma cell line U2OS and generated a stable cell line with conditional Myc-estrogen receptor (ER) fusion protein (U2OS-MycER). These cells were then transfected with either a siRNA against human Rad21 (siRad21) or a non-targeting siRNA (siCtrl) as a negative control and simultaneously were treated with OHT, to activate Myc, or ethanol, as a control. Cell proliferation and cell death were monitored at 24, 48 and 72 hours post siRNA transfection/Myc activation. The growth curve of siRad21-transfected cells displayed a reduction in cellular growth compared to control cells (Figure 3.20A), while cell viability was not dramatically changed, suggesting a role for Rad21 in cell cycle progression and proliferation. Activation of Myc in Rad21-silenced cells showed a further decrease in cell growth which was mostly because of the cell death. These cells displayed a striking

reduction in cell number at 72 hours post siRad21 transfection/Myc activation that was concordant with robust cell death at this time (Figure 3.20B and 20C).

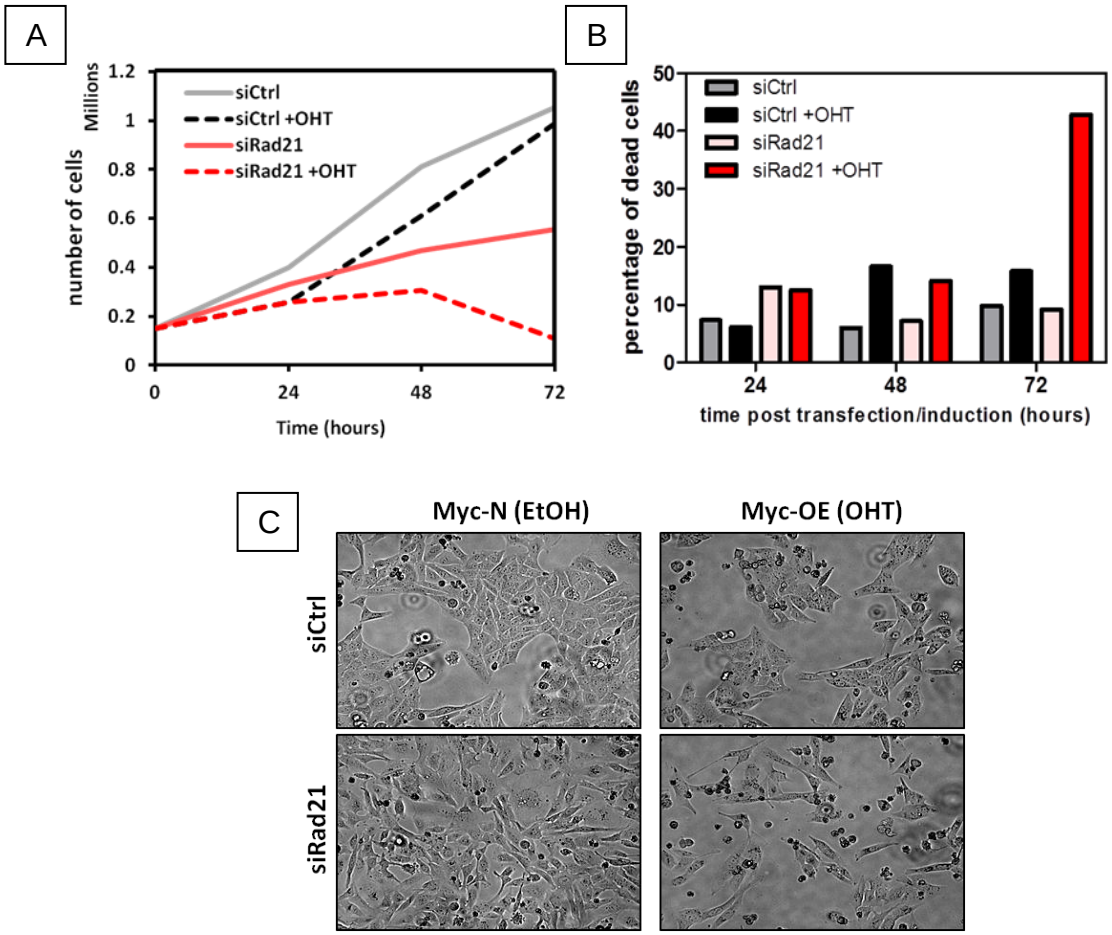

Figure 3.20. The effect of Rad21 silencing on the cell growth of normal and Myc-overexpressing cells

At time 0, U2OS-MycER cells were transfected with Rad21 siRNA (siRad21) or a non-targeting siRNA (siCtrl) and simultaneously treated with ethanol or OHT. The cells were counted at 24, 48 and 72 hours post transfection. (A) Growth curve of siRNA-transfected cells over a period of 3 days post transfection. (B) Percentages of the dead cells assessed by trypan blue staining. (C) Representative picture of transfected/treated cells after 72 hours. Comparable results were obtained in at least five independent experiments. siCtrl: control siRNA, siRad21: siRNA against Rad21, Myc-N: normal Myc level, Myc-OE: Myc overexpression, EtOH: ethanol.

Previously in our siRNA screen Myc-Rad21 synthetic lethality was paralleled by an increase in the percentage of ϒH2AX positive cells, for this reason we examined H2AX phosphorylation in U2OS-MycER transfected cells over time. siRNA-transfected cells

were harvested at 24, 48 and 72 hours post transfection and analyzed by ϒH2AX western blotting (Figure 3.21A). Consistent with previous data, we observed a substantial increase of ϒH2AX in Rad21-depleted cells that were treated with OHT. The enhancement in H2AX phosphorylation was more evident starting from 48 hours post siRNA transfection and Myc overexpression, when there was no massive cell death in the population, implicating that the accumulation of DNA damage preceded by time and most likely account for the cytotoxic effect seen at later time points.

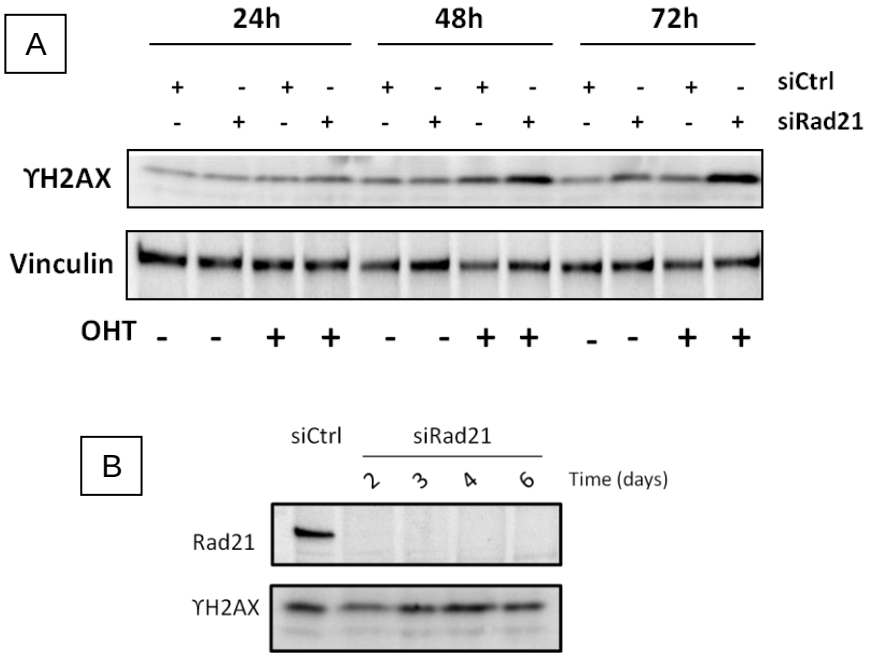

Figure 3.21. Western blot analysis of U2OS-MycER transfected cells
(A) U2OS-MycER cells were transfected with siRad21 or siCtrl and were treated with OHT or ethanol at the same time. Cells were harvested at 24, 48 and 72 hours post transfection and analyzed for H2AX phosphorylation by western blotting. Vinculin used as a loading control. (B) Western blot analysis of Rad21 (upper panel) and ϒH2AX (bottom panel) in U2OS-MycER cells transfected with siRad21 and harvested at the indicated times after transfection. siCtrl-transfected cells at 48 hours post transfection were used as a control. Note that cells were not treated with OHT. Western blot analyses were repeated twice with comparable results.

Therefore, we concluded that while Rad21 knock-down *per se* did not trigger DNA damage (up to 6 days after siRad21 transfection, Figure 3.21B), it synergized with Myc overexpression to induce DNA damage response. This notion was supported by ϒH2AX immunofluorescence staining. Cell staining at 48 hours post siRNA transfection displayed an increased ϒH2AX foci in siRad21-transfected Myc-activated cells compared to other experimental groups, whereas at the time of 72 hours most of these cells displayed apoptotic features with uniform ϒH2AX staining on the nuclei (Figure 3.22).

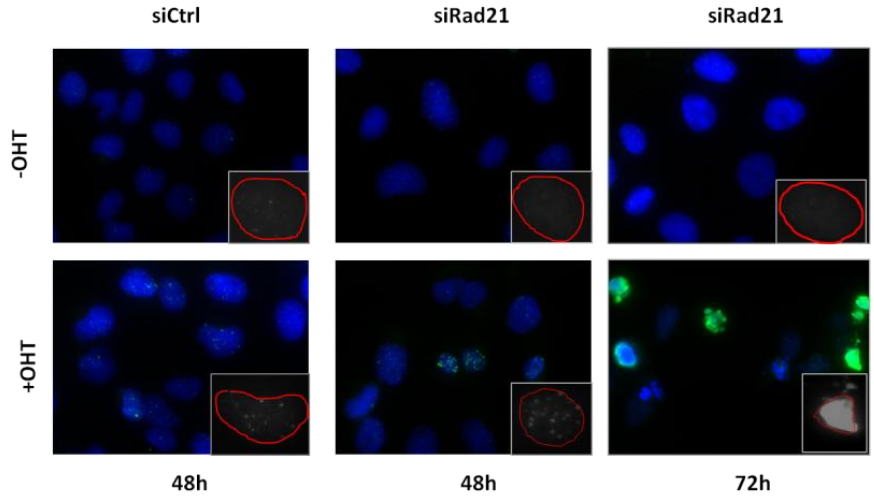

Figure 3.22. ϒH2AX immunofluorescence in U2OS-MycER cells
siCtrl- or siRad21-transfected cells treated with OHT or ethanol, were fixed at 48 and 72 hours post transfection, stained with ϒH2AX (green) and counterstained with DAPI (blue). The nuclei are outlined by a red line in the enlarged images. ϒH2AX immunofluorescence was repeated twice with comparable results.

3.8.2 Rad21 depletion does not sensitize cells to DNA damaging agents

The cohesin complex has been shown to facilitate double strand break repair via homologous recombination, therefore it is conceivable that depletion of cohesion subunits under DNA damage condition -such as Myc-induced RS- might affect genome stability and cell survival. To understand the impact of Rad21 depletion on different DNA damage signaling pathways, we examined the sensitivity of Rad21-silenced cells to other types of DNA damage. For this purpose, first Rad21 was depleted in U2OS cells by the specific

siRNA and then Rad21-depleted and control cells were exposed to several different DNA damaging agents. Comparing Rad21-silenced cells with control cells, we did not see any further sensitivity in these cells when cells were irradiated with ionizing radiation (IR) or treated with DNA damagereplication stress inducing agents camptothecin (CPT) or Hydroxyurea (HU) (data not shown). We also measured the DNA damage response in these cells by western blot analysis of ϒH2AX (Figure 3.23). The enhancement of ϒH2AX in irradiated Rad21-depleted cells was comparable to irradiated control cells after 4 hours of recovery. In addition, the increased level of ϒH2AX was declined to a similar level in control and in Rad21-silenced cells at 24 hours after irradiation, suggesting that Rad21-depleted cells were able to sense and respond to DNA damage induced by IR. Furthermore, siRad21-transfected cells subjected to CPT or HU for 4 hours, showed reduced H2AX phosphorylation compared to siCtrl-transfected cells treated with the same drug. This low level of ϒH2AX in CPT-treated cells increased with time and reached the same level as in siCtrl-transfected cells after 24 hours of treatment. Since CPT-mediated DNA damage is shown to be largely replication-dependent (Cliby et al., 2002), the lower ϒH2AX level in siRad21-transfected cells after 4 hours of treatment may refer to the lower percentage of cells in S-phase compared to siCtrl-transfected cells. The amount of ϒH2AX in Rad21-depleted cells after 24 hours treatment with HU was still lower than the control cells, which may be due to the role of HU in preventing S-phase progression in cells.

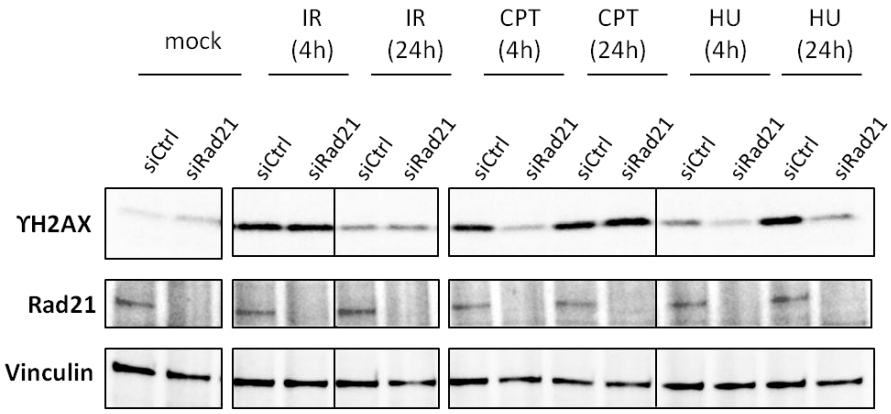

Figure 3.23. Analysis of DNA damage response in siCtrl- and siRad21-transfected cells upon exposure to different DNA damage agents
U2OS cells were first transfected with siCtrl or siRad21 and at 48 hours post transfection cells were exposed to different DNA damaging agents. At the indicated times, the cells were harvested and subjected to western blot analysis for ϒH2AX (upper panel), Rad21 (middle panel) and vinculin (bottom panel). The dose of IR used was 10 Gy. The final concentration of the drugs was 1 μM for CPT and 2 mM for HU. The times indicated for IR irradiation are the recovery time after 10 Gy IR. For CPT and HU the incubation times with the drug are shown. The experiment was performed once.

3.8.3 Myc overexpression in Rad21-depleted cells enforces DNA synthesis and provokes replicative stress

Considering the direct role of Myc in promoting DNA synthesis and the fact that Rad21 depletion was reported to slow down S-phase (Guillou et al., 2010), we asked whether Myc activation would alter the cell cycle distribution of Rad21-silenced cells. To address this question we determined the cell cycle profile of siCtrl- or siRad21-transfected U2OS-MycER cells (with and without Myc activation) at 24, 48 and 72 hours post transfection. Cell cycle analysis of Rad21-depleted cells showed a progressive decrease in the percentage of S-phase and an increase in the G1 phase of the cell cycle over time (Figure 3.24), confirming that Rad21 down-regulation affected S-phase entry in these cells. However, the population of S-phase cells in Rad21-silenced cells that were overexpressing Myc, was not significantly affected compared to control cells.

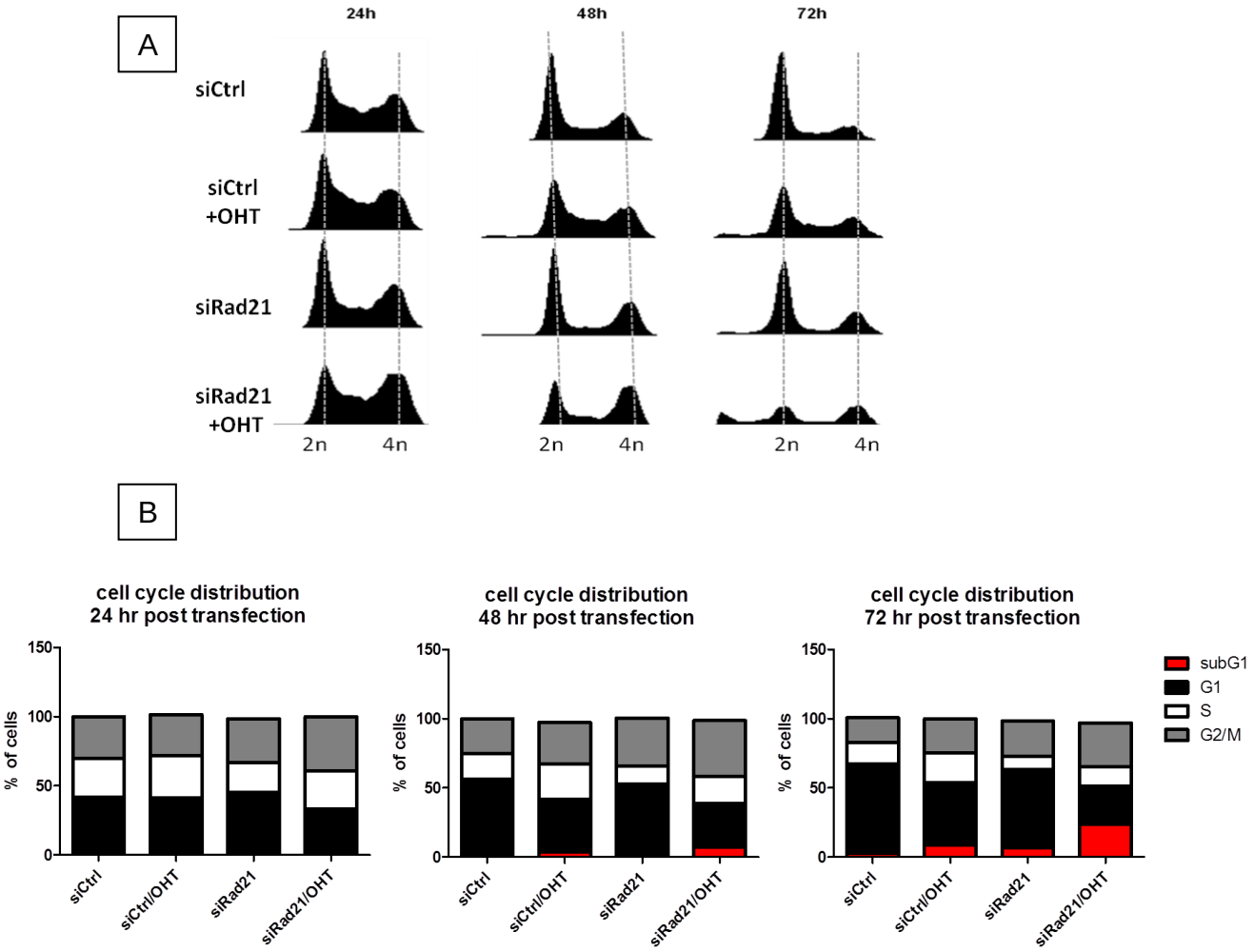

Figure 3.24. Cell cycle analysis of U2OS-MycER cells at different time post siRNA transfection

U2OS-MycER cells were transfected with siCtrl or siRad21 and treated with OHT or ethanol. Cells were collected after 24, 48 and 72 hours of transfection/treatment and stained with propidium iodide (PI). (A) FACS profiles of PI-stained cells showing DNA content. (B) Percentage of cells in each phase of the cell cycle is plotted. Comparable results were obtained in at least three independent experiments.

To measure DNA synthesis more precisely, we assessed the level of BrdU incorporation in Rad21-depleted cells and in relative controls, by BrdU pulse labeling of the cells at 48 hours post siRNA transfection (siCtrl or siRad21) and Myc activation. FACS analysis showed a higher percentage of BrdU positive cells in Myc-overexpressing cells (57%) compared to control cells (47%). Moreover, Rad21-depleted cells showed a striking reduction in BrdU incorporation (18%) while the G1 population was remarkably

increased (Figure 3.25). However, the BrdU positive population in Myc-overexpressing cells that were transfected with siRad21 just showed a slight reduction (35%) compared to siCtrl-transfected cells with normal Myc level (47%). Noteworthy, we also noticed a significant increase in G2/M phase of Rad21-depleted cells overexpressing Myc (Figure 3.25B) that could be due to the activation of G2 checkpoint in these cells.

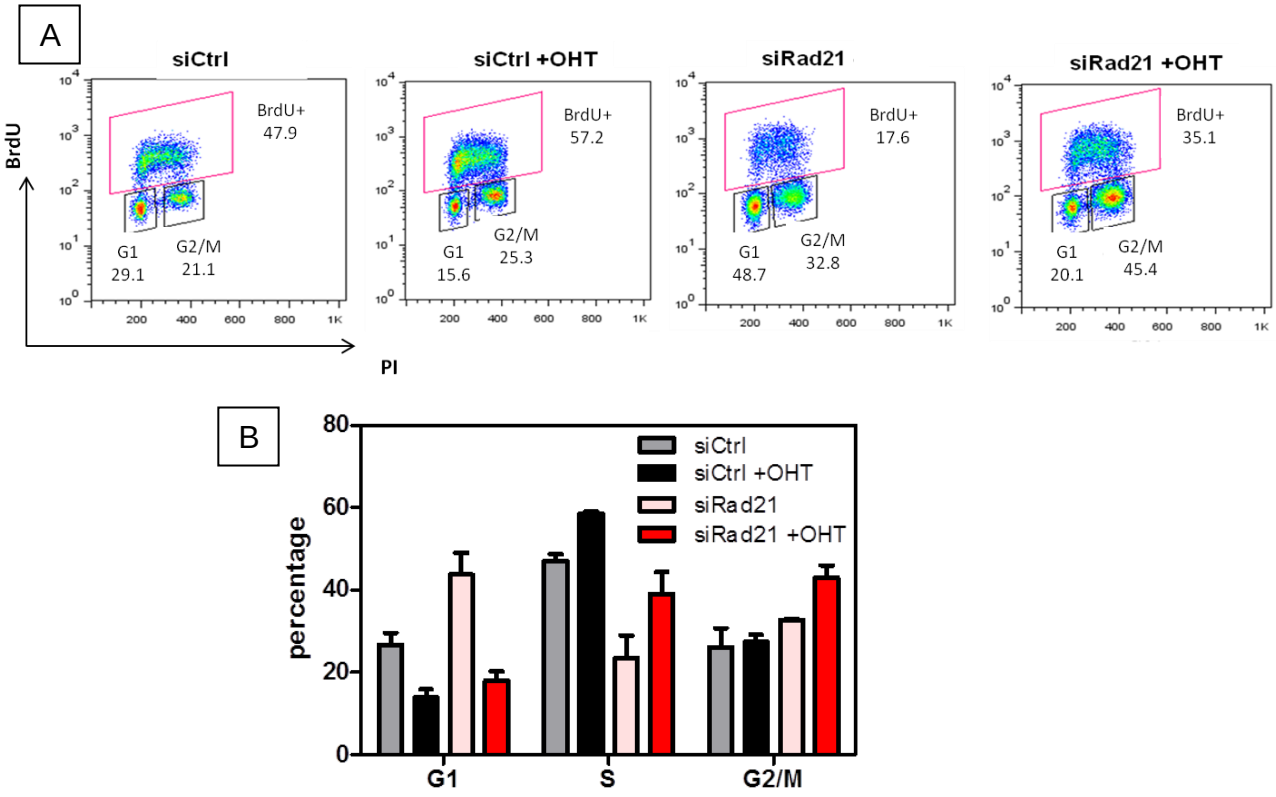

Figure 3.25. FACS analysis of BrdU incorporation in U2OS-MycER transfected cells

Cells were transfected with siCtrl and siRad21 and simultaneously were treated with OHT or ethanol. At 48 hours post transfection, cells were pulsed with BrdU for 30 minutes, then collected and subjected to BrdU staining followed by flow cytometry analysis. (A) FACS profiles depicting BrdU incorporated population in pink gates. The G1 and G2/M populations were shown in black gates. (B) The percentage of cells is each phase of the cell cycle as determined by BrdU staining is plotted. Values are the means from three independent replications. Error bars indicate standard deviation.

Taken together we hypothesized that while Rad21 depletion negatively affects DNA synthesis, ectopic activation of Myc is able to enforce the cells into S-phase. As Myc activation was performed simultaneously with siRad21 transfection, we wondered whether Myc prevents or whether it rescues the S-phase defect of Rad21-silenced cells. To address this question, Rad21 was first depleted in U2OS-MycER cells by using specific siRNA and 24 hours post transfection the transfected cells were synchronized in G2/M by Nocodazole treatment. The mitotic-arrested cells were then collected by mitotic shake off and released into the medium containing OHT (to activate Myc) or ethanol (as control) supplemented with BrdU. Quantification of BrdU-immunofluorescent cells over time after nocodazole release displayed a significant increase in the percentage of BrdU positive cells in Myc-overexpressing cells compared to cells with endogenous level of Myc (Figure 3.26). In addition there was a remarkable decrease in the percentage of BrdU positive cells that were transfected with siRad21. Interestingly, Myc overexpression in these cells led to a significant increase in the S-phase population measured by BrdU incorporation (Figure 3.26). This enhancement in the percentage of BrdU-positive cells was still lower than control cells suggesting that Myc is able to promote DNA synthesis in slow-growing Rad21-depleted cells and thus partially rescue the S-phase defect and the G1 arrest observed in these cells.

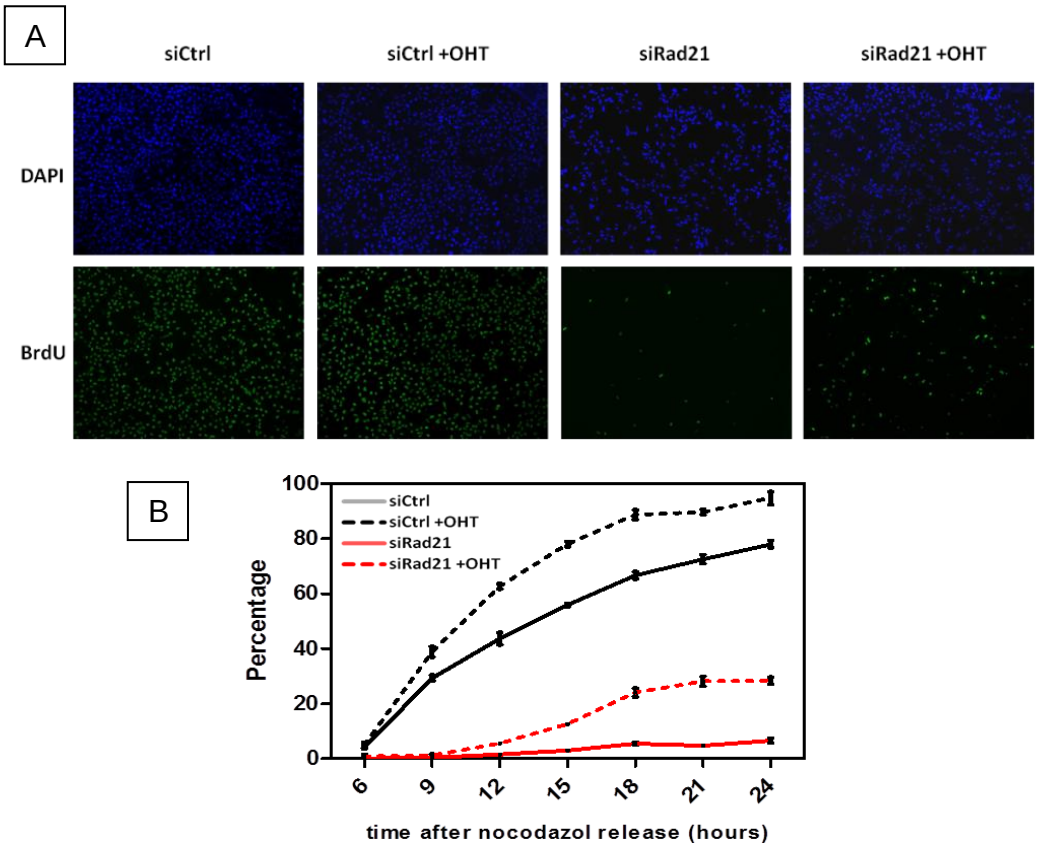

Figure 3.26. Immunofluorescence analysis of BrdU incorporation in U2OS-MycER cells released from nocodazole arrest

siCtrl or siRad21-transfected cells, at 24 hours post transfection, were synchronized in G2/M phase by nocodazole treatment. Mitotic arrested cells were then collected and released into the medium containing OHT or ethanol and supplemented with BrdU. Cells were fixed at specified time points and stained with an anti-BrdU antibody. (A) Representative images of BrdU immunostaining in cells at 18 hours post release. (B) Quantification of the percentage of BrdU-positive cells in 24 hours time frame post release. The experiment was performed once. Values are the mean ± sd of five field of view (magnification ×4) with total number of 1500 nuclei.

Notably, BrdU immunofluorescence in Rad21–silenced cells in asynchronous population exhibited a large number of nuclei having very few dispersed BrdU spots (Figure 3.27A). This staining pattern is known to be typical of late S-phase cells, however sub-dividing S-phase cells based on FACS profile to early, middle and late S-phase in siRad21-transfected population yielded equal percentages in each sub-class, that was comparable with control cells. This led us think that Rad21-depleted cells may have defects in DNA replication. The dispersed BrdU foci were also present in siRad21-transfected cells

overexpressing Myc, though the percentage was lower (Figure 3.27B), suggesting that Myc may rescue the replication defects in Rad21-depleted cells. Noteworthy, these cells also showed higher percentage of late S-phase and G2/M population. Therefore the nuclei with few BrdU foci, at least partly, could be the late S-phase cells.

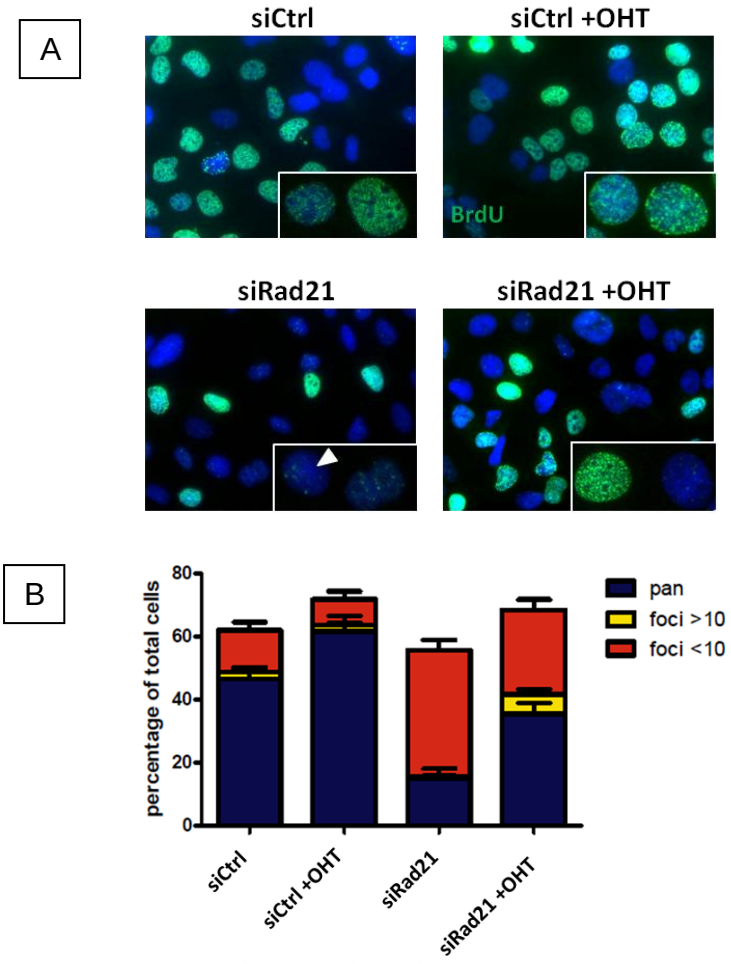

Figure 3.27. Immunofluorescence analysis of BrdU incorporation in asynchronous population of U2OS-MycER cells

siCtrl- or siRad21-transfected cells, treated with OHT or ethanol, were fixed at 48 hours post transfection and subjected to BrdU staining. (A) Representative images of BrdU immunofluorescence. Examples of nuclei having BrdU dispersed foci are depicted by arrowheads. (B) Quantification of the percentage of total BrdU-positive cells subdivided to pan, foci>10 and foci<10. The experiment was performed once. Values are mean ± sd of ten field of view (magnification ×40), with total number of 150 cells.

To investigate DNA replication kinetics and see if and how DNA replication is affected by Rad21-depletion and Myc-overexpression, we used DNA combing assay. U2OS-MycER cells were transfected with siRad21 or siCtrl and treated with OHT or ethanol. After 48 hours from transfection and Myc activation, cells were sequentially pulsed-labeled first with the thymidine analogue IdU for 30 minutes and then with CldU for 30 minutes. After genomic DNA extraction, DNA fibers were prepared by molecular combing and newly synthesized DNA, labeled with IdU and CIdU, was detected by fluorescent antibodies. Fork speed was calculated by dividing the length of each fluorescent signal by the time of the pulse. Symmetry of replication fork progression was also analyzed considering the velocity of the left and right arms of replication fork of a given origin. The inter-origin distance that reflects the number of fired replication origins was also measured on individual DNA fibers.

The DNA combing results displayed a higher fork progression rate in Rad21-depleted cells regardless of Myc overexpression (0.8 Kb/min in siCtrl and 1.2 Kb/min in siRad21) and a slightly higher inter-origin distance in Rad21-depleted cells (Figure 3.28A and Figure 3.28B). Notably, Rad21 silencing caused a dramatic increase in the percentage of unidirectional forks (20% in siCtrl and 45% in siRad21) revealing that a considerable fraction of replication forks was prematurely terminated (Figure 3.28C).

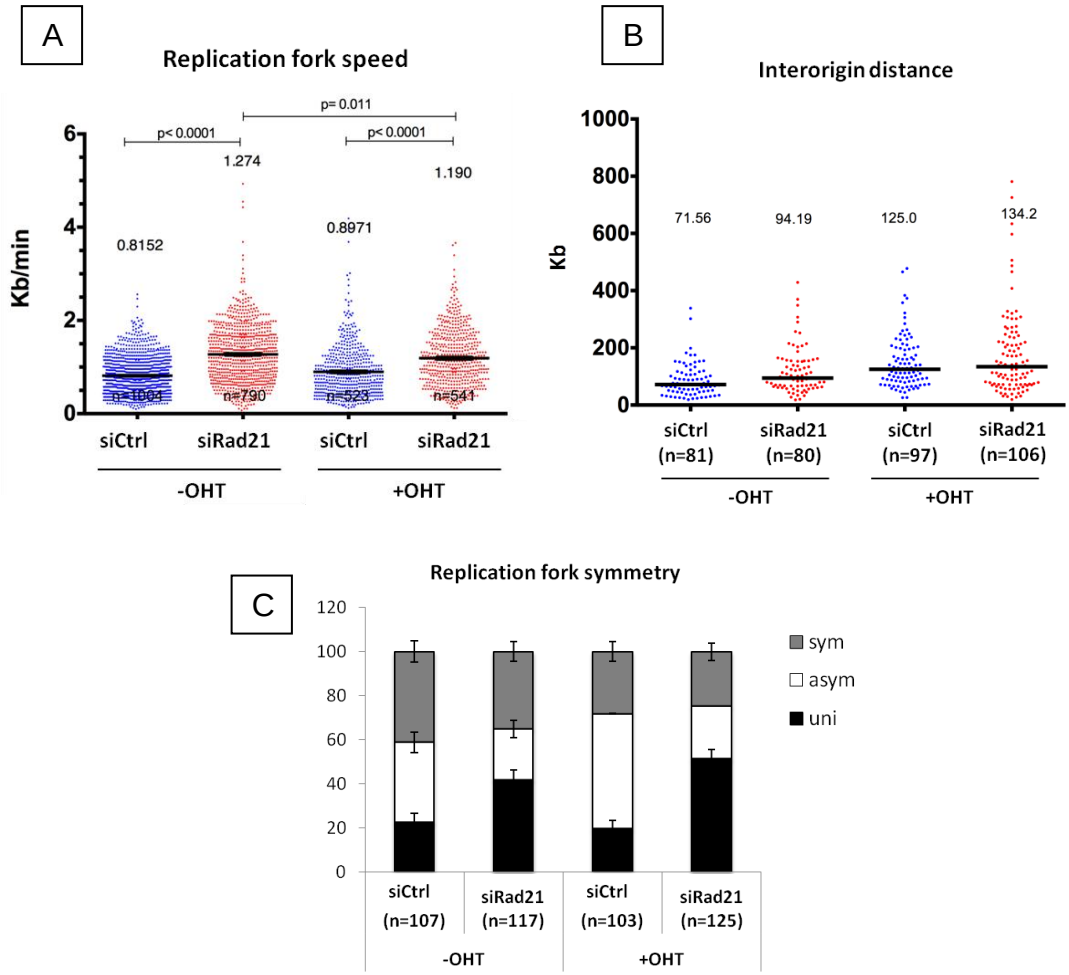

Figure 3.28. Analysis of DNA replication by DNA combing

U2OS-MycER cells were transfected with siCtrl or siRad21 and treated with OHT or ethanol at the same time. At 48 hours post transfection cells were sequentially pulsed with IdU and CldU for 30 minutes and then collected for DNA combing. Fork rate values (A) and inter-origin distances (B) were shown in scatter plots. Horizontal lines and the numbers above the plots represent mean values for fork velocity and median for interorigin distance. (C) Quantification of the symmetry of fork progression. Forks were considered as symmetric if the difference between two replication forks were less than 30%. If the difference was more than 30%, fork was considered as asymmetric. Unidirectional forks were defined if only one replication fork departs from origin. (DNA combing was performed once and in collaboration with Dr. Aurora Cerutti and Dr. Fabrizio d'Adda di Fagagna).

Given the fact that Myc induction enforces DNA synthesis in Rad21-depleted cells, we hypothesized that the Myc-induced synthetic lethality in the absence of Rad21 could be originated by boosting the replicative stress in these cells. To investigate the presence of replication stress in these cells, we analyzed H2AX phosphorylation as cells traverse into the S-phase of the cell cycle. The experimental design is shown in figure 3.29A. Briefly, U2OS-MycER cells were transfected with siCtrl or siRad21 and after 24 hours of siRNA transfection, cells were subjected to two rounds of thymidine arrest. Excess of thymidine inhibits DNA synthesis and thus synchronizes cells in G1/S boundary. After the first synchronization, Rad21-silenced cells, as well as the control cells, were released into a medium containing either OHT or ethanol. EdU, an analogue of thymdine, was also given to the released cells to discriminate the S-phase cells. Cells were harvested 12 hours post release and analyzed by FACS. FACS analysis of EdU incorporation and H2AX phosphorylation showed a slight increase in ϒH2AX in the EdU-positive population of Rad21-depleted cells that were treated with OHT (Figure 3.29B). To monitor ϒH2AX enhancement that may happen in the S-phase of the next cell cycle, released cells from the first thymidine block were subjected to a second round of thymidine arrest. EdU was added as the cells were released into a fresh medium. These cells were then collected at 4, 8 and 12 hours post release for FACS analysis. Cell staining using the antibodies reacting with ϒH2AX and EdU following fluorescence-activated cell sorting, exhibited progressive accumulation of ϒH2AX in the EdU-positive population of Myc-activated cells that were depleted of Rad21 compared to either Myc-activated cells or Rad21-silenced cells. In contrast, neither thymidine-arrested cells nor the cells that did not incorporate EdU displayed ϒH2AX accumulation, suggesting that the synergy between Myc overexpression and Rad21 depletion in enhancing DDR is occurring mostly in S-phase of the cell cycle and is more pronounced after long-term Myc activation.

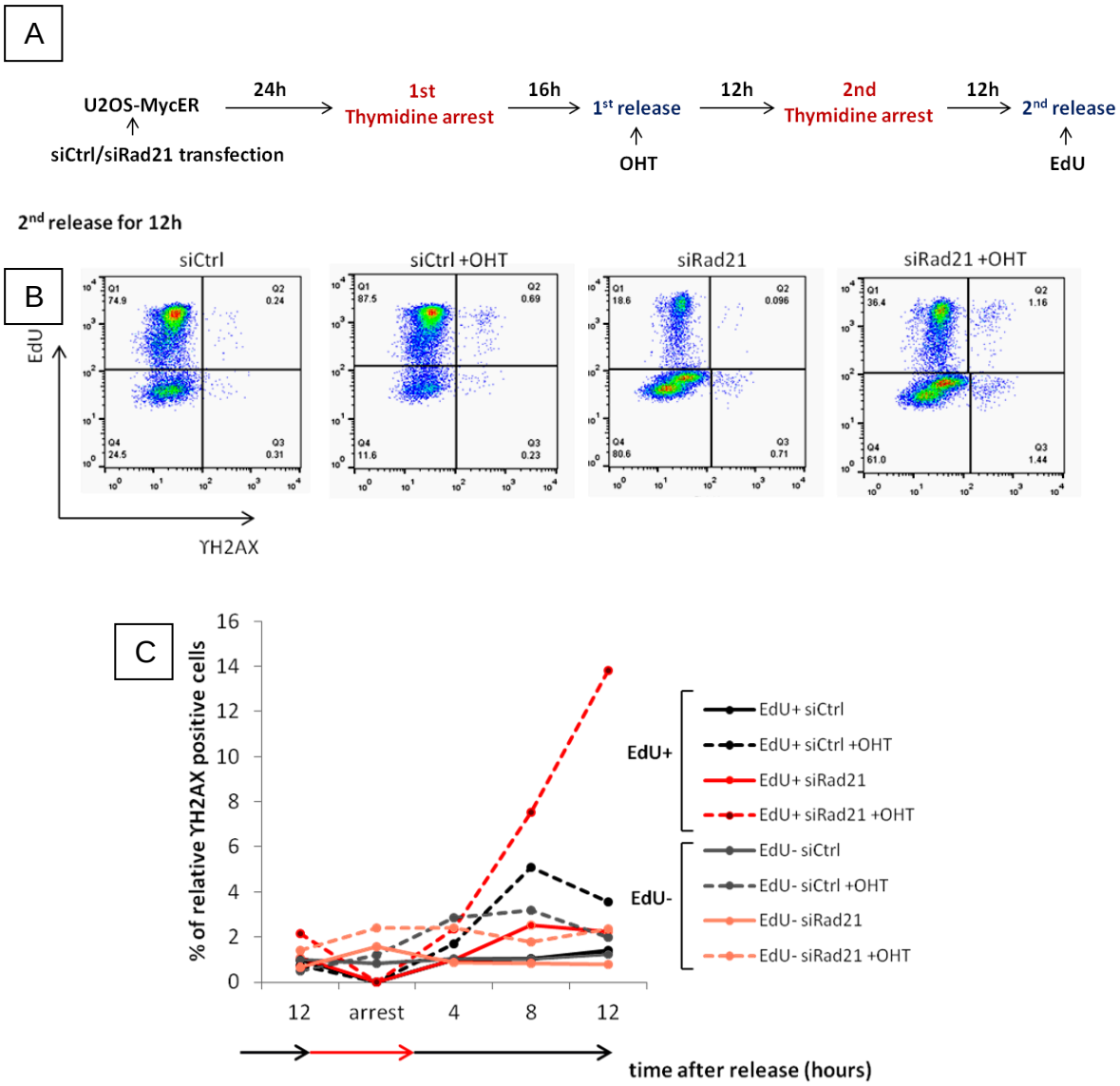

Figure 3.29. FACS analysis of ϒH2AX and EdU in U2OS-MycER cells released from thymidine arrest

Twenty-four hours post siRNA transfection, siCtrl- or siRad21-transfected cells were subjected to two rounds of thymidine arrest and release. Cells were treated with OHT or ethanol as they released from the first thymdine arrest and were kept in OHT- or ethanol-containing medium through the second arrest and release. EdU was added to the medium when the cells were released or when they were arrested by thymidine. Cells were collected at the indicated time (12 hours after the first release - before the second release - 4, 8 and 12 hours after the second release), subjected to ϒH2AX and EdU staining and followed by FACS analysis. (A) Experimental design of double thymdine arrest is depicted. (B) Representative FACS profile of ϒH2AX and EdU staining in the released cells from the second thymidine arrest for 12 hours. (C) Quantification of ϒH2AX positive cells in EdU-positive and EdU-negative populations during thymidine arrest and release. The experiment was performed once and values are normalized to the population size and are relative to control sample (siCtrl).

We also analyzed RPA foci formation as a marker of single stranded DNA that can be generated by replication stress. Quantification of the number of RPA foci in asynchronous population of transfected cells, at 48 hours post transfection, showed an increase in DNA-bound RPA in Rad21-depleted cells in the presence of elevated Myc level (Figure 3.30). All together, these results led us to propose that Rad21-depleted cells undergo replicative stress upon Myc overexpression.

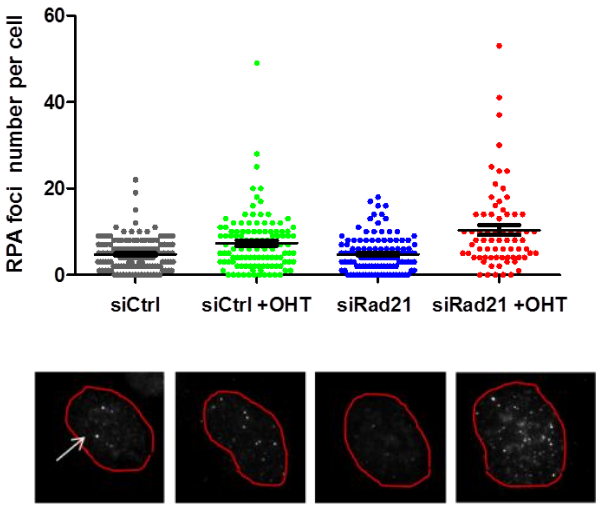

Figure 3.30. Quantification of RPA foci in U2OS-MycER cells determined by immunofluorescence
Cells were transfected with siCtrl or siRad21 and simultaneously treated with OHT or ethanol. Forty-eight hours post transfection/treatment, cells were pre-extracted, then fixed and stained for RPA. Representative immunofluorescence images of RPA staining for the indicated treatment are shown under the graph. The experiment was repeated once. Each bar represents mean ± SEM.

3.8.4 Rad21 is present in replication sites and may have a direct role in DNA replication

Since the lack of Rad21 was shown to reduce DNA synthesis by several studies as well as the current study, we asked whether RAD21 protein has a direct function in DNA synthesis. Therefore we applied native iPOND technique to isolate the proteins on newly-synthesized DNA and to see whether RAD21 is among the replication associated proteins. To this end, asynchronous U2OS cells were shortly pulsed with EdU (10

minutes), then harvested and lysed with the nuclear extraction buffer. After a step of adding biotin-azide to EdU (named click reaction), biotinylated chromatin was captured by streptavidin beads and western blot analysis was used to identify RAD21 protein. To distinguish the replication-associated proteins from the other chromatin bound proteins, a part of U2OS cells after EdU pulse was briefly washed with equilibrated media (37°C and 5% CO_2) and then chased with thymidine for an hour. Thymidine competes with residual EdU inside the cells to be incorporated into DNA and in this way the replication-associated proteins travel far from the EdU incorporated region.

Along with replisome component PCNA, native iPOND revealed an enrichment of RAD21 protein in EdU-pulsed sample, but not in the thymidine-chased sample or the sample that omits the biotin-azide during the click reaction (Figure. 3.31).

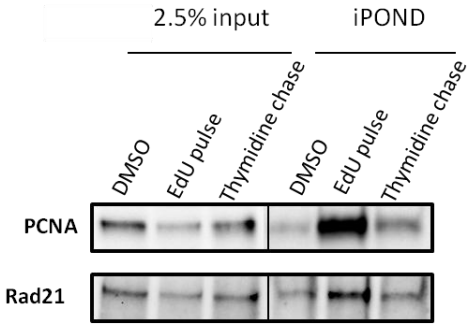

Figure 3.31. Western blot analysis of the input and the captured proteins following native iPOND on U2OS-MycER cells
U2OS-MycER cells were pulsed with EdU for 10 minutes and then harvested for iPOND. In thymidine chase sample, after EdU pulse, the medium was washed out and cells were incubated with thymidine-containing medium for 1 hour. In DMSO control, no biotin was added in the click reaction. Comparable results were obtained with two independent experiments.

3.8.5 Myc overexpression induces phosphorylation of p53 and leads to G2/M arrest in Rad21-depleted cells

Cell cycle analysis showed the majority of Myc-activated siRad21-transfected cells arrested in G2/M phase of the cell cycle (Figure 3.25), therefore we hypothesized that

accumulation of DNA damage during S-phase in these cells may lead to activation of G2 checkpoint and eventually cell cycle arrest. To test this hypothesis, we sought for the different DDR-mediated modifications on the DNA damage response factors in Myc-activated Rad21-silenced cells by western blotting.

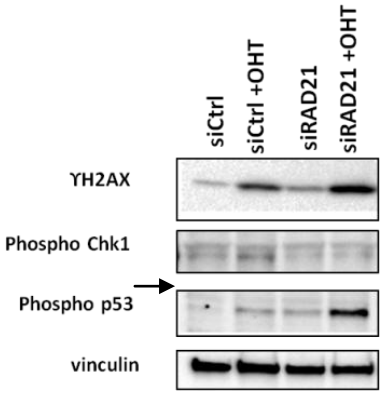

Figure 3.32. Western blot analysis for different DDR marker in U2OS-MycER cells

U2OS-MycER cells were transfected with siCtrl or siRad21 and simultaneously were treated with OHT or ethanol. Cells were harvested at 48 hours post transfection and subjected to western blot analysis. Comparable results were obtained with two independent experiments.

Western blot analysis for phospho-Chk1 showed a slight increase in the phospho-Chk1 band in Myc-overexpressing cells, however Rad21-depleted cells with normal or high level of Myc did not show any band corresponding to phospho-Chk1 (Figure 3.32), indicating that the ATR/Chk1-mediated checkpoint may not be strongly engaged in these cells. We also looked at the phosphorylation of p53 as one of the downstream targets of the ATR/ATM signaling pathway. Western blot analysis showed that p53 is strongly phosphorylated at serine 15 in Rad21-depleted/Myc-overexpressing cells in comparison with a slight increase observed in Myc-overexpressing cells or Rad21-depleted cells (Figure 3.32). Since these cells are mainly arrested in G2/M, we hypothesized that activation of ATM and its downstream target, p53, is responsible for this phenotype. In agreement with our hypothesis, ATM inhibition by caffeine treatment decreased the

percentage of G2/M population of Rad21-depleted/Myc-overexpressing cells compared to the cells that were not treated with caffeine (Figure 3.33). In addition, the reduction in G2/M population was accompanied by a slight increase in the sub-G1 population, while the percentage of G1 and S-phase was not remarkably changed. These results propose that most probably ATM-mediated checkpoint was activated upon Myc activation in Rad21-depleted cells and by causing G2 arrest may exert a protective role against mitotic catastrophe in these cells.

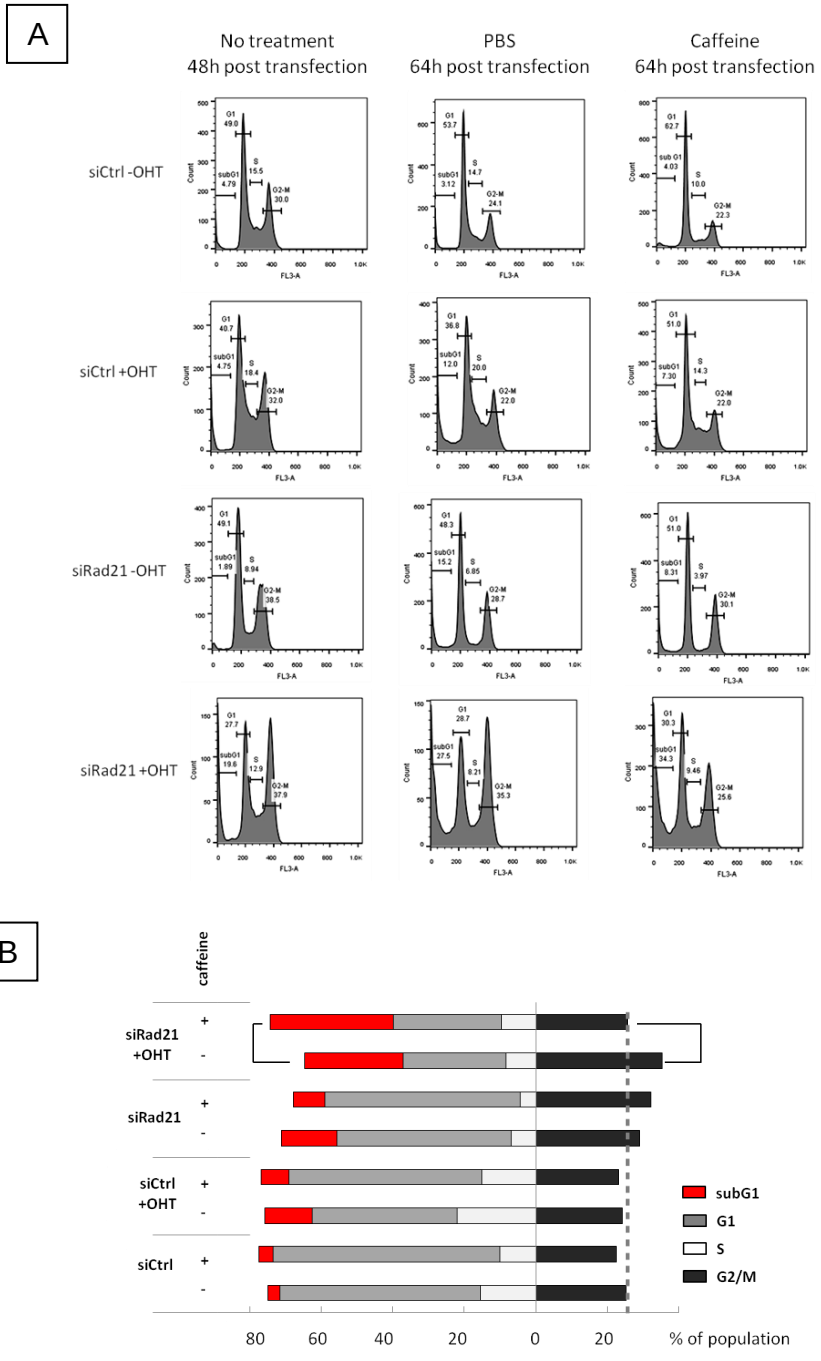

Figure 3.33. The effect of ATM inhibition in cell cycle profile of U2OS-MycER cells

Cells were transfected with siRad21 or siCtrl and simultaneously treated with ethanol or OHT. At 48 hours post transfection, cells were treated with caffeine (5 mM) or PBS (as control) for additional 16 hours. Cells were then collected and stained with propidium iodide (PI). (A) FACS profile of PI-stained cells showing the cell cycle distribution of the cells at 48 hours post transfection (before starting the treatment) and 16 hours later after caffeine or PBS treatment. (B) The percentage of cells in each phase is plotted. The experiment was performed once.

To further characterize the role of p53 in G2/M arrest observed in these cells, we depleted p53 in p53-proficient Bz1 R26MycER MEF cell line by stably overexpressing a potent shRNA targeting p53. The efficiency of p53 knock-down in these cells was assessed by treating cells with doxorubicin, a potent p53 inducer. Western blot analysis for the total p53 level showed an accumulation of the protein in doxorubicine-treated cells that stably overexpressed a non-targeting shRNA (shRenilla). In contrast in doxorubicin-treated cells stably overexpressing shp53 we did not detect any band corresponding to p53 (Figure 3.35A), indicating the potency of p53 knock-down by shRNA.

We then transfected shp53- and shRenilla-overexpressing cells with siRad21 or siCtrl and examined cell viability, cell cycle and DDR. shp53-overexpressing cells that were transfected with siRad21, unlike shRenilla-overexpressing cells, showed a slight increase in cell death upon Myc activation (Figure 3.34). However, the level of ϒH2AX accumulation detected upon Myc activation in Rad21-depleted cells was mostly unchanged between p53-silenced and control cells (Figure 3.35A and Figure 3.35B).

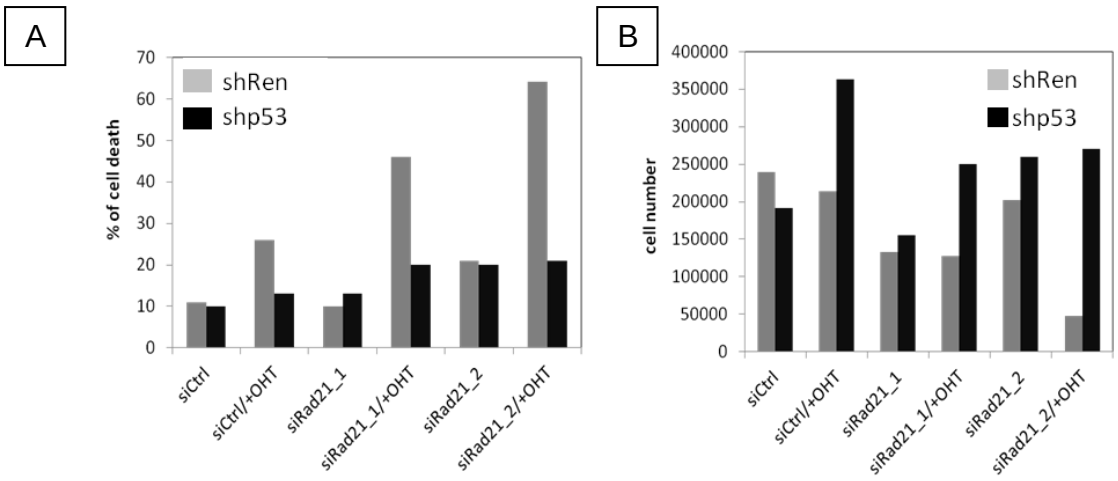

Figure 3.34. The effect of Rad21 depletion on cell death and cell growth of Bz1 R26-MycER MEF cell line

Bz1 R26-MycER cell line overexpressing shp53 or shRenilla cells were reverse transfected with 2 different siRNAs against Rad21 (siRad21_1 and siRad21_2) and simultaneously were treated with OHT or ethanol. After 48 hours from transfection, cells were collected and counted. (A) Percentage of cell death measured by trypan blue staining. (B) Quantification of the number of live cells (initial cell number was 9×10^4). The experiment was performed once.

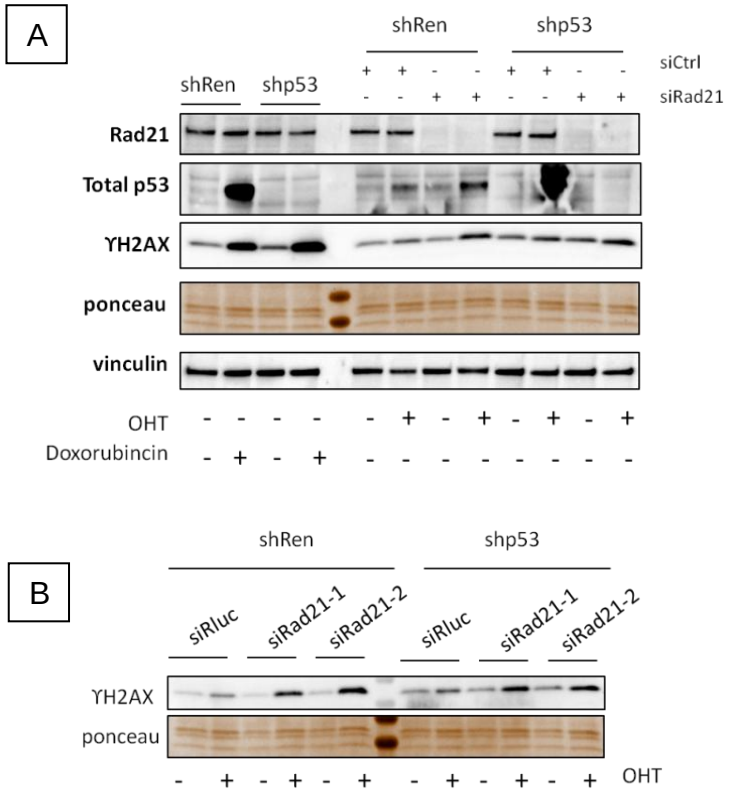

Figure 3.35. Western blot analysis of shp53- and shRenilla-overexpressing Bz1 R26-MycER MEF cell line (See figure legend next page)

(A) Cells were transfected with siRad21 or siCtrl and treated with OHT or ethanol at the same time. Cells were harvested at 48 hours post transfection and subjected to western blot analysis. The efficiency of p53 knockdown was also evaluated by detecting the accumulation of stabilized p53 upon doxorubicin treatment (1 μM for 16 h). (B) Western blot analysis for H2AX phosphorylation was repeated with two different siRad21 (siRad21_1 and siRad21_2). Vinculin and Ponceau staining for histones are shown as loading controls.

More interestingly, cell cycle analysis of Myc-induced shp53-overexpressing cells transfected with siRad21 showed a higher fraction of cells with more than 4n DNA content (Figure 3.36). These polyploid cells may be the source of reduced cell death that underwent aberrant endoreduplication. Therefore it could be interesting to monitor the cell death in long term after Rad21 knock-down to appreciate the cell death delay in p53-inactivated cells.

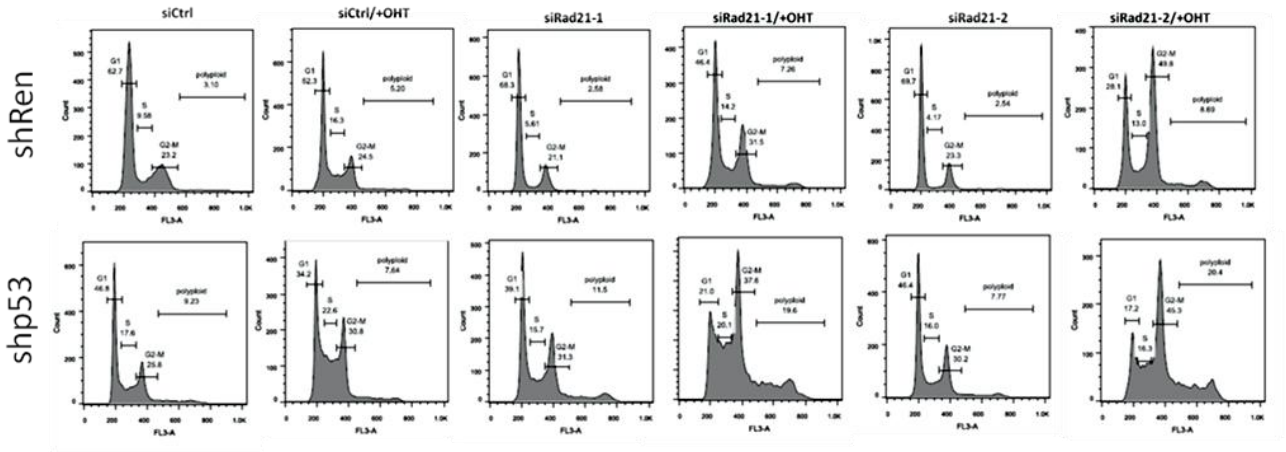

Figure 3.36. Cell cycle profile of shp3- and shRenilla-overexpressing Bz1 R26-MycER MEF line upon Rad21 depletion and Myc activation

A non-targeting siRNA (siCtrl) and two different siRNAs against Rad21 (siRad21_1 and siRad21_2) were used to transfect the cells. Cells were treated with OHT or ethanol the same time of transfection. Forty-eight hours post transfection cells were harvested and stained with propidium iodide followed by FACS analysis. The experiment was performed once.

3.8.6 Depletion of other cohesin component and cohesin loader recapitulates Rad21-Myc synthetic lethality

Although we focused on Rad21 subunit of the cohesin complex, it was interesting to know if the other cohesin components can also recapitulate Rad21-Myc synthetic lethal interaction and increase H2AX phosphorylation. For this reason, we examined the effect of depletion of the other cohesin complex Smc1, the cohesin loader Nipbl as well as Ctcf which was shown to interact with cohesin in some genomic sites on Bz1 R26-MycER MEF cell line. Silencing of Smc1, Nipbl and Ctcf significantly increased the percentage of ϒH2AX-positive cells in Myc-overexpressing cells compared to cells with normal Myc level. However the cell viability was not remarkably affected in these cells (Figure 3.37).

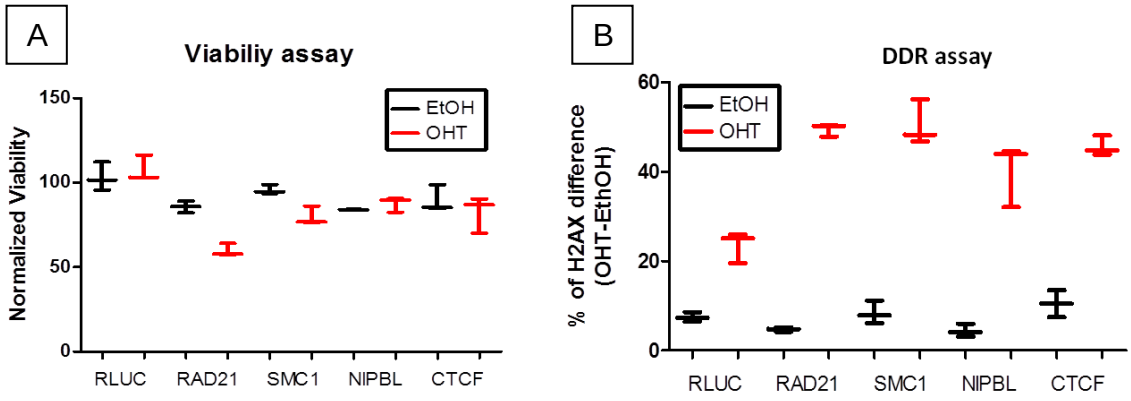

Figure 3.37. Viability and DDR assay of Bz1 R26-MycER cell line after cohesins knock-down

Cells were transfected with siRNA against Rluc (negative control), Rad21, Smc1, Nipbl and Ctcf and simultaneously treated with OHT or ethanol. Forty-eight hours post siRNA transfection, the transfected cells were fixed and were subjected to DAPI and ϒH2AX immunostaining. (A) Viability ratio of Myc-overexpressing cells (Myc-OE) to cells with normal Myc level (Myc-N) assessed by DAPI staining. Values are normalized to the siRluc-transfected cells. (B) Percentage of ϒH2AX pan-positive nuclei in transfected cells in the presence or absence of OHT. The assays were performed in triplicates (The data is produced by IIT screening unit).

To further characterize the impact of cohesin depletion on Myc-overexpressing cells, U2OS-MycER cells were transfected with siRNAs against Smc3 and Nipbl and simultaneously treated with OHT -to induce Myc activation- or ethanol as control. These cells were collected at 48 hours post transfection for RNA and protein extraction as well as for cell viability and cell cycle analyses.

First, we checked the efficiency of gene knock-down by measuring the mRNA expression level of Smc3 and Nipbl. Real time RT-PCR showed an efficient knock-down of Smc3 and Nipbl at the RNA level (Figure 3.38).

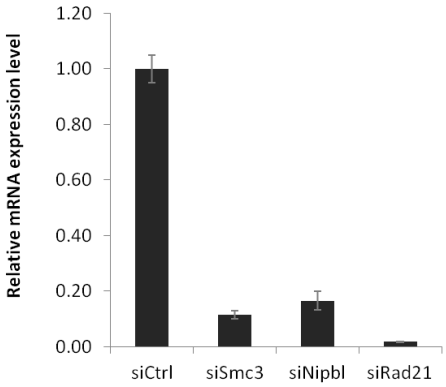

Figure 3.38. RT-qPCR analysis of Smc3, Nipbl and Rad21 expression level after siRNA knock-down

U2OS cells were transfected with the corresponding siRNA and 48 hours later were harvested for RNA extraction and cDNA synthesis. Relative mRNA expression was measured using ΔCt method, normalized with a housekeeper gene (RPLPO) and is plotted relative to the control (siCtrl) cells. Error bars indicate standard deviation.

We also assessed the viability of the cells by trypan blue staining. Comparable to Rad21-Myc synthetic lethality, we observed a significant reduction in the viability of cohesin-depleted cells in the presence of elevated Myc level (Figure 3.39).

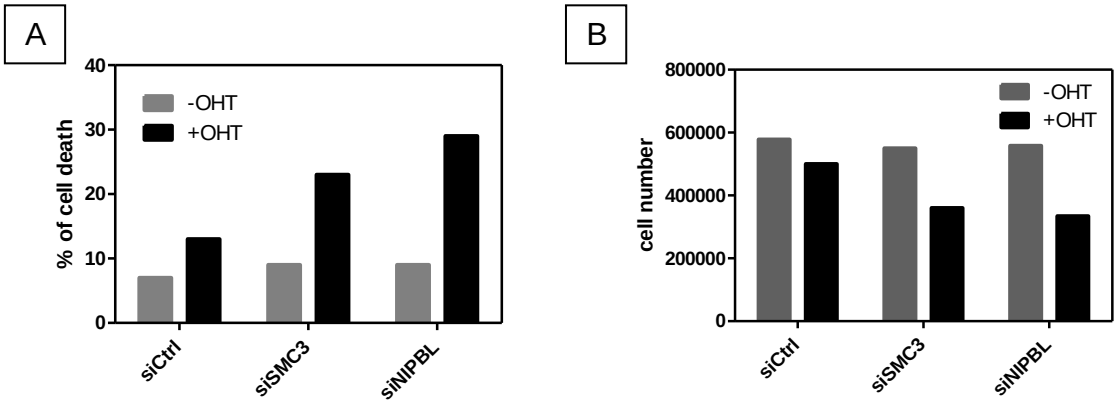

Figure 3.39. The effect of Smc3 and Nipbl depletion on cell death and cell growth of U2OS-MycER cells

Cells were transfected with siRNAs against Smc3 and Nipbl and treated with or without OHT. Forty-eight hours post transfection/treatment the cells were collected, stained with trypan blue and counted. (A) Percentage of dead cells and (B) the number of live cells were plotted. The experiment was performed once.

In addition, western blot analysis for ϒH2AX displayed a synergy between cohesin-depletion and Myc-induced DDR (Figure 3.40).

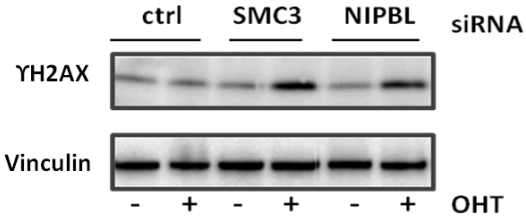

Figure 3.40. Western blot analysis for H2AX phosphorylation in U2OS-MycER cells

U2OS-MycER cells were transfected with siSmc3, siNipbl and siCtrl and were treated either with OHT or with ethanol. Cells were harvested 48 hours after transfection. Vinculin served as a loading control.

Unlike the remarkable reduction of S-phase in Rad21-silenced cells, cell cycle analysis of Smc3- and Nipbl-depleted cells revealed just a slight reduction in the S-phase population (Figure 3.41). This difference could be due to the presence of residual functional protein after the gene knock-down. As RAD21 is the cleavable part of the cohesin, it may be

more feasible to achieve higher knock-down level of RAD21 compared to SMC proteins or NIPBL.

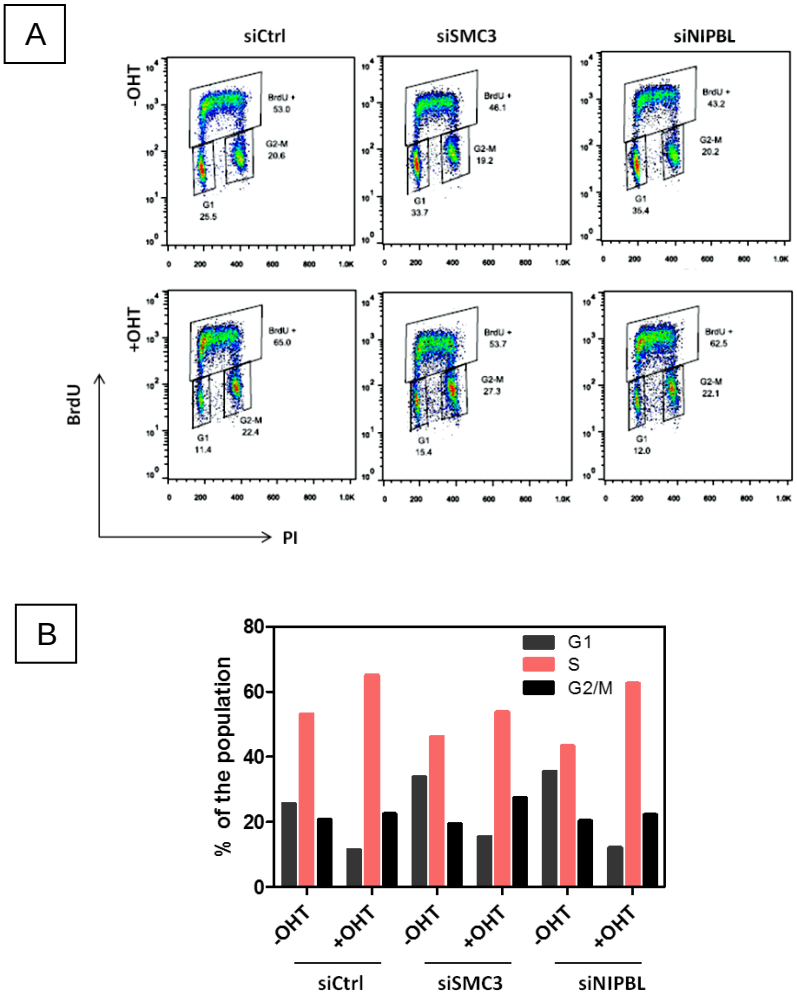

Figure 3.41. FACS analysis of BrdU incorporation in U2OS-MycER cells transfected with siSmc3 or siNipbl

At 48 hours post transfection and Myc activation, cells were pulsed with BrdU for 30 minutes, then harvested and stained with anti-BrdU antibody and propidium iodide. (A) FACS profiles showing the BrdU positive cells and the population of cells in G1 and G2/M phase of the cell cycle. (B) The percentage of cells in each phase of the cell cycle, as determined by BrdU staining, is plotted. FACS analysis was performed once.

3.8.7 Myc is unique among other oncogenes in inducing DNA synthesis in Rad21-depleted cells

We observed that Rad21 silencing synergized with Myc in inducing DNA damage and eventually lead to synthetic lethality. To investigate whether this synergy could be

generalized to other oncogenes that similarly to Myc are able to induce replication stress and subsequently DDR, we generated a stable U2OS cell lines constitutively overexpressing several oncogenes such as Cyclin E1, Ras and E2F1. These oncogene-overexpressing U2OS cell lines along with U2OS cells infected with empty vector (mock) were transfected with siRad21 and siCtrl and then were harvested 48 hours later for ϒH2AX western blot and cell cycle analyses. The analysis of DNA damage marker ϒH2AX in the oncogene-overexpressing cells displayed an increase of the ϒH2AX signal (with different extent among different oncogene-overexpressing cells) compared to mock cells (

Figure 3.42).

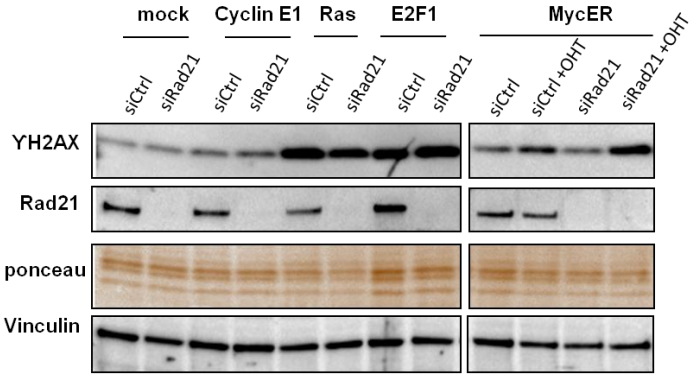

Figure 3.42. Western blot analysis of ϒH2AX in oncogene-overexpressing U2OS cells

U2OS cells stably overexpressing Cyclin E1, Ras and E2F1 along with mock cells were transfected with siCtrl or siRad21. U2OS-MycER cells were transfected with siCtrl or siRad21 and treated with OHT or ethanol at the same time. At 48 hours post transfection, cells were harvested and subjected to western blot analysis. Vinculin was used as a loading control.

Moreover, unlike Myc-overexpressing cells, cells overexpressing oncogenes (Cyclin E1, Ras and E2F1) did not show further enhancement in H2AX phosphorylation when transfected with siRad21 (Figure 3.42). Noteworthy, no sign of massive cell death was seen in these oncogene-overexpressing cells up to 72 hours post siRad21 transfection (data not shown).

Notably, cell cycle analysis of oncogene-overexpressing cells (Cyclin E1, Ras and E2F1-overexpressing U2OS cells) transfected with siRad21 revealed a reduction in S-phase population similar to mock transfected cells (Figure 3.43) suggesting that, in contrast to Myc, none of these oncogenes is capable of enforcing DNA replication and entry into S-phase under Rad21 depleted condition.

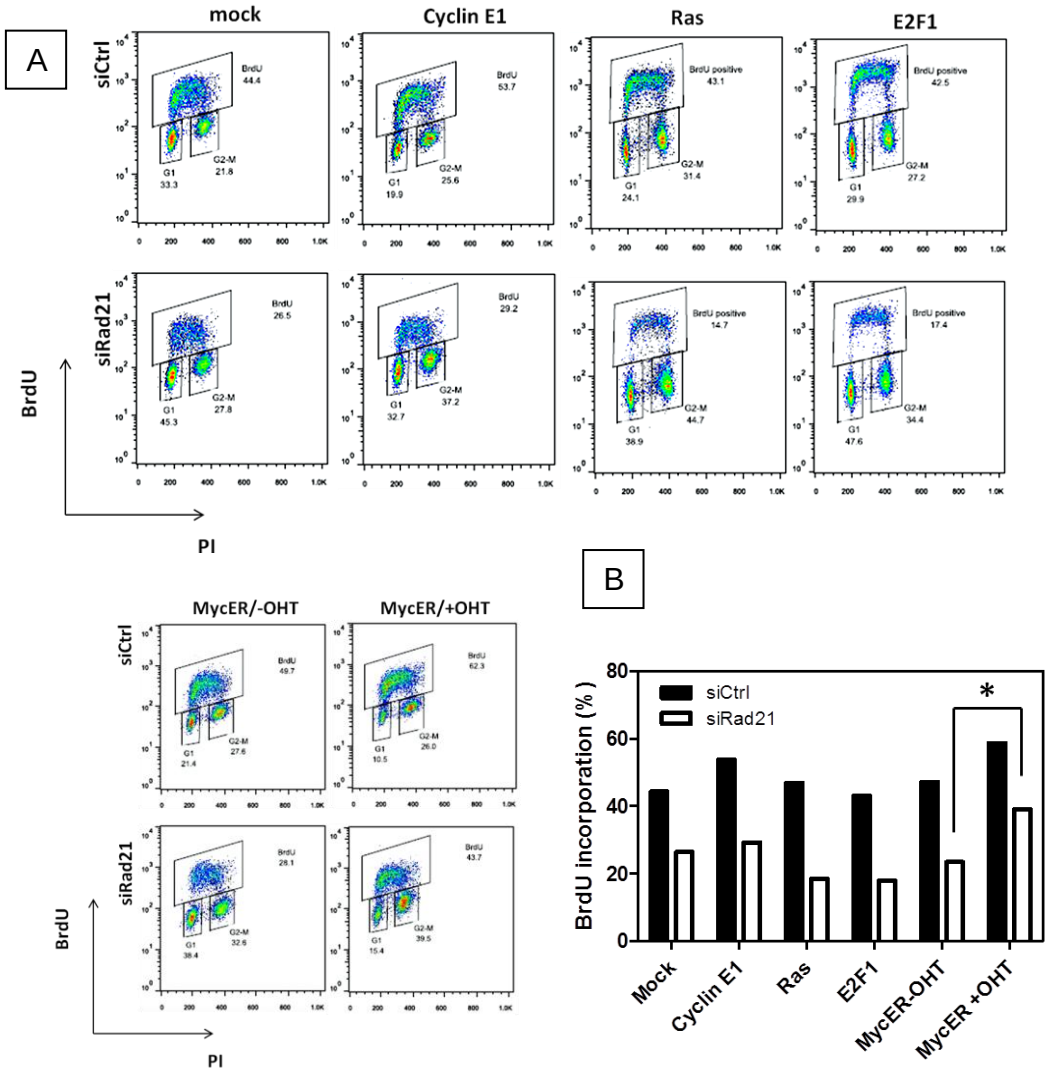

Figure 3.43. FACS analysis of BrdU incorporation in U2OS cells stably overexpressing oncogenes upon Rad21 depletion

(A) FACS profiles depicting BrdU positive population as well as population of cells residing in G1 and G2/M phase. (B) Percentage of BrdU positive cells is plotted. FACS analysis was performed three times for MycER cells (mean values are shown) and once for the rest of the cells. Asterisk indicates p-value <0.01 with the Student *t* test.

3.8.8 Myc ectopic activation partially rescues the gene expression alterations observed in Rad21-depleted cells

Since we observed that Myc is unique among other oncogenes in inducing DNA synthesis in Rad21-depleted cells, we reasoned that this effect could be at least partly due to the role of Myc in activating the transcription of a subset of genes involved in S-phase entry and progression. To investigate this possibility, we tested the expression level of several Myc-responsive genes including genes involved in nucleotide and ribosomal biosynthesis, cell cycle, DNA replication and DNA repair at 24 and 72 hours post siRNA transfection and OHT/ethanol treatment. RT-qPCR analysis revealed a modest reduction in the expression levels of most of the genes in Rad21-depleted cells, though Myc overexpression could partially rescue this effect and support gene expression to the levels seen in control Myc-overexpressing cells (Figure 3.44). These results were in line with the role of cohesin in regulating gene transcription and suggest a dominant role for Myc in inducing the transcription of at least the aforementioned subset of genes that are down-regulated as a consequence of Rad21 depletion.

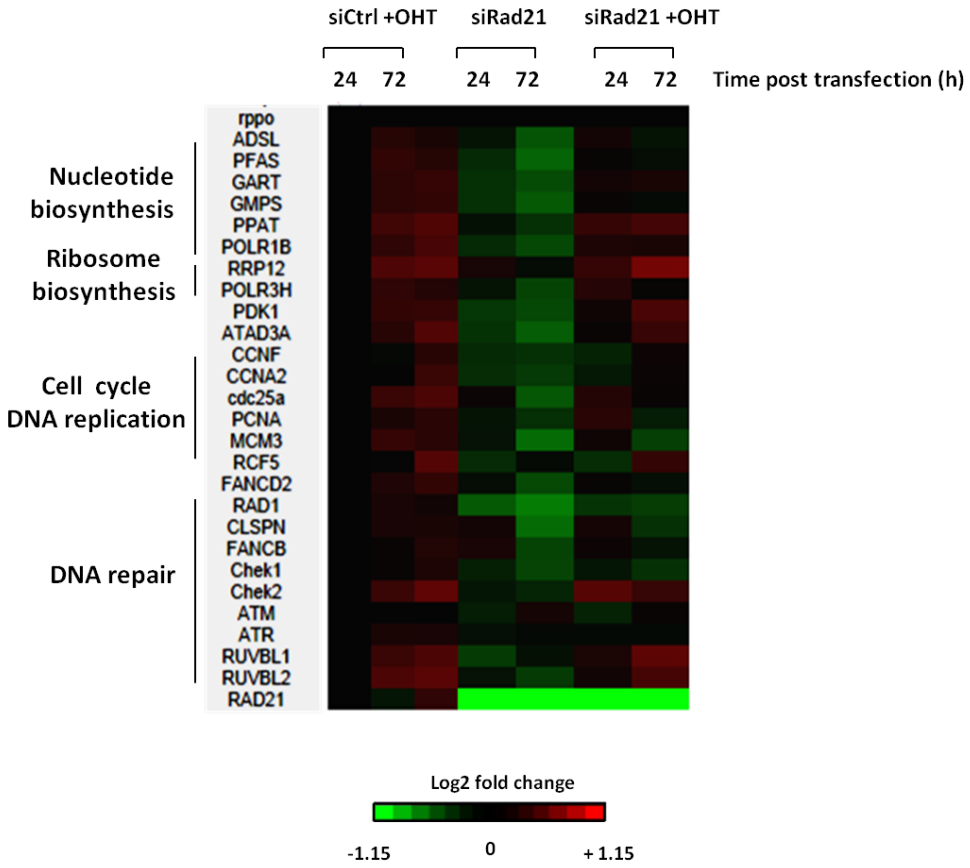

Figure 3.44. Heatmap of gene expression ratio for a subset of Myc-responsive genes

The heatmap depicts the log2 fold change expression level relative to control sample (siCtrl) measured by RT-qPCR. Red indicates up-regulation while green shows down-regulation. The RT-qPCR analysis was performed once with three biological replicates.

To have a global view of gene expression profile under Rad21 depletion and Myc overexpression conditions, we profiled RNA expression level of transfected U2OS-MycER cells by RNA-sequencing. To minimize the secondary effect that cell cycle distribution may have on global gene expression, cells were harvested 24 hours post siRNA transfection and Myc activation, a time point where cell cycle profiles of the different samples were still comparable. We then used unsupervised hierarchical clustering to classify the samples based on their expression profile. Consistent with the RT-qPCR analysis, we observed that siRad21-transfected cells that were overexpressing

Myc clustered with Myc-activated control cells but not with siRad21-silenced cells having normal Myc level (Figure 3.45A), suggesting a dominant role for Myc in regulating gene transcription in Rad21-depleted cells.

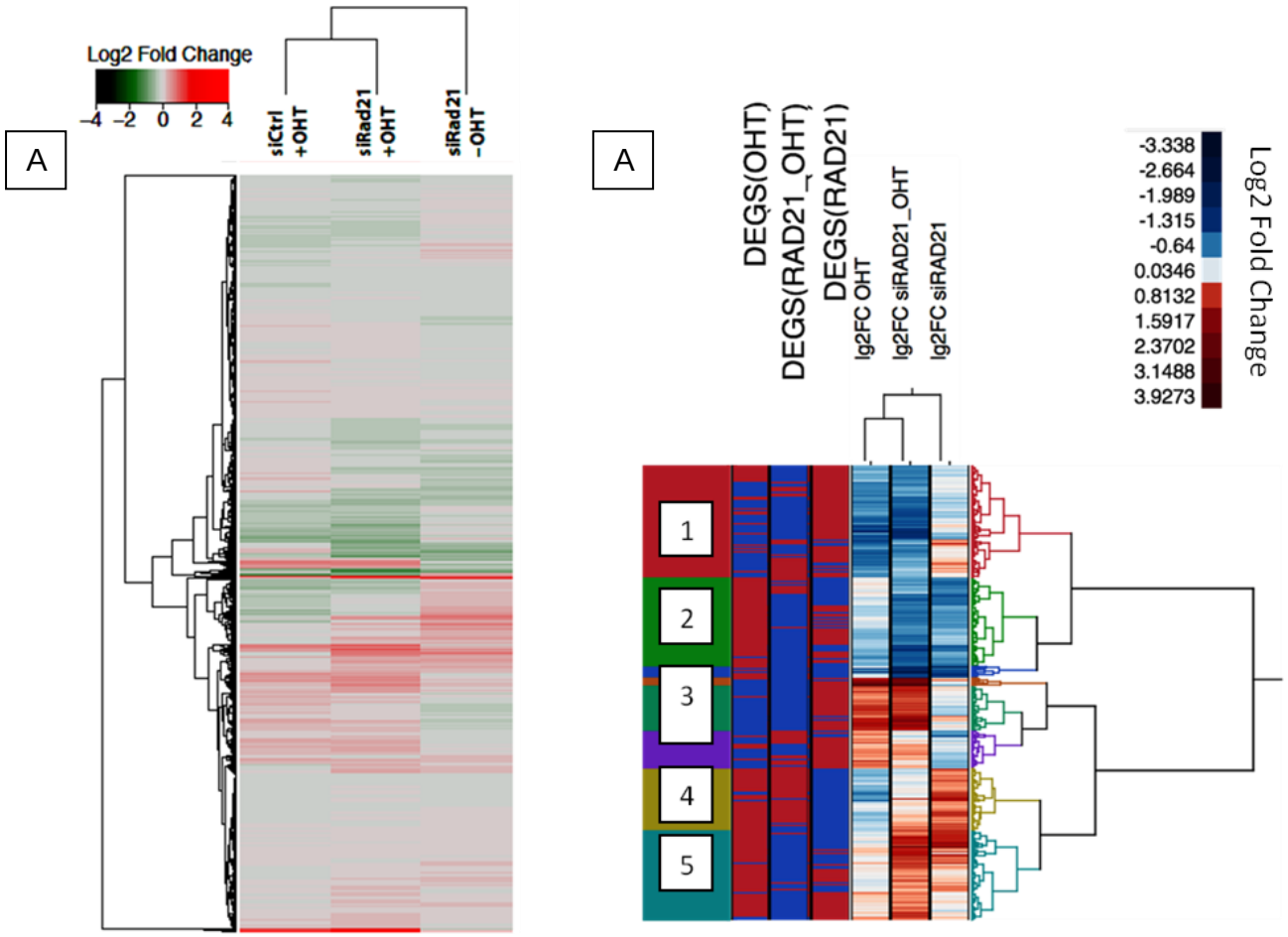

Figure 3.45. Expression profiling of U2OS-MycER cells as measured by RNA-seq

(A) Heatmap of global expression pattern of U2OS-MycER cells at 24 hours after siRNA transfection and Myc activation. Log2 fold change was measured in different experimental group compared to siCtrl-transfected cells. Red and green show up- and down-regulated genes respectively. (B) Hierarchical clustering of differentially expressed genes. Red in the heatmap denotes up-regulation while blue denotes down-regulation. The statistical significance of the expression level of each gene cluster was depicted in a flat heatmap on the left. In this heatmap, blue corresponds to statistical significant clusters while red means insignificant change. RNA-Seq analysis was performed once with two biological replicates.

Next, the differentially expressed genes were classified based on the expression profile (Figure 3.45B) and then were annotated based on the biological processes by DAVID

annotation tool. Using hierarchical clustering we identified five different gene clusters as following:

1. Cluster 1 that composed of genes that were down-regulated in Myc-overexpressing siCtrl- and siRad21-transfected cells but did not show a significant alteration in Rad21-depleted cells. This cluster mainly consisted of genes encoding cell adhesion molecules as well as several developmental factors. This observation is in agreement with the role of Myc in repressing genes involved in cell differentiation and cell adhesion (Kleine-Kohlbrecher et al., 2006).

2. Cluster 2 contained genes that were down-regulated to a same extent in siRad21-transfected cells in the presence or absence of high level of Myc, whereas Myc-activated control cells displayed no or slight change. This cluster was enriched in genes related to regulation of cell proliferation such as FGFR and TGFB2, and may argue, at least partly, the reason of slow-growing feature of cells depleted of Rad21.

3. Cluster 3 acted in a similar way as cluster 1 and was composed of a group of genes that were up-regulated in Myc-overexpressing cells (regardless of Rad21 knock-down) while was mainly unchanged or slightly down-regulated in Rad21-silenced cells. This group consisted of genes involved in ion transport such as potassium and sodium ion transport genes. Apart from the role in maintaining cellular homeostasis through regulation of bioelectrical charges, recently several investigations have addressed the role of ion transport factors in cellular proliferation and in particular their role in cancer development and progression (Blackiston et al., 2009). Therefore, it would be interesting to characterize the role of this cluster of genes in Myc-induced cellular proliferation.

3. In cluster 4, the genes were up-regulated in siRad21-transfected cells and were down-regulated in Myc-activated cells, however transcription was not largely affected (or may

be compensated) in Myc-activated Rad21-depleted cells. This group contained several genes that were associated with cell motility, migration and adhesion.

4. Lastly, genes in cluster 5 displayed significant up-regulation mostly in Myc-overexpressing Rad21-silenced cells compared to Myc-overexpressing or Rad21-depleted cells. The genes in this cluster revealed to be linked to cell death and apoptosis and composed of pro-apoptotic and anti-apoptotic genes as well as several DNA-damage associated genes.

We also compared the expression ratio obtained from RNA-seq analysis with RT-qPCR results (performed at 24 hours post siRNA transfection and Myc activation). The computed correlation coefficient (r) displayed a strong linear correlation between RNA-seq and RT-qPCR analyses in OHT-treated cells transfected with siCtrl or siRad21. For siRad21-transfected cells, although the r value was not high, there was still a positive correlation between two analyses (Figure 3.46). Noteworthy, the log2 fold change was not similar between two methods, with RT-qPCR displaying higher values rather than RNA-seq. This may be the reason that RNA-seq analysis did not call any of the examined genes in RT-qPCR as differentially deregulated genes.

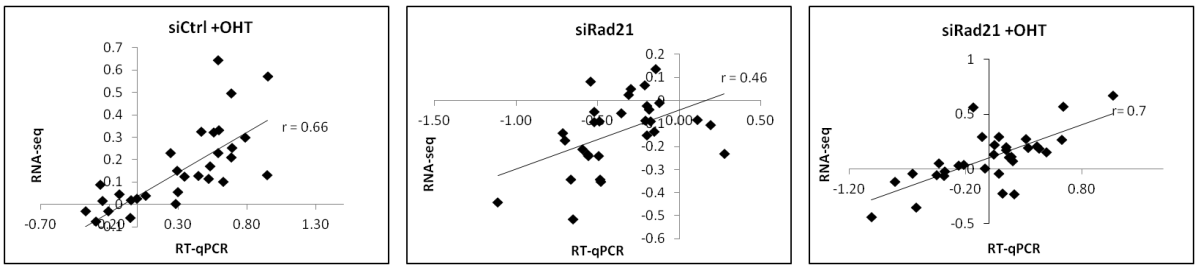

Figure 3.46. Correlation of gene expression ratio between RNA-seq and RT-qPCR analyses

Log2 fold change from RNA-seq analysis (Y axis) is plotted against log2 fold change determined by RT-qPCR (X axis). Correlation coefficiency (r) is shown in the plots

3.8.9 Myc-overexpression in Rad21-depleted cells increased the formation of DNA-RNA hybrids

Considering the dual role of Myc in prompting DNA synthesis and transcription, one possible source of DNA damage in Myc-overexpressing cells could be the conflict that may arise between DNA replication and transcription machineries. As a consequence of a head on collision between DNA replication apparatus and the transcription complex, a DNA-RNA hybrid called R-loop may be generated. If unresolved, R-loops may lead to DNA damage. Therefore, we sought to examine if Myc overexpression in control and Rad21-depleted cells increases R-loop formation. To this end, we performed genome wide profiling of DNA-RNA hybrids by DNA-RNA immunoprecipitation (DRIP) using a specific antibody that recognizes DNA-RNA hybrids. We then applied next generation sequencing to map the regions in the genome harboring R-loops.

DRIP-seq analysis did not show any increase in the number of S9.6 peaks in Myc-overexpressing cells (625), compared to control cells (756). However this number was slightly increased in Rad21-depleted cells (1325) and was remarkably increased in Myc-induced Rad21-silenced cells (3580, Figure 3.47A). The majority of the peaks in Myc-overexpressing or siRad21-transfected cells were also found in Myc-activated Rad21-depleted cells. These cells also acquired additional S9.6 peaks (Figure 3.47B).

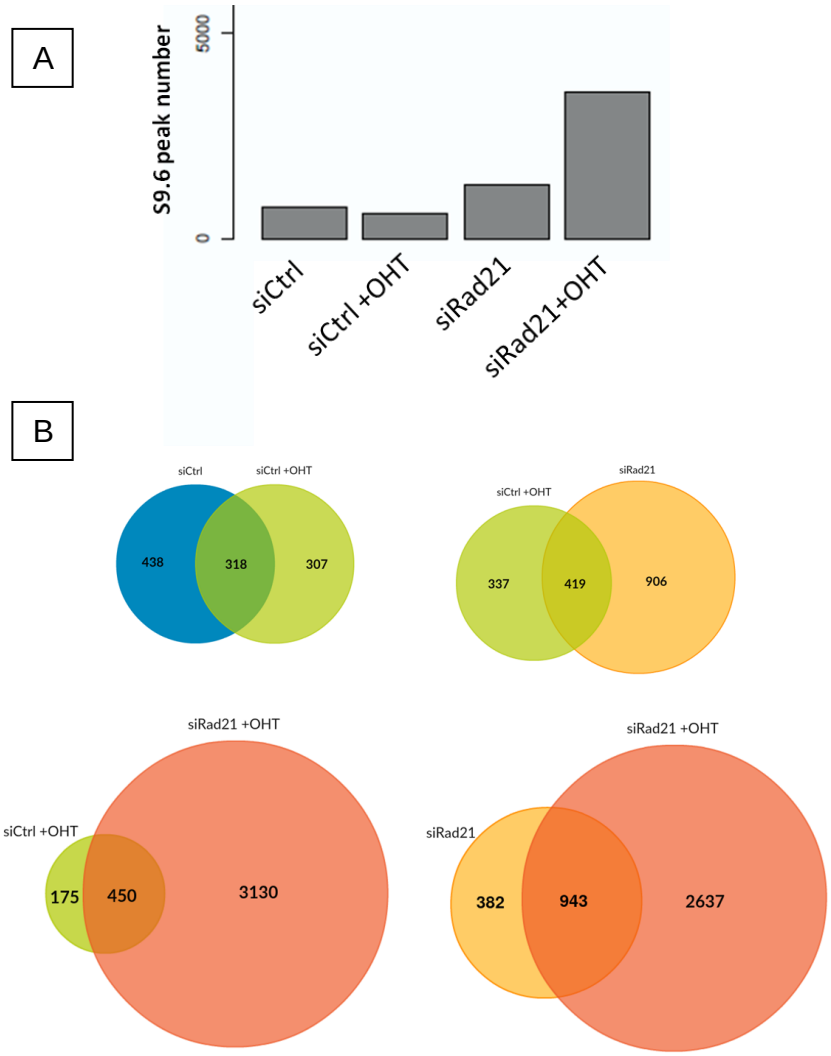

Figure 3.47. S9.6 peak number resulted from DRIP-seq analysis
U2OS-MycER cells were transfected with siCtrl or siRad21 and treated with ethanol or OHT. At 48 hours post transfection, the cells were fixed and then lysed in a DRIP buffer. Immunoprecipitated material by S9.6 was followed by high-throughput sequencing. (A) Quantification of the total number of peaks. (B) Pair wise overlap of S9.6 peaks between different experimental conditions. S9.6 DRIP was performed once.

Moreover, the S9.6 peaks were mapped to intergenic and intragenic regions and to a less extent were found in promoters. This pattern was similar between different experimental groups (Figure 3.48).

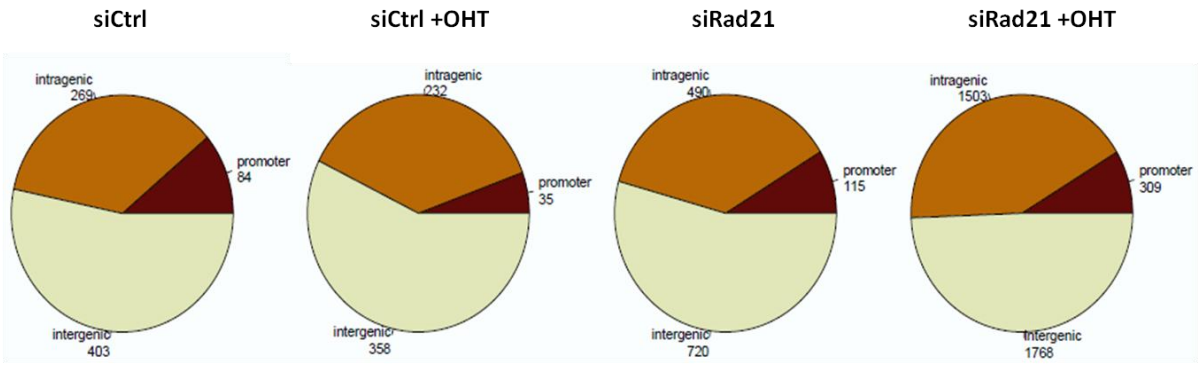

Figure 3.48. Distribution of the S9.6 peaks in different genomic sites
promoters (brown), intragenic (mustard) and intergenic (light cream).

We also looked at the Myc-bound genes and analyzed whether the S9.6 preferentially enriched in those genomic sites. For this, we retrieved the Myc ChIP-seq datasets on U2OS cells that overexpress Myc in a doxycycline-inducible manner (treatment time 30 hr) [GEO accession GSM1231598, (Walz et al., 2014)]. Myc-bound genes were defined as a subset of genes having a Myc peak on the promoter (-2000,1000) in Dox-induced cells. We also defined Myc-target genes as those genes that are bound by Myc in both un-induced and Dox-induced cells, but the binding intensity is increased upon Myc induction. By computing the fraction of gene bodies associated with Myc and overlapping them with the S9.6 peaks, we did not see any enrichment of S9.6 signal in Myc-bound or Myc-target gene bodies compared to the overall gene bodies overlapped with S9.6 peaks (Figure 3.49), indicating that DNA-RNA hybrids, in Myc-activated siRad21-transfected cells are not formed selectively on Myc target genes .

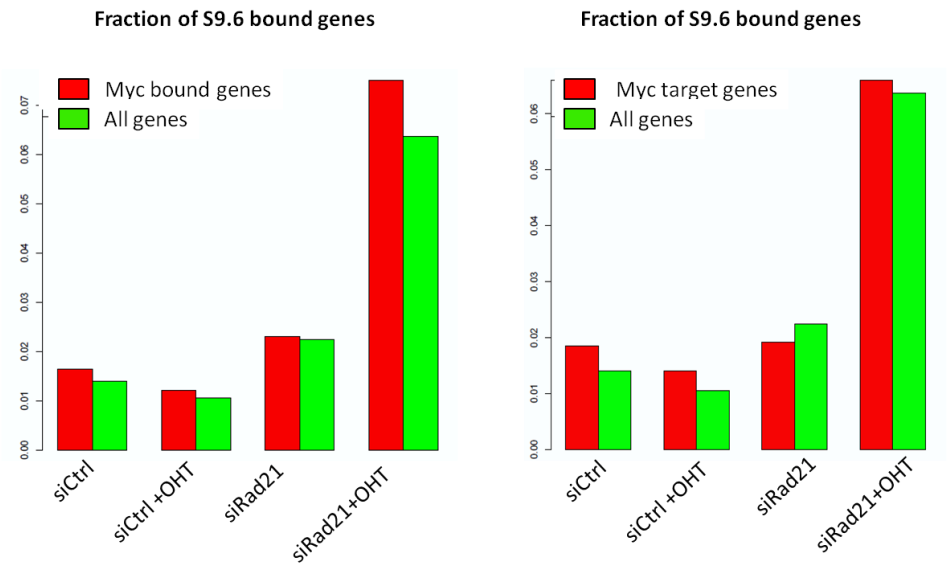

Figure 3.49. Quantification of S9.6 enrichment in Myc-bound genes (left) and Myc-target genes (right) compared to its enrichment in all genes.

It has been shown that early replication fragile sites (that are replicated early in the genome and are susceptible to fork collapse under replication stress) map to actively transcribed genes (Barlow et al., 2013). To see if the S9.6 signal maps to early replication zones, we retrieved Repli-seq datasets on human embryonic stem cells [GEO accession GSE51334, (Pope et al., 2014)] and associated the S9.6 peaks to early and late replication sites. We found S9.6 peaks both in early and late replication regions, although the signal tended to be preferentially associated with early replication zones. The fraction of the S9.6 peaks residing in early replication sites in siRad21-depleted Myc-overexpressing cells was slightly higher compared to other samples, indicating that although DNA-RNA hybrid may form preferentially in early replication sites, the frequency of R-loop formation is similar in both early and late replication sites (Figure 3.50).

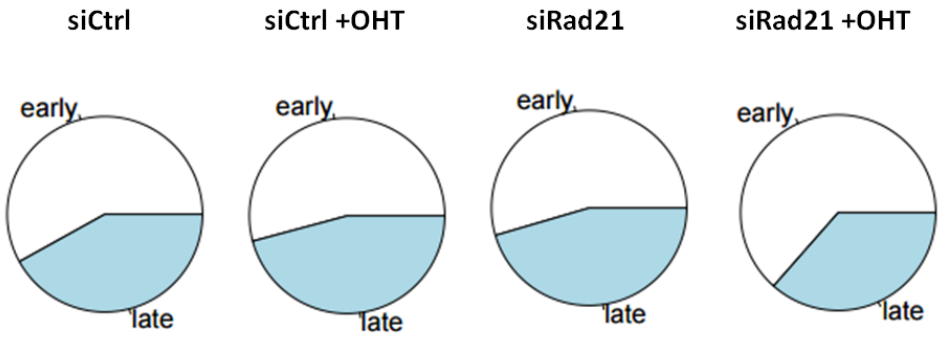

Figure 3.50. Distribution of the S9.6 peaks in early (white) and late (blue) replication sites.

4 Discussion

Considering the role of Myc as an oncoprotein, Myc inhibition has been proposed as a promising strategy for the treatment of Myc-driven cancers. However, concerns are often raised regarding the side effects of Myc inhibition on normal cells. There are also some practical difficulties in designing inhibitors against Myc (Soucek et al., 2008). Recently the concept of "synthetic lethality" has been suggested for the development of selective and less toxic anticancer targets and drugs (Kaelin, 2005). For example, reminiscent to the synthetic lethality of ATR and Chk1 inhibition in Myc-overexpressing cancer cells, several clinical trials are ongoing with the Chk1-inhibitors (LY2606368 and SCH 900776) and ATR inhibitors (AZD6738 and VX-970) in patients with variety of cancers (ClinicalTrials.Gov). A prerequisite of these studies is the thorough knowledge of the underlying pathways through which Myc can act.

In order to identify genes involved in modulating Myc-induced replicative stress, we carried out a high-throughput RNAi screen, using a conditional Myc-overexpressing MEF cell line (MycER-MEF), across 1400 potentially druggable genes and 1200 genes with the potential role in genome instability. Our siRNA screen revealed a subset of "positive hits" including Myc-synthetic lethal genes as well as genes whose knock-down increased ϒH2AX, selectively in Myc-overexpressing cells. We noticed that some of the synthetic lethal hits also displayed higher percentage of ϒH2AX-positive cells. Without ruling out the possibility that H2AX phosphorylation might be a consequence of cell death, accumulation of cytotoxic DNA damage could also be a cause of the reduction in cell viability. We also identified a group of genes whose knock-down increased cell viability and/or reduced ϒH2AX immunofluorescence signal. Though, having low statistical power and low signal-to-noise ratio in this case, limited our confidence in calling the hits.

The initial hit rate of the druggable and genome instability screens -considering only the high confidence positive hits were 6.8% and 7.7% respectively. Validation of the positive

hits from the druggable libraries in a secondary screen yielded a validation rate of 26%. Interestingly, we found several common hits between Myc-SL candidates reported by Toyoshima et al. (Toyoshima et al., 2012) and our screen hits, providing confidence in our screening data. Similarly to the tested libraries, validated hits were dispersed in a variety of pathways and biological processes, suggesting that the events cooperating with Myc in reducing DDR may not be confined to the DNA damage response and repair pathways. Indeed, we identified several hit candidates involved in RNA transcription and processing as well as translation, protein synthesis and degradation.

Interestingly, in a previous study (Paulsen et al., 2009) the mRNA processing module was also the most significantly enriched group of genes whose knock-down induced significant H2AX phosphorylation. While it is conceivable that mRNA processing could affect gnome stability indirectly by altering protein level, recent studies pointed to a more direct mechanism linking some mRNA processing genes to genome maintenance. For example, depletion of splicing factor ASF/SF2 led to increased R-loop formation and generation of DNA double-strand breaks (Li and Manley, 2005). Moreover, pharmacological inhibition of the spliceosome was shown to impair survival and tumorigenesis of Myc-dependent breast cancers *in vivo* (Hsu et al., 2015). It has also been demonstrated that several RNA processing factors such as SRSF1 and the core snRNP assembly genes are direct targets of Myc and are necessary for Myc oncogenic activity (Das et al., 2012, Koh et al., 2015). Taken together, these data indicate the important role of mRNA processing machinery and splicing factors in Myc-overexpressing cells.

In line with the previous data, we found a number of splicing factors such as Serine/Arginine-Rich Splicing Factor 3 (SRSF3), Splicing Factor 3a (SF3A3) and several subunits of Splicing Factor 3b (SF3b) among SL and/or DDR-up hits. The core spliceosomal factor SF3B1 (together with BUD31 and U2AF1) was also shown by

another group recently as a synthetic lethal gene in Myc-overexpressing cells (Hsu et al., 2015). In addition, we validated the Myc-synthetic lethal interaction with SRSF3 depletion in human osteosarcoma U2OS-MycER cells and showed that this synthetic lethality was accompanied with accumulation of ϒH2AX. Thus, while it has been proposed that Myc transcription factor via its ability to increase the synthesis of precursor mRNAs, relies heavily on effective mRNA processing, it would be interesting to understand how the disruption in mRNA splicing synergized with Myc in inducing DDR. In this regard, one may assume that disrupted mRNA splicing by increasing R-loop formation may generate replication fork barrier and boost Myc-induced replicative stress. In addition, we and the others have observed an increased expression of splicing factors (such as SRSF3 in current study and SRSF1 in Das et al. study) upon Myc activation, whether this can be generalized to other splicing factors or whether Myc overexpression engages specific splicing factors for efficient proliferation remains to be determined. Also, the consequences of altered mRNA expression level as well as new alternative splicing events upon depletion of splicing factors in the context of Myc overexpression may be an interesting issue to be addressed.

In addition to mRNA processing factors, our siRNA screen also identified a number of candidates involved in mRNA transcription. Of particular interest, we found Cyclin dependent kinase 12 (CDK12) among DDR-up hits. CDK12 was previously linked to DNA damage response (Blazek et al., 2011) and was also identified as a Myc-synthetic lethal candidate (Toyoshima et al., 2012). CDK12 has been demonstrated to interact with CCNK (Cyclin K) to phosphorylate the RNA polymerase II C-terminal domain (CTD), thus positively regulating gene expression. Different studies have shown that depletion of CdK12/Cyclin K resulted in decreased expression of long genes with high number of exons including DDR genes such as ATR, BRCA1, FANCI and FANCD2 and in this way

sensitized cells to a variety of DNA damage agents (Blazek et al., 2011, Liang et al., 2015).

Validating the preliminary result from screen in U2OS-MycER cells, we demonstrated that Myc activation resulted in synergistic accumulation of ϒH2AX in cells depleted of either Cdk12 or Cdk13 (Cdk12 paralog) or Cyclin K. We also observed a significant reduction in the viability of Myc-overexpressing cells once CDK12, Cdk13 or Cyclin K (but not Cdk12) was silenced. We reasoned that the effect of accumulation of ϒH2AX on cell viability and survival of Myc-activated cells depleted of Cdk12 might be more evident at later time points. However, inconsistent with the previous studies, we could not detect any change in the expression of the examined DDR genes (ATR, ATM and FANCD2) upon Cdk12 and Cyclin K depletion, therefore it would be of merit to analyze the global expression profiles upon Cdk12 and Cyclin K gene knock-down. Of note, since it was shown that each of these proteins, besides some common genes, controls the expression of distinct subset of genes, dissecting gene expression profiles of Cdk12-, Cdk13- and Cyclin K-depleted cells, would be informative to understand how these proteins are linked to DNA damage response and whether or not these proteins, at least in their transcriptional role, are functionally redundant. As it was previously shown that CDK12 and CDK13 have positive effects on gene transcription (Liang et al., 2015, Blazek et al., 2011), it would be interesting to know if and how Myc overexpression affects the expression of down-regulated genes in the cells depleted of Cdk12 or Cdk13 or Cyclin K.

CDK12 and CDK13 seem to also interact with mRNA processing factor through their N-terminal serine-arginine dipeptide-rich regions (Liang et al., 2015, Berro et al., 2008). Indeed, not only many splicing factors including some of our aforementioned hits were co-purified with Cdk12 and Cdk13, also Cdk12 and Cdk13 knock-down affected the

expression of genes involved in RNA processing (Liang et al., 2015). Therefore, it may be intriguing to investigate the functional link between Cdk12/Cdk13 and splicing factors particularly in the context of Myc hyper-activation.

In the second part of our study, we sought to better understand the molecular mechanism underlying the synthetic lethal interaction between Myc and Rad21 (a component of the cohesin complex). Rad21 was among the Myc-synthetic lethal candidates in Toyoshima et al. study (Toyoshima et al., 2012) and, due to the robust effect, was selected to serve as a positive SL/DDR-up control in our RNAi screen. Further validation by us, revealed that Rad21 depletion in different Myc overexpressing cell types (MEF-, U2OS- and NMuMG-MycER cells) caused a massive cell death, demonstrating that the synthetic lethality is not cell type specific. Moreover, Rad21 silencing caused a remarkable increase in ϒH2AX level selectively in Myc-activated cells, suggesting that the synthetic lethality is subsequent to the accumulation of cytotoxic DNA damage. Moreover, Rad21-depleted cells with endogenous level of Myc were viable and did not exhibit accumulation of ϒH2AX. These results support the idea that DNA damage response in Myc activated cells depleted of Rad21 is unlikely to be due to the lack of chromosomal cohesion and missegregation of the sister chromatids. In line with this notion, cohesin-depleted cells or cells that are heterozygous for NIPBL (a cohesin loader) showed normal mitosis (Liu et al., 2009), implying that even very low levels of cohesin may be sufficient for proper and functional sister chromatid cohesion. An alternative (yet not mutually exclusive) explanation is that other mechanisms such as DNA catenations can act redundantly with the cohesin complex to provide a cohesive force during mitosis (Díaz-Martínez et al., 2007).

Cohesins have also been shown to facilitate repair of double strand breaks by homologous recombination (Wu and Yu, 2012). However, in contrast to the previous data, we did not

see any further sensitivity in U2OS cells to DNA damaging agents when Rad21 was depleted. In addition, we observed that irradiated U2OS cells, after one day recovery, were able to efficiently repair DNA damage, as was shown by ϒH2AX reduction. This discrepancy may be due to the difference in irradiation dose and to the preferred DNA repair pathway cells may choose under certain circumstances. While ϒH2AX was suggested by several studies as a valid measure of DNA repair (Rothkamm et al., 2003), examining the other DNA repair markers involved in homologous-directed repair and non-homologous end joining repair such as RAD51, 53BP1 and BRCA1 would give us better understandings on the efficiency of DNA repair in Rad21-depleted cells in face of DNA damage.

Recently the role of RAD21 as a part of cohesion complex is expanding far more than just involving in sister chromatid cohesion and DNA repair. Recent findings showed not only an enrichment of cohesin at replication origins, but also a physical interaction between cohesin and pre-replication complex (Guillou et al., 2010). In line with these data, we detected RAD21 protein enriched on newly synthesized DNA by iPOND technique. Although the "cohesin barrier" model suggests that cohesins deposited before DNA replication are stable and block subsequent fork progression, our data support the notion that cohesins are highly dynamic and transiently chromatin-associated complexes before S-phase (Gerlich et al., 2006). Moreover, evidence of cohesin interactions with fork stability factors such as PCNA, argues that functional cohesin loading probably takes place during DNA replication and may be coordinated with fork progression. In this way cohesins may be deposited at higher levels on both sister chromatids (on leading and lagging strands) during replication. After fork passage, as a result of the activity of ESCO1/2 acetyltransferase, the cohesin complex may be converted to a state competent for sister pairing.

This data together with the results of DNA combing analysis that displayed a remarkable increase in unidirectional replication fork in Rad21-depleted cells, may explain the essential role of the cohesin complex in fork stability and progression. Unexpectedly, DNA combing analysis also showed higher fork speed in Rad21-depleted cells compared to control cells. This data seem difficult to reconcile with the high frequency of unidirectional replication forks in Rad21-depleted cells. One possible reason to account for the higher fork speed in these cells could be the size of the chromatin loops under cohesin-depleted condition.

We also found that Myc is able to partially rescue DNA synthesis in Rad21-depleted cells, however, replication reinforcement imposed by Myc overexpression results in a replicative stress over time. How Myc is able to restore DNA replication in Rad21-depleted cells? One explanation could be that Myc hyper-activation leads to unscheduled origin firing, however, in the absence of RAD21, DNA replication cannot proceed long enough, resulting in replication fork stalling and collapse. Although our results on DNA combing do not favor the effect of Myc on origin activation, it has been shown by several studies that Myc overexpression boosts origin firing (Dominguez-Sola et al., 2007, Srinivasan et al., 2013). It should also be noted that due to the high percentage of unidirectional forks which were not taken into account in the DNA combing analysis (particularly in siRad21-transfected cells), the measured inter-origin distances may be biased toward the tracks with symmetric labeling and not be reflective of the real situation. More precise techniques, such as Repli-seq, may be required to clarify the replication profile of the cells in this case.

We propose that as a result of the progressive accumulation of DNA damage in S-phase and activation of G2 checkpoint, at least through phosphorylation of p53, Myc-activated cells depleted of Rad21 get arrested in G2/M phase to avoid mitotic catastrophe. In an

effort to relieve the G2 checkpoint in these cells, we saw that ATM inhibition led to increased cell death while p53 knock-down, without affecting cell viability, enhanced the percentage of the polyploid population. This controversy may stem from the difference between inhibiting ATM -that acts upstream of p53 in the DDR pathway- and knocking-down p53 that acts at the downstream of the cascade. In line with our observation, it has been shown that irradiated p53-mutated cells before undergoing cell death, entered aberrant endoreduplication resulting in the formation of polyploid cells (Illidge et al., 2000). Therefore, it would be interesting to see whether Myc synthetic lethality with Rad21, though with a delay, can occur also in the absence of functional p53.

Comparing Myc with the other oncogenes, that similarly to Myc induces replication stress, we found that Myc is unique in enforcing DNA synthesis and triggering DDR in Rad21-silenced cells. As a result, we think that the combination of transcriptional and non-transcriptional roles of Myc is important for the observed effect of Myc on DNA replication in Rad21-depleted cells. RNA expression analysis in Rad21-depleted cells show several deregulated genes, including genes involved in cell cycle progression and DNA replication, however Myc overexpression in these cells was able to partially re-establish gene expression profile toward the expression profile of Myc activated cells. This result also exclude the possibility that the Myc-induced replication stress in Rad21-silenced cells might be due to the deregulation of Myc target genes necessary for DNA synthesis.

The dominant effect of Myc in provoking gene transcription in Rad21-depleted cells, also led us think that the increased DDR in these cells may originate from the dual role of Myc in inducing DNA replication and in directing RNA transcription. Supporting this idea, DRIP-seq analysis on Rad21-depleted cells upon Myc overexpression, revealed a remarkable increase in the DNA-RNA hybrids, as an indication of R-loop formation.

Although we did not find any preferential enrichment of R-loops in the vicinity of Myc-bound genes, we cannot rule out the R-loops generated as a result of Myc-induced replication. This became more interesting as we saw R-loops preferentially occurring in early replication sites. Therefore, more thorough analyses of replication dynamics as well as Myc-mediated transcription are needed to dissect the impact of Myc overexpression on R-loop formation in Rad21-depleted cells.

Recently Yan et al. showed the presence of dense clusters of different transcription factors (TF) in the genome that are exclusively formed around the cohesin complex and act as a memory for TF establishing. These transcriptional dense clusters were shown to localize close to the transcription sites and interestingly Myc is almost exclusively present in such clusters (Yan et al., 2013). Given the fact that replication origins are shown to preferentially locate close to transcription start site, one may assume that by Rad21 depletion, the TF dense clusters might be disassembled and this may result in a disruption of the coordination of transcription and DNA replication in these sites. Further studies are needed to investigate the impact of the cohesins depletion on such TF clusters and their neighboring genomic regions.

Taken together, our data highlights the pleiotropic roles of Rad21 in particular (and the cohesin complex in general) in different cellular processes such as cohesion, DNA replication and gene transcription. In addition, we showed that Myc overexpression by counteracting the effect of Rad21 depletion on DNA replication and transcription, imposes a severe replicative stress in cells and eventually leads to cell death.

In summary, by means of a high-throughput siRNA screen, we identified several genes that are required to ensure genome stability in Myc-overexpressing cells, followed by validation of the selected hits. Prospective studies will elucidate how targeting these

molecules can influence the malignant phenotypes of cancer cells with deregulated Myc *in vitro* and *in vivo*, and may ultimately used for therapeutic intervention.

References

ABRAHAM, R. T. 2001. Cell cycle checkpoint signaling through the ATM and ATR kinases. *Genes & development,* 15**,** 2177-2196.

ADHIKARY, S. & EILERS, M. 2005. Transcriptional regulation and transformation by Myc proteins. *Nat Rev Mol Cell Biol,* 6**,** 635-45.

AGUILERA, A. & GARCÍA-MUSE, T. 2012. R Loops: From Transcription Byproducts to Threats to Genome Stability. *Molecular Cell,* 46**,** 115-124.

ARIAS, E. E. & WALTER, J. C. 2007. Strength in numbers: preventing rereplication via multiple mechanisms in eukaryotic cells. *Genes & development,* 21**,** 497-518.

ARVANITIS, C. & FELSHER, D. W. 2005. Conditionally MYC:insights from novel transgenic models. *Cancer Letters,* 226**,** 95-99.

BAKKENIST, C. J. & KASTAN, M. B. 2003. DNA damage activates ATM through intermolecular autophosphorylation and dimer dissociation. *Nature,* 421**,** 499-506.

BANIN, S., MOYAL, L., SHIEH, S.-Y., TAYA, Y., ANDERSON, C. W., CHESSA, L., SMORODINSKY, N. I., PRIVES, C., REISS, Y., SHILOH, Y. & ZIV, Y. 1998. Enhanced Phosphorylation of p53 by ATM in Response to DNA Damage. *Science,* 281**,** 1674-1677.

BAO, S., WU, Q., MCLENDON, R. E., HAO, Y., SHI, Q., HJELMELAND, A. B., DEWHIRST, M. W., BIGNER, D. D. & RICH, J. N. 2006. Glioma stem cells promote radioresistance by preferential activation of the DNA damage response. *nature,* 444**,** 756-760.

BARLOW, C., HIROTSUNE, S., PAYLOR, R., LIYANAGE, M., ECKHAUS, M., COLLINS, F., SHILOH, Y., CRAWLEY, J. N., RIED, T. & TAGLE, D. 1996. Atm-deficient mice: a paradigm of ataxia telangiectasia. *Cell,* 86**,** 159-171.

BARLOW, J. H., FARYABI, R. B., CALLÉN, E., WONG, N., MALHOWSKI, A., CHEN, H. T., GUTIERREZ-CRUZ, G., SUN, H.-W., MCKINNON, P. & WRIGHT, G. 2013. Identification of early replicating fragile sites that contribute to genome instability. *Cell,* 152**,** 620-632.

BARTEK, J., BARTKOVA, J. & LUKAS, J. 1997. The retinoblastoma protein pathway in cell cycle control and cancer. *Experimental cell research,* 237**,** 1-6.

BARTEK, J., LUKAS, C. & LUKAS, J. 2004. Checking on DNA damage in S phase. *Nature reviews Molecular cell biology,* 5**,** 792-804.

BARTEK, J. & LUKAS, J. 2001. Mammalian G1-and S-phase checkpoints in response to DNA damage. *Current opinion in cell biology,* 13**,** 738-747.

BARTKOVA, J., HOREJSI, Z., KOED, K., KRAMER, A., TORT, F., ZIEGER, K., GULDBERG, P., SEHESTED, M., NESLAND, J. M., LUKAS, C., ORNTOFT, T., LUKAS, J. & BARTEK, J. 2005. DNA damage response as a candidate anti-cancer barrier in early human tumorigenesis. *Nature,* 434**,** 864-870.

BARTKOVA, J., REZAEI, N., LIONTOS, M., KARAKAIDOS, P., KLETSAS, D., ISSAEVA, N., VASSILIOU, L. V., KOLETTAS, E., NIFOROU, K., ZOUMPOURLIS, V. C., TAKAOKA, M., NAKAGAWA, H., TORT, F., FUGGER, K., JOHANSSON, F., SEHESTED, M., ANDERSEN, C. L., DYRSKJOT, L., ORNTOFT, T., LUKAS, J., KITTAS, C., HELLEDAY, T., HALAZONETIS, T. D., BARTEK, J. & GORGOULIS, V. G. 2006. Oncogene-induced senescence is part of the tumorigenesis barrier imposed by DNA damage checkpoints. *Nature,* 444**,** 633-7.

BASSING, C. H., SUH, H., FERGUSON, D. O., CHUA, K. F., MANIS, J., ECKERSDORFF, M., GLEASON, M., BRONSON, R., LEE, C. & ALT, F. W. 2003. Histone H2AX: a dosage-dependent suppressor of oncogenic translocations and tumors. *Cell,* 114**,** 359-370.

BATES, S. & VOUSDEN, K. H. 1996. p53 in signaling checkpoint arrest or apoptosis. *Current opinion in genetics & development,* 6**,** 12-18.

BELL, D. W., VARLEY, J. M., SZYDLO, T. E., KANG, D. H., WAHRER, D. C., SHANNON, K. E., LUBRATOVICH, M., VERSELIS, S. J., ISSELBACHER, K. J. & FRAUMENI, J. F. 1999. Heterozygous germ line hCHK2 mutations in Li-Fraumeni syndrome. *Science,* 286**,** 2528-2531.

BERRO, R., PEDATI, C., KEHN-HALL, K., WU, W., KLASE, Z., EVEN, Y., GENEVIÈRE, A.-M., AMMOSOVA, T., NEKHAI, S. & KASHANCHI, F. 2008. CDK13, a new potential human immunodeficiency virus type 1 inhibitory factor regulating viral mRNA splicing. *Journal of virology,* 82**,** 7155-7166.

BESTER, A. C., RONIGER, M., OREN, Y. S., IM, M. M., SARNI, D., CHAOAT, M., BENSIMON, A., ZAMIR, G., SHEWACH, D. S. & KEREM, B. 2011. Nucleotide deficiency promotes genomic instability in early stages of cancer development. *Cell,* 145**,** 435-46.

BIRKENBIHL, R. P. & SUBRAMANI, S. 1992. Cloning and characterization of rad21 an essential gene of Schizosaccharomyces pombe involved in DNA double-strand-break repair. *Nucleic acids research,* 20**,** 6605-6611.

BLACKISTON, D. J., MCLAUGHLIN, K. A. & LEVIN, M. 2009. Bioelectric controls of cell proliferation: ion channels, membrane voltage and the cell cycle. *Cell cycle,* 8**,** 3527-3536.

BLAZEK, D., KOHOUTEK, J., BARTHOLOMEEUSEN, K., JOHANSEN, E., HULINKOVA, P., LUO, Z., CIMERMANCIC, P., ULE, J. & PETERLIN, B. M. 2011. The Cyclin K/Cdk12 complex maintains genomic stability via regulation of expression of DNA damage response genes. *Genes & development,* 25**,** 2158-2172.

BOSE, T. & GERTON, J. L. 2010. Cohesinopathies, gene expression, and chromatin organization. *J Cell Biol,* 189**,** 201-10.

BOUCHARD, C., THIEKE, K., MAIER, A., SAFFRICH, R., HANLEY- HYDE, J., ANSORGE, W., REED, S., SICINSKI, P., BARTEK, J. & EILERS, M. 1999. Direct induction of cyclin D2 by Myc contributes to cell cycle progression and sequestration of p27. *The EMBO journal,* 18**,** 5321-5333.

BRENNER, C., DEPLUS, R., DIDELOT, C., LORIOT, A., VIRÉ, E., DE SMET, C., GUTIERREZ, A., DANOVI, D., BERNARD, D. & BOON, T. 2005. Myc represses transcription through recruitment of DNA methyltransferase corepressor. *The EMBO journal,* 24**,** 336-346.

BROWN, E. J. & BALTIMORE, D. 2000. ATR disruption leads to chromosomal fragmentation and early embryonic lethality. *Genes & development,* 14**,** 397-402.

BUNZ, F., DUTRIAUX, A., LENGAUER, C., WALDMAN, T., ZHOU, S., BROWN, J., SEDIVY, J., KINZLER, K. & VOGELSTEIN, B. 1998. Requirement for p53 and p21 to sustain G2 arrest after DNA damage. *Science,* 282**,** 1497-1501.

CANMAN, C. E., LIM, D.-S., CIMPRICH, K. A., TAYA, Y., TAMAI, K., SAKAGUCHI, K., APPELLA, E., KASTAN, M. B. & SILICIANO, J. D. 1998. Activation of the ATM kinase by ionizing radiation and phosphorylation of p53. *Science,* 281**,** 1677-1679.

CELESTE, A., DIFILIPPANTONIO, S., DIFILIPPANTONIO, M. J., FERNANDEZ-CAPETILLO, O., PILCH, D. R., SEDELNIKOVA, O. A., ECKHAUS, M., RIED, T., BONNER, W. M. & NUSSENZWEIG, A. 2003. H2AX haploinsufficiency modifies genomic stability and tumor susceptibility. *Cell,* 114**,** 371-383.

CHANG, T.-C., YU, D., LEE, Y.-S., WENTZEL, E. A., ARKING, D. E., WEST, K. M., DANG, C. V., THOMAS-TIKHONENKO, A. & MENDELL, J. T. 2008. Widespread microRNA repression by Myc contributes to tumorigenesis. *Nature genetics,* 40**,** 43-50.

CHEN, Z., XIAO, Z., GU, W. Z., XUE, J., BUI, M. H., KOVAR, P., LI, G., WANG, G., TAO, Z. F. & TONG, Y. 2006. Selective Chk1 inhibitors differentially sensitize p53- deficient cancer cells to cancer therapeutics. *International journal of cancer,* 119**,** 2784-2794.

CHENG, S. W. G., DAVIES, K. P., YUNG, E., BELTRAN, R. J., YU, J. & KALPANA, G. V. 1999. c-MYC interacts with INI1/hSNF5 and requires the SWI/SNF complex for transactivation function. *Nat Genet,* 22**,** 102-105.

CLIBY, W. A., LEWIS, K. A., LILLY, K. K. & KAUFMANN, S. H. 2002. S phase and G2 arrests induced by topoisomerase I poisons are dependent on ATR kinase function. *Journal of Biological Chemistry,* 277**,** 1599-1606.

CLIBY, W. A., ROBERTS, C. J., CIMPRICH, K. A., STRINGER, C. M., LAMB, J. R., SCHREIBER, S. L. & FRIEND, S. H. 1998. Overexpression of a kinase- inactive ATR

protein causes sensitivity to DNA- damaging agents and defects in cell cycle checkpoints. *The EMBO Journal,* 17**,** 159-169.

CORTEZ, D., GUNTUKU, S., QIN, J. & ELLEDGE, S. J. 2001. ATR and ATRIP: Partners in Checkpoint Signaling. *Science,* 294**,** 1713-1716.

D'ADDA DI FAGAGNA, F. 2008. Living on a break: cellular senescence as a DNA-damage response. *Nat Rev Cancer,* 8**,** 512-522.

DANG, C. V. 2013. MYC, metabolism, cell growth, and tumorigenesis. *Cold Spring Harb Perspect Med,* 3.

DAS, S., ANCZUKÓW, O., AKERMAN, M. & KRAINER, A. R. 2012. Oncogenic splicing factor SRSF1 is a critical transcriptional target of MYC. *Cell reports,* 1**,** 110-117.

DE ALBORÁN, I. M., BAENA, E. & MARTINEZ-A, C. 2004. c-Myc-deficient B lymphocytes are resistant to spontaneous and induced cell death. *Cell Death & Differentiation,* 11**,** 61-68.

DE KLEIN, A., MUIJTJENS, M., VAN OS, R., VERHOEVEN, Y., SMIT, B., CARR, A., LEHMANN, A. & HOEIJMAKERS, J. 2000. Targeted disruption of the cell-cycle checkpoint gene ATR leads to early embryonic lethality in mice. *Current Biology,* 10**,** 479-482.

DELGADO, M. D., LERGA, A., CANELLES, M., GOMEZ-CASARES, M. T. & LEÓN, J. 1995. Differential regulation of Max and role of c-Myc during erythroid and myelomonocytic differentiation of K562 cells. *Oncogene,* 10**,** 1659-1665.

DI MICCO, R., FUMAGALLI, M., CICALESE, A., PICCININ, S., GASPARINI, P., LUISE, C., SCHURRA, C., GARRE, M., NUCIFORO, P. G., BENSIMON, A., MAESTRO, R., PELICCI, P. G. & D'ADDA DI FAGAGNA, F. 2006. Oncogene-induced senescence is a DNA damage response triggered by DNA hyper-replication. *Nature,* 444**,** 638-42.

DÍAZ-MARTÍNEZ, L. A., GIMÉNEZ-ABIÁN, J. F. & CLARKE, D. J. 2007. Cohesin is dispensable for centromere cohesion in human cells.

DOMINGUEZ-SOLA, D., YING, C. Y., GRANDORI, C., RUGGIERO, L., CHEN, B., LI, M., GALLOWAY, D. A., GU, W., GAUTIER, J. & DALLA-FAVERA, R. 2007. Non-transcriptional control of DNA replication by c-Myc. *Nature,* 448**,** 445-451.

DONZELLI, M. & DRAETTA, G. F. 2003. Regulating mammalian checkpoints through Cdc25 inactivation. *EMBO reports,* 4**,** 671-677.

DUROCHER, D. & JACKSON, S. P. 2001. DNA-PK, ATM and ATR as sensors of DNA damage: variations on a theme? *Current opinion in cell biology,* 13**,** 225-231.

EBERHARDY, S. R. & FARNHAM, P. J. 2002. Myc Recruits P-TEFb to Mediate the Final Step in the Transcriptional Activation of the cad Promoter. *Journal of Biological Chemistry,* 277**,** 40156-40162.

EIJPE, M., HEYTING, C., GROSS, B. & JESSBERGER, R. 2000. Association of mammalian SMC1 and SMC3 proteins with meiotic chromosomes and synaptonemal complexes. *Journal of Cell Science,* 113**,** 673-682.

EIJPE, M., OFFENBERG, H., JESSBERGER, R., REVENKOVA, E. & HEYTING, C. 2003. Meiotic cohesin REC8 marks the axial elements of rat synaptonemal complexes before cohesins SMC1β and SMC3. *The Journal of Cell Biology,* 160**,** 657-670.

EISCHEN, C. M., WEBER, J. D., ROUSSEL, M. F., SHERR, C. J. & CLEVELAND, J. L. 1999. Disruption of the ARF–Mdm2–p53 tumor suppressor pathway in Myc-induced lymphomagenesis. *Genes & development,* 13**,** 2658-2669.

ELLEDGE, S. J. 1996. Cell Cycle Checkpoints: Preventing an Identity Crisis. *Science,* 274**,** 1664-1672.

EVAN, G. I., WYLLIE, A. H., GILBERT, C. S., LITTLEWOOD, T. D., LAND, H., BROOKS, M., WATERS, C. M., PENN, L. Z. & HANCOCK, D. C. 1992. Induction of apoptosis in fibroblasts by c-myc protein. *Cell,* 69**,** 119-128.

FANG, Y., TSAO, C. C., GOODMAN, B. K., FURUMAI, R., TIRADO, C. A., ABRAHAM, R. T. & WANG, X. F. 2004. ATR functions as a gene dosage- dependent tumor suppressor on a mismatch repair- deficient background. *The EMBO journal,* 23**,** 3164-3174.

FERRAO, P. T., BUKCZYNSKA, E. P., JOHNSTONE, R. W. & MCARTHUR, G. A. 2012. Efficacy of CHK inhibitors as single agents in MYC-driven lymphoma cells. *Oncogene,* 31**,** 1661-1672.

FOGAL, V., RICHARDSON, A. D., KARMALI, P. P., SCHEFFLER, I. E., SMITH, J. W. & RUOSLAHTI, E. 2010. Mitochondrial p32 protein is a critical regulator of tumor metabolism via maintenance of oxidative phosphorylation. *Molecular and cellular biology,* 30**,** 1303-1318.

FROELICH-AMMON, S. J. & OSHEROFF, N. 1995. Topoisomerase poisons: harnessing the dark side of enzyme mechanism. *Journal of Biological Chemistry,* 270**,** 21429-21432.

GAILLARD, H., GARCIA-MUSE, T. & AGUILERA, A. 2015. Replication stress and cancer. *Nat Rev Cancer,* 15**,** 276-89.

GARTEL, A. L. & SHCHORS, K. 2003. Mechanisms of c-myc-mediated transcriptional repression of growth arrest genes. *Experimental cell research,* 283**,** 17-21.

GARTEL, A. L., YE, X., GOUFMAN, E., SHIANOV, P., HAY, N., NAJMABADI, F. & TYNER, A. L. 2001. Myc represses the p21 (WAF1/CIP1) promoter and interacts with Sp1/Sp3. *Proceedings of the National Academy of Sciences,* 98**,** 4510-4515.

GERLICH, D., KOCH, B., DUPEUX, F., PETERS, J. M. & ELLENBERG, J. 2006. Live-cell imaging reveals a stable cohesin-chromatin interaction after but not before DNA replication. *Current Biology,* 16, 1571-1578.

GEWURZ, B. E. & HARPER, J. W. 2006. DNA-damage control: Claspin destruction turns off the checkpoint. *Current biology,* 16**,** R932-R934.

GILAD, O., NABET, B. Y., RAGLAND, R. L., SCHOPPY, D. W., SMITH, K. D., DURHAM, A. C. & BROWN, E. J. 2010. Combining ATR suppression with oncogenic Ras synergistically increases genomic instability, causing synthetic lethality or tumorigenesis in a dosage-dependent manner. *Cancer research,* 70**,** 9693-9702.

GOMEZ-ROMAN, N., GRANDORI, C., EISENMAN, R. N. & WHITE, R. J. 2003. Direct activation of RNA polymerase III transcription by c-Myc. *Nature,* 421**,** 290-294.

GORGOULIS, V. G., VASSILIOU, L.-V. F., KARAKAIDOS, P., ZACHARATOS, P., KOTSINAS, A., LILOGLOU, T., VENERE, M., DITULLIO, R. A., KASTRINAKIS, N. G. & LEVY, B. 2005. Activation of the DNA damage checkpoint and genomic instability in human precancerous lesions. *Nature,* 434**,** 907-913.

GRANDORI, C., GOMEZ-ROMAN, N., FELTON-EDKINS, Z. A., NGOUENET, C., GALLOWAY, D. A., EISENMAN, R. N. & WHITE, R. J. 2005. c-Myc binds to human ribosomal DNA and stimulates transcription of rRNA genes by RNA polymerase I. *Nature cell biology,* 7**,** 311-318.

GUILLOU, E., IBARRA, A., COULON, V., CASADO-VELA, J., RICO, D., CASAL, I., SCHWOB, E., LOSADA, A. & MENDEZ, J. 2010. Cohesin organizes chromatin loops at DNA replication factories. *Genes Dev,* 24**,** 2812-22.

HALAZONETIS, T. D., GORGOULIS, V. G. & BARTEK, J. 2008. An oncogene-induced DNA damage model for cancer development. *science,* 319**,** 1352-1355.

HARPER, J. W. & ELLEDGE, S. J. 2007. The DNA damage response: ten years after. *Mol Cell,* 28**,** 739-45.

HEIDINGER-PAULI, J. M., MERT, O., DAVENPORT, C., GUACCI, V. & KOSHLAND, D. 2010. Systematic reduction of cohesin differentially affects chromosome segregation, condensation, and DNA repair. *Current biology,* 20**,** 957-963.

HEIDINGER-PAULI, J. M., ÜNAL, E., GUACCI, V. & KOSHLAND, D. 2008. The Kleisin Subunit of Cohesin Dictates Damage-Induced Cohesion. *Molecular Cell,* 31**,** 47-56.

HEIDINGER-PAULI, J. M., ÜNAL, E. & KOSHLAND, D. 2009. Distinct Targets of the Eco1 Acetyltransferase Modulate Cohesion in S Phase and in Response to DNA Damage. *Molecular Cell,* 34**,** 311-321.

HEMANN, M. T., BRIC, A., TERUYA-FELDSTEIN, J., HERBST, A., NILSSON, J. A., CORDON-CARDO, C., CLEVELAND, J. L., TANSEY, W. P. & LOWE, S. W. 2005. Evasion of the p53 tumour surveillance network by tumour-derived MYC mutants. *Nature,* 436**,** 807-811.

HENRIKSSON, M., SELIVANOVA, G., LINDSTRÖM, M. & WIMAN, K. 2001. Inactivation of Myc-induced p53-dependent apoptosis in human tumors. *Apoptosis,* 6**,** 133-137.

HERMEKING, H., RAGO, C., SCHUHMACHER, M., LI, Q., BARRETT, J. F., OBAYA, A. J., O'CONNELL, B. C., MATEYAK, M. K., TAM, W., KOHLHUBER, F., DANG, C. V., SEDIVY, J. M., EICK, D., VOGELSTEIN, B. & KINZLER, K. W. 2000. Identification of CDK4 as a target of c-MYC. *Proceedings of the National Academy of Sciences,* 97**,** 2229-2234.

HIRAO, A., KONG, Y.-Y., MATSUOKA, S., WAKEHAM, A., RULAND, J., YOSHIDA, H., LIU, D., ELLEDGE, S. J. & MAK, T. W. 2000. DNA Damage-Induced Activation of p53 by the Checkpoint Kinase Chk2. *Science,* 287**,** 1824-1827.

HOFFMAN, B. & LIEBERMANN, D. A. 2008. Apoptotic signaling by c-MYC. *Oncogene,* 27**,** 6462-72.

HÖGLUND, A., NILSSON, L. M., MURALIDHARAN, S. V., HASVOLD, L. A., MERTA, P., RUDELIUS, M., NIKOLOVA, V., KELLER, U. & NILSSON, J. A. 2011. Therapeutic implications for the induced levels of Chk1 in Myc-expressing cancer cells. *Clinical Cancer Research,* 17**,** 7067-7079.

HORSFIELD, J., PRINT, C. G. & MÖNNICH, M. 2012. Diverse developmental disorders from The One Ring: distinct molecular pathways underlie the cohesinopathies. *Frontiers in Genetics,* 3.

HSU, T. Y.-T., SIMON, L. M., NEILL, N. J., MARCOTTE, R., SAYAD, A., BLAND, C. S., ECHEVERRIA, G. V., SUN, T., KURLEY, S. J. & TYAGI, S. 2015. The spliceosome is a therapeutic vulnerability in MYC-driven cancer. *Nature,* 525**,** 384-388.

ILLIDGE, T. M., CRAGG, M. S., FRINGES, B., OLIVE, P. & ERENPREISA, J. A. 2000. Polyploid giant cells provide a survival mechanism for p53 mutant cells after DNA damage. *Cell biology international,* 24**,** 621-633.

JESSBERGER, R. 2002. The many functions of SMC proteins in chromosome dynamics. *Nat Rev Mol Cell Biol,* 3**,** 767-78.

JESSBERGER, R. 2003. SMC proteins at the crossroads of diverse chromosomal processes. *IUBMB Life,* 55**,** 643-52.

JESSBERGER, R., PODUST, V., HÜBSCHER, U. & BERG, P. 1993. A mammalian protein complex that repairs double-strand breaks and deletions by recombination. *Journal of Biological Chemistry,* 268**,** 15070-15079.

JESSBERGER, R., RIWAR, B., BAECHTOLD, H. & AKHMEDOV, A. T. 1996. SMC proteins constitute two subunits of the mammalian recombination complex RC-1. *The EMBO Journal,* 15**,** 4061.

JONES, R. M., MORTUSEWICZ, O., AFZAL, I., LORVELLEC, M., GARCIA, P., HELLEDAY, T. & PETERMANN, E. 2013. Increased replication initiation and conflicts with transcription underlie Cyclin E-induced replication stress. *Oncogene,* 32**,** 3744-53.

KAELIN, W. G. 2005. The concept of synthetic lethality in the context of anticancer therapy. *Nature reviews cancer,* 5**,** 689-698.

KAGEY, M. H., NEWMAN, J. J., BILODEAU, S., ZHAN, Y., ORLANDO, D. A., VAN BERKUM, N. L., EBMEIER, C. C., GOOSSENS, J., RAHL, P. B., LEVINE, S. S., TAATJES, D. J., DEKKER, J. & YOUNG, R. A. 2010. Mediator and cohesin connect gene expression and chromatin architecture. *Nature,* 467**,** 430-5.

KASTAN, M. B. & BARTEK, J. 2004. Cell-cycle checkpoints and cancer. *Nature,* 432**,** 316-323.

KIM, J., LEE, J. & IYER, V. R. 2008. Global identification of Myc target genes reveals its direct role in mitochondrial biogenesis and its E-box usage in vivo. *PloS one,* 3**,** e1798.

KIM, J. S., KRASIEVA, T. B., LAMORTE, V., TAYLOR, A. M. & YOKOMORI, K. 2002a. Specific recruitment of human cohesin to laser-induced DNA damage. *J Biol Chem,* 277**,** 45149-53.

KIM, S. T., XU, B. & KASTAN, M. B. 2002b. Involvement of the cohesin protein, Smc1, in Atm-dependent and independent responses to DNA damage. *Genes Dev,* 16**,** 560-70.

KING, M.-C., MARKS, J. H. & MANDELL, J. B. 2003. Breast and ovarian cancer risks due to inherited mutations in BRCA1 and BRCA2. *Science,* 302**,** 643-646.

KITAGAWA, R., BAKKENIST, C. J., MCKINNON, P. J. & KASTAN, M. B. 2004. Phosphorylation of SMC1 is a critical downstream event in the ATM-NBS1-BRCA1 pathway. *Genes Dev,* 18**,** 1423-38.

KLEIN, F., MAHR, P., GALOVA, M., BUONOMO, S. B. C., MICHAELIS, C., NAIRZ, K. & NASMYTH, K. 1999. A Central Role for Cohesins in Sister Chromatid Cohesion, Formation of Axial Elements, and Recombination during Yeast Meiosis. *Cell,* 98**,** 91-103.

KLEINE-KOHLBRECHER, D., ADHIKARY, S. & EILERS, M. 2006. Mechanisms of transcriptional repression by Myc. *The Myc/Max/Mad Transcription Factor Network.* Springer.

KLOSE, R. J., KALLIN, E. M. & ZHANG, Y. 2006. JmjC-domain-containing proteins and histone demethylation. *Nat Rev Genet,* 7**,** 715-27.

KOH, C. M., BEZZI, M., LOW, D. H., ANG, W. X., TEO, S. X., GAY, F. P., AL-HADDAWI, M., TAN, S. Y., OSATO, M. & SABÒ, A. 2015. MYC regulates the core pre-mRNA splicing machinery as an essential step in lymphomagenesis. *Nature*.

KONDO, T., KOBAYASHI, M., TANAKA, J., YOKOYAMA, A., SUZUKI, S., KATO, N., ONOZAWA, M., CHIBA, K., HASHINO, S. & IMAMURA, M. 2004. Rapid degradation of Cdt1 upon UV-induced DNA damage is mediated by SCFSkp2 complex. *Journal of Biological Chemistry,* 279**,** 27315-27319.

KRETZNER, L., BLACKWOOD, E. M. & EISENMAN, R. N. 1992. Myc and Max proteins possess distinct transcriptional activities.

KURLAND, J. F. & TANSEY, W. P. 2008. Myc-mediated transcriptional repression by recruitment of histone deacetylase. *Cancer research,* 68**,** 3624-3629.

LEON, J., FERRANDIZ, N., ACOSTA, J. C. & DELGADO, M. D. 2014. Inhibition of cell differentiation: A critical mechanism for MYC-mediated carcinogenesis? *Cell Cycle,* 8**,** 1148-1157.

LEUNG, K. H. T., EL HASSAN, M. A. & BREMNER, R. 2013. A rapid and efficient method to purify proteins at replication forks under native conditions. *BioTechniques,* 55**,** 204-206.

LI, F., WANG, Y., ZELLER, K. I., POTTER, J. J., WONSEY, D. R., O'DONNELL, K. A., KIM, J.-W., YUSTEIN, J. T., LEE, L. A. & DANG, C. V. 2005. Myc stimulates nuclearly encoded mitochondrial genes and mitochondrial biogenesis. *Molecular and cellular biology,* 25**,** 6225-6234.

LI, X. & MANLEY, J. L. 2005. Inactivation of the SR protein splicing factor ASF/SF2 results in genomic instability. *Cell,* 122**,** 365-378.

LIANG, K., GAO, X., GILMORE, J. M., FLORENS, L., WASHBURN, M. P., SMITH, E. & SHILATIFARD, A. 2015. Characterization of human CDK12 and CDK13 complexes in CTD phosphorylation, gene transcription and RNA processing. *Molecular and Cellular Biology***,** MCB. 01426-14.

LIU, J., ZHANG, Z., BANDO, M., ITOH, T., DEARDORFF, M. A., CLARK, D., KAUR, M., TANDY, S., KONDOH, T. & RAPPAPORT, E. 2009. Transcriptional dysregulation in NIPBL and cohesin mutant human cells. *PLoS biology,* 7**,** 1136.

LIU, Y.-C., LI, F., HANDLER, J., HUANG, C., XIANG, Y., NERETTI, N., SEDIVY, J. M., ZELLER, K. I. & DANG, C. V. 2008. Global regulation of nucleotide biosynthetic genes by c-Myc. *PloS one,* 3**,** e2722.

LOSADA, A. 2014. Cohesin in cancer: chromosome segregation and beyond. *Nat Rev Cancer,* 14**,** 389-93.

MACHERET, M. & HALAZONETIS, T. D. 2015. DNA Replication Stress as a Hallmark of Cancer. *Annual Review of Pathology: Mechanisms of Disease,* 10**,** 425-448.

MAILAND, N., PODTELEJNIKOV, A. V., GROTH, A., MANN, M., BARTEK, J. & LUKAS, J. 2002. Regulation of G2/M events by Cdc25A through phosphorylation- dependent modulation of its stability. *The EMBO journal,* 21**,** 5911-5920.

MATSUOKA, S., BALLIF, B. A., SMOGORZEWSKA, A., MCDONALD, E. R., HUROV, K. E., LUO, J., BAKALARSKI, C. E., ZHAO, Z., SOLIMINI, N., LERENTHAL, Y., SHILOH, Y., GYGI, S. P. & ELLEDGE, S. J. 2007. ATM and ATR Substrate Analysis

Reveals Extensive Protein Networks Responsive to DNA Damage. *Science,* 316**,** 1160-1166.

MAYA, R., BALASS, M., KIM, S.-T., SHKEDY, D., LEAL, J.-F. M., SHIFMAN, O., MOAS, M., BUSCHMANN, T., RONAI, Z. E. & SHILOH, Y. 2001. ATM-dependent phosphorylation of Mdm2 on serine 395: role in p53 activation by DNA damage. *Genes & development,* 15**,** 1067-1077.

MCKINNON, P. 1987. Ataxia-telangiectasia: an inherited disorder of ionizing-radiation sensitivity in man. *Human Genetics,* 75**,** 197-208.

MCMAHON, S. B., WOOD, M. A. & COLE, M. D. 2000. The Essential Cofactor TRRAP Recruits the Histone Acetyltransferase hGCN5 to c-Myc. *Molecular and Cellular Biology,* 20**,** 556-562.

MEYER, N. & PENN, L. Z. 2008. Reflecting on 25 years with MYC. *Nature Reviews Cancer,* 8**,** 976-990.

MOSER, R., TOYOSHIMA, M., ROBINSON, K., GURLEY, K. E., HOWIE, H. L., DAVISON, J., MORGAN, M., KEMP, C. J. & GRANDORI, C. 2012. MYC-driven tumorigenesis is inhibited by WRN syndrome gene deficiency. *Mol Cancer Res,* 10**,** 535-45.

MURGA, M., CAMPANER, S., LOPEZ-CONTRERAS, A. J., TOLEDO, L. I., SORIA, R., MONTAÑA, M. F., D'ARTISTA, L., SCHLEKER, T., GUERRA, C. & GARCIA, E. 2011a. Exploiting oncogene-induced replicative stress for the selective killing of Myc-driven tumors. *Nature structural & molecular biology,* 18**,** 1331-1335.

NASMYTH, K. & HAERING, C. H. 2009. Cohesin: its roles and mechanisms. *Annu Rev Genet,* 43**,** 525-58.

NIIDA, H. & NAKANISHI, M. 2006. DNA damage checkpoints in mammals. *Mutagenesis,* 21**,** 3-9.

NYBERG, K. A., MICHELSON, R. J., PUTNAM, C. W. & WEINERT, T. A. 2002. Toward maintaining the genome: DNA damage and replication checkpoints. *Annual review of genetics,* 36**,** 617-656.

ONG, C. T. & CORCES, V. G. 2014. CTCF: an architectural protein bridging genome topology and function. *Nat Rev Genet,* 15**,** 234-46.

OSTER, S. K., HO, C. S., SOUCIE, E. L. & PENN, L. Z. 2002. The myc oncogene: marvelously complex. *Advances in cancer research,* 84**,** 81-154.

PAINTER, R. & YOUNG, B. 1980. Radiosensitivity in ataxia-telangiectasia: a new explanation. *Proceedings of the National Academy of Sciences,* 77**,** 7315-7317.

PASIERBEK, P., JANTSCH, M., MELCHER, M., SCHLEIFFER, A., SCHWEIZER, D. & LOIDL, J. 2001. A Caenorhabditis elegans cohesion protein with functions in meiotic chromosome pairing and disjunction. *Genes & development,* 15**,** 1349-1360.

PAULSEN, R. D., SONI, D. V., WOLLMAN, R., HAHN, A. T., YEE, M.-C., GUAN, A., HESLEY, J. A., MILLER, S. C., CROMWELL, E. F. & SOLOW-CORDERO, D. E. 2009. A genome-wide siRNA screen reveals diverse cellular processes and pathways that mediate genome stability. *Molecular cell,* 35**,** 228-239.

PICHIERRI, P., AMMAZZALORSO, F., BIGNAMI, M. & FRANCHITTO, A. 2011. The Werner syndrome protein: linking the replication checkpoint response to genome stability. *Aging (Albany NY),* 3**,** 311.

POPE, B. D., RYBA, T., DILEEP, V., YUE, F., WU, W., DENAS, O., VERA, D. L., WANG, Y., HANSEN, R. S. & CANFIELD, T. K. 2014. Topologically associating domains are stable units of replication-timing regulation. *Nature,* 515**,** 402-405.

POTTS, P. R., PORTEUS, M. H. & YU, H. 2006. Human SMC5/6 complex promotes sister chromatid homologous recombination by recruiting the SMC1/3 cohesin complex to double- strand breaks. *The EMBO journal,* 25**,** 3377-3388.

PRICE, B. D. & D'ANDREA, A. D. 2013. Chromatin remodeling at DNA double-strand breaks. *Cell,* 152**,** 1344-1354.

PUSAPATI, R. V., ROUNBEHLER, R. J., HONG, S., POWERS, J. T., YAN, M., KIGUCHI, K., MCARTHUR, M. J., WONG, P. K. & JOHNSON, D. G. 2006. ATM promotes apoptosis and suppresses tumorigenesis in response to Myc. *Proceedings of the National Academy of Sciences of the United States of America,* 103**,** 1446-1451.

REINHARDT, H. C. & YAFFE, M. B. 2009. Kinases that control the cell cycle in response to DNA damage: Chk1, Chk2, and MK2. *Current Opinion in Cell Biology,* 21**,** 245-255.
REMESEIRO, S., CUADRADO, A., CARRETERO, M., MARTINEZ, P., DROSOPOULOS, W. C., CANAMERO, M., SCHILDKRAUT, C. L., BLASCO, M. A. & LOSADA, A. 2012. Cohesin-SA1 deficiency drives aneuploidy and tumourigenesis in mice due to impaired replication of telomeres. *EMBO J,* 31**,** 2076-89.
ROBINSON, K., ASAWACHAICHARN, N., GALLOWAY, D. A. & GRANDORI, C. 2009. c-Myc accelerates S-phase and requires WRN to avoid replication stress. *PLoS One,* 4**,** e5951.
ROHBAN, S. & CAMPANER, S. 2015. Myc induced replicative stress response: How to cope with it and exploit it. *Biochim Biophys Acta,* 1849**,** 517-24.
ROTHKAMM, K., KRÜGER, I., THOMPSON, L. H. & LÖBRICH, M. 2003. Pathways of DNA double-strand break repair during the mammalian cell cycle. *Molecular and cellular biology,* 23**,** 5706-5715.
SANCAR, A., LINDSEY-BOLTZ, L. A., UNSAL-KACMAZ, K. & LINN, S. 2004. Molecular mechanisms of mammalian DNA repair and the DNA damage checkpoints. *Annu Rev Biochem,* 73**,** 39-85.
SANTOS-PEREIRA, J. M. & AGUILERA, A. 2015. R loops: new modulators of genome dynamics and function. *Nat Rev Genet,* 16**,** 583-597.
SANTOS, M. A., JOHN, S. & NUSSENZWEIG, A. 2014. Tumor promoting role of the DNA damage response. *Cell Cycle,* 13**,** 2807-2808.
SCHMITZ, J., WATRIN, E., LÉNÁRT, P., MECHTLER, K. & PETERS, J.-M. 2007. Sororin is required for stable binding of cohesin to chromatin and for sister chromatid cohesion in interphase. *Current Biology,* 17**,** 630-636.
SHECHTER, D., COSTANZO, V. & GAUTIER, J. 2004. Regulation of DNA replication by ATR: signaling in response to DNA intermediates. *DNA repair,* 3**,** 901-908.
SHI, Y., GLYNN, J. M., GUILBERT, L. J., COTTER, T. G., BISSONNETTE, R. P. & GREEN, D. R. 1992. Role for c-myc in activation-induced apoptotic cell death in T cell hybridomas. *Science,* 257**,** 212-214.
SHICHIRI, M., HANSON, K. & SEDIVY, J. 1993. Effects of c-myc expression on proliferation, quiescence, and the G0 to G1 transition in nontransformed cells. *Cell growth & differentiation: the molecular biology journal of the American Association for Cancer Research,* 4**,** 93-104.
SHILOH, Y. 2003. ATM and related protein kinases: safeguarding genome integrity. *Nature Reviews Cancer,* 3**,** 155-168.
SHILOH, Y. & KASTAN, M. B. 2001. ATM: genome stability, neuronal development, and cancer cross paths. *Advances in cancer research,* 83**,** 209-254.
SHILOH, Y. & ZIV, Y. 2013. The ATM protein kinase: regulating the cellular response to genotoxic stress, and more. *Nat Rev Mol Cell Biol,* 14**,** 197-210.
SHINOZAKI, T., NOTA, A., TAYA, Y. & OKAMOTO, K. 2003. Functional role of Mdm2 phosphorylation by ATR in attenuation of p53 nuclear export. *Oncogene,* 22**,** 8870-8880.
SMITS, V. A., KLOMPMAKER, R., ARNAUD, L., RIJKSEN, G., NIGG, E. A. & MEDEMA, R. H. 2000. Polo-like kinase-1 is a target of the DNA damage checkpoint. *Nature cell biology,* 2**,** 672-676.
SOUCEK, L., WHITFIELD, J., MARTINS, C. P., FINCH, A. J., MURPHY, D. J., SODIR, N. M., KARNEZIS, A. N., SWIGART, L. B., NASI, S. & EVAN, G. I. 2008. Modelling Myc inhibition as a cancer therapy. *Nature,* 455**,** 679-683.
SRINIVASAN, S. V., DOMINGUEZ-SOLA, D., WANG, L. C., HYRIEN, O. & GAUTIER, J. 2013. Cdc45 is a critical effector of myc-dependent DNA replication stress. *Cell Rep,* 3**,** 1629-39.
STEWART, G. S., MASER, R. S., STANKOVIC, T., BRESSAN, D. A., KAPLAN, M. I., JASPERS, N. G., RAAMS, A., BYRD, P. J., PETRINI, J. H. & TAYLOR, A. M. R. 1999. The DNA double-strand break repair gene hMRE11 is mutated in individuals with an ataxia-telangiectasia-like disorder. *Cell,* 99**,** 577-587.

STEWART, G. S., WANG, B., BIGNELL, C. R., TAYLOR, A. M. R. & ELLEDGE, S. J. 2003. MDC1 is a mediator of the mammalian DNA damage checkpoint. *Nature,* 421**,** 961-966.

STOKES, M. P., RUSH, J., MACNEILL, J., REN, J. M., SPROTT, K., NARDONE, J., YANG, V., BEAUSOLEIL, S. A., GYGI, S. P. & LIVINGSTONE, M. 2007. Profiling of UV-induced ATM/ATR signaling pathways. *Proceedings of the National Academy of Sciences,* 104**,** 19855-19860.

STROM, L., LINDROOS, H. B., SHIRAHIGE, K. & SJOGREN, C. 2004. Postreplicative recruitment of cohesin to double-strand breaks is required for DNA repair. *Mol Cell,* 16**,** 1003-15.

STUCKI, M. & JACKSON, S. P. 2006. γH2AX and MDC1: anchoring the DNA-damage-response machinery to broken chromosomes. *DNA repair,* 5**,** 534-543.

SULLI, G., DI MICCO, R. & DI FAGAGNA, F. D. A. 2012. Crosstalk between chromatin state and DNA damage response in cellular senescence and cancer. *Nature Reviews Cancer,* 12**,** 709-720.

TAKAHASHI, K. & YAMANAKA, S. 2006. Induction of pluripotent stem cells from mouse embryonic and adult fibroblast cultures by defined factors. *cell,* 126**,** 663-676.

TAYLOR, W. R. & STARK, G. R. 2001. Regulation of the G2/M transition by p53. *Oncogene,* 20**,** 1803-1815.

TIBBETTS, R. S., BRUMBAUGH, K. M., WILLIAMS, J. M., SARKARIA, J. N., CLIBY, W. A., SHIEH, S.-Y., TAYA, Y., PRIVES, C. & ABRAHAM, R. T. 1999. A role for ATR in the DNA damage-induced phosphorylation of p53. *Genes & development,* 13**,** 152-157.

TOLEDO, L. I., MURGA, M. & FERNANDEZ-CAPETILLO, O. 2011. Targeting ATR and Chk1 kinases for cancer treatment: a new model for new (and old) drugs. *Mol Oncol,* 5**,** 368-73.

TOYOSHIMA, M., HOWIE, H. L., IMAKURA, M., WALSH, R. M., ANNIS, J. E., CHANG, A. N., FRAZIER, J., CHAU, B. N., LOBODA, A. & LINSLEY, P. S. 2012. Functional genomics identifies therapeutic targets for MYC-driven cancer. *Proceedings of the National Academy of Sciences,* 109**,** 9545-9550.

TSANTOULIS, P. K., KOTSINAS, A., SFIKAKIS, P. P., EVANGELOU, K., SIDERIDOU, M., LEVY, B., MO, L., KITTAS, C., WU, X. R., PAPAVASSILIOU, A. G. & GORGOULIS, V. G. 2008. Oncogene-induced replication stress preferentially targets common fragile sites in preneoplastic lesions. A genome-wide study. *Oncogene,* 27**,** 3256-64.

ÜNAL, E., ARBEL-EDEN, A., SATTLER, U., SHROFF, R., LICHTEN, M., HABER, J. E. & KOSHLAND, D. 2004. DNA damage response pathway uses histone modification to assemble a double-strand break-specific cohesin domain. *Molecular cell,* 16**,** 991-1002.

UZIEL, T., LERENTHAL, Y., MOYAL, L., ANDEGEKO, Y., MITTELMAN, L. & SHILOH, Y. 2003. Requirement of the MRN complex for ATM activation by DNA damage. *The EMBO journal,* 22**,** 5612-5621.

VAFA, O., WADE, M., KERN, S., BEECHE, M., PANDITA, T. K., HAMPTON, G. M. & WAHL, G. M. 2002. c-Myc can induce DNA damage, increase reactive oxygen species, and mitigate p53 function: a mechanism for oncogene-induced genetic instability. *Molecular cell,* 9**,** 1031-1044.

VAN LOHUIZEN, M., VERBEEK, S., SCHELJEN, B., WIENTJENS, E., VAN DER GUIDON, H. & BERNS, A. 1991. Identification of cooperating oncogenes in Eμ-myc transgenic mice by provirus tagging. *Cell,* 65**,** 737-752.

VARON, R., VISSINGA, C., PLATZER, M., CEROSALETTI, K. M., CHRZANOWSKA, K. H., SAAR, K., BECKMANN, G., SEEMANOVÁ, E., COOPER, P. R. & NOWAK, N. J. 1998. Nibrin, a novel DNA double-strand break repair protein, is mutated in Nijmegen breakage syndrome. *Cell,* 93**,** 467-476.

VITA, M. & HENRIKSSON, M. 2006. The Myc oncoprotein as a therapeutic target for human cancer. *Seminars in Cancer Biology,* 16**,** 318-330.

VITALE, I., GALLUZZI, L., VIVET, S., NANTY, L., DESSEN, P., SENOVILLA, L., OLAUSSEN, K. A., LAZAR, V., PRUDHOMME, M. & GOLSTEYN, R. M. 2007.

Inhibition of Chk1 kills tetraploid tumor cells through a p53-dependent pathway. *PloS one,* 2**,** e1337-e1337.

WAHL, G. M. & CARR, A. M. 2001. The evolution of diverse biological responses to DNA damage: insights from yeast and p53. *Nature cell biology,* 3**,** E277-E286.

WALZ, S., LORENZIN, F., MORTON, J., WIESE, K. E., VON EYSS, B., HEROLD, S., RYCAK, L., DUMAY-ODELOT, H., KARIM, S. & BARTKUHN, M. 2014. Activation and repression by oncogenic MYC shape tumour-specific gene expression profiles. *Nature,* 511**,** 483-487.

WARD, I. M., MINN, K., VAN DEURSEN, J. & CHEN, J. 2003. p53 Binding protein 53BP1 is required for DNA damage responses and tumor suppression in mice. *Molecular and cellular biology,* 23**,** 2556-2563.

WENDT, K. S., YOSHIDA, K., ITOH, T., BANDO, M., KOCH, B., SCHIRGHUBER, E., TSUTSUMI, S., NAGAE, G., ISHIHARA, K., MISHIRO, T., YAHATA, K., IMAMOTO, F., ABURATANI, H., NAKAO, M., IMAMOTO, N., MAESHIMA, K., SHIRAHIGE, K. & PETERS, J. M. 2008. Cohesin mediates transcriptional insulation by CCCTC-binding factor. *Nature,* 451**,** 796-801.

WISE, D. R., DEBERARDINIS, R. J., MANCUSO, A., SAYED, N., ZHANG, X.-Y., PFEIFFER, H. K., NISSIM, I., DAIKHIN, E., YUDKOFF, M. & MCMAHON, S. B. 2008. Myc regulates a transcriptional program that stimulates mitochondrial glutaminolysis and leads to glutamine addiction. *Proceedings of the National Academy of Sciences,* 105**,** 18782-18787.

WRIGHT, J. A., KEEGAN, K. S., HERENDEEN, D. R., BENTLEY, N. J., CARR, A. M., HOEKSTRA, M. F. & CONCANNON, P. 1998. Protein kinase mutants of human ATR increase sensitivity to UV and ionizing radiation and abrogate cell cycle checkpoint control. *Proceedings of the National Academy of Sciences,* 95**,** 7445-7450.

WU, N. & YU, H. 2012. The Smc complexes in DNA damage response. *Cell Biosci,* 2**,** 5.

XU, B., KIM, S.-T., LIM, D.-S. & KASTAN, M. B. 2002. Two molecularly distinct G2/M checkpoints are induced by ionizing irradiation. *Molecular and cellular biology,* 22**,** 1049-1059.

YAN, J., ENGE, M., WHITINGTON, T., DAVE, K., LIU, J., SUR, I., SCHMIERER, B., JOLMA, A., KIVIOJA, T., TAIPALE, M. & TAIPALE, J. 2013. Transcription factor binding in human cells occurs in dense clusters formed around cohesin anchor sites. *Cell,* 154**,** 801-13.

ZELLER, K. I., JEGGA, A. G., ARONOW, B. J., O'DONNELL, K. A. & DANG, C. V. 2003. An integrated database of genes responsive to the Myc oncogenic transcription factor: identification of direct genomic targets. *Genome Biol,* 4**,** R69.

ZEMAN, M. K. & CIMPRICH, K. A. 2014. Causes and consequences of replication stress. *Nature cell biology,* 16**,** 2-9.

ZHANG, H., GAO, P., FUKUDA, R., KUMAR, G., KRISHNAMACHARY, B., ZELLER, K. I., DANG, C. V. & SEMENZA, G. L. 2007. HIF-1 inhibits mitochondrial biogenesis and cellular respiration in VHL-deficient renal cell carcinoma by repression of C-MYC activity. *Cancer cell,* 11**,** 407-420.

ZHOU, B.-B. S. & ELLEDGE, S. J. 2000. The DNA damage response: putting checkpoints in perspective. *Nature,* 408**,** 433-439.

ZINDY, F., EISCHEN, C. M., RANDLE, D. H., KAMIJO, T., CLEVELAND, J. L., SHERR, C. J. & ROUSSEL, M. F. 1998. Myc signaling via the ARF tumor suppressor regulates p53-dependent apoptosis and immortalization. *Genes & development,* 12**,** 2424-2433.

ZOU, L. & ELLEDGE, S. J. 2003. Sensing DNA damage through ATRIP recognition of RPA-ssDNA complexes. *Science,* 300**,** 1542-1548.

Acknowledgement

First of all, I would like to express my sincere gratitude to my supervisor Dr. Stefano Campaner for his guidance, patience, motivation and the immense knowledge and skills.

Next, I would like to thank my thesis committee members: Dr. Anja Groth and Dr. Vincenzo Costanzo for agreeing to serve on my dissertation committee. I would truly appreciate all of their time, feedbacks and comments.

I would like to extend my gratitude to my internal advisor Dr. Fabrizio d'Adda di Fagagna and my external advisor Dr. Axel Behrens for reading my reports, commenting on my views and taking the time out of their schedule to meet with me and provide me valuable feedbacks.

I would like to express my sincere thanks and appreciation to Dr. Bruno Amati for his support and assistance when I needed.

I also wish to thank the members of IIT screening unit: Dr. Mark Wade, Dr. Michela Mattioli, Dr. Fernanda Ricci and Dr. Adrian Andronache for performing RNAi screen, providing resources and contributing to this study.

I would like to thank Dr. Macro Morelli for performing ChIP and RNA-seq analysis, and Dr. Aurora Cerutti for performing DNA combing experiment.

This work would have not been possible without the great core facilities of IFOM-IEO Campus, specially: Tissue culture facility, Imaging unit, Genomic unit and IEO kitchen unit. I would like to thank all staffs of these facilities.

A very special thanks is due to my friends and colleagues in the lab specially Elisa Donato, Mirko Doni, Alessandro Verrecchia, Manuel Colucci, Ottavio Croci, Dr. Chiara Biancotto, Dr. Serena De Fazio, Dr. Marieta Caganova and Dr. Francesca Biagioni, for the stimulating discussions, exchanges of knowledge, skills and for all the fun we have had in these years.

I am also grateful to Francesa Fiore and Veronica Viscardi in SEMM office for their support during my doctoral studies.

I would like to express my heart-felt gratitude to my parents, my sister and my brother for their encouragement and the continued support over the years and their enthusiasm. I would also like to express appreciation to my beloved husband, who is my best friend and supporter.

I could not have completed my doctoral study without the support of all these wonderful people!